Molecular Conductors and Superconductors Based on Trihalides of BEDT-TTF and Some of Its Analogues

ARTICLE *in* CHEMICAL REVIEWS · NOVEMBER 2004

Impact Factor: 46.57 · DOI: 10.1021/cr0306642 · Source: PubMed

2 AUTHORS:

Rimma Shibaeva
Institute of Solid State Physics RAS
227 PUBLICATIONS **1,712** CITATIONS
SEE PROFILE

Eduard Borisovich Yagubskii
Russian Academy of Sciences
63 PUBLICATIONS **566** CITATIONS
SEE PROFILE

Molecular Conductors and Superconductors Based on Trihalides of BEDT-TTF and Some of Its Analogues

Rimma P. Shibaeva*,† and Eduard B. Yagubskii‡

Institute of Solid State Physics and Institute of Problems of Chemical Physics, Russian Academy of Sciences, Chernogolovka, Moscow District, 142432 Russia

Received April 15, 2004

Contents

1. Introduction

Low-dimensional organic conductors based on charge-transfer salts of bis(ethylenedithio)tetrathiafulvalene (BEDT-TTF or ET) and its analogues are very versatile systems for studying the relationship between their crystal structures and physical properties.[1−8] These salts have a layer structure in which layers of π-donor molecules alternate with layers of anions. Electronic properties of the salts are essentially determined by the packing pattern of their donor molecule layers, which in turn, depends on a counterion. Actually, the donor layer arrangements are strongly controlled by donor···anion interactions. That is why inorganic counterions play a crucial role in physical properties of ET-based materials. Variation of an anion component in organic conductors based on radical cation salts is one of the approaches for modifying their physical properties. Although a great number of molecular conductors have already been found among radical cation salts, those of the $(ET)_2X$ family, where X = trihalide anion I_3, IBr_2, ICl_2, etc., are still very interesting as both quite simple and very informative systems.

Organic molecular crystals of $(ET)_2X$ are low-dimensional electronic systems showing a wide range of physical properties, from semiconductors to superconductors. One of the member of this family, β-$(ET)_2I_3$, was the first quasi-two-dimensional (2D) organic superconductor at ambient pressure.[9−11] The synthesis of β-$(ET)_2I_3$ in 1983 was an important historical step in the study of ET salts. Soon after [information on these results became known to the community at the Conference in Abano Terme (June, 1984) and has been published in ref 12], it was found that this compound can exist in low-temperature (β_L) and high-temperature (β_H) superconducting states.[12] Shubnikov-de Haas and angle-dependent magnetoresistance oscillations were for the first time observed in the ET trihalide salt[13,14] and, in fact, that study was an initial contribution to fermiology of quasi-2D organic metals. Quite recently, the other member of the $(ET)_2X$ family, β'-$(ET)_2ICl_2$, has become "intriguingly famous". This compound being a Mott insulator transforms to a superconductor with T_c = 14.2 K under very high pressure.[15]

The compounds of the $(ET)_2X$ series are characterized by extensive polymorphism, associated with different molecule arrangements in the donor layer. The ET tri-iodide, $(ET)_2I_3$, can exist in four polymorphous modifications (α, β, κ, and θ). Moreover, it is a unique compound among radical cation salts of ET by a number of superconducting polymorphous phases (β_L, β_H, κ, and θ, with T_c from 1.5 to 8 K). The ability to crystallize in several different phases provides the opportunity to correlate structures and physical properties in this class of organic conductors.

The reason for the current intense interest in these conductors is that they form an easily variable system. Physical properties of ET salts can change dramatically when their structures are altered by a

* To whom correspondence should be addressed. E-mail: shibaeva@issp.ac.ru.
† Institute of Solid State Physics.
‡ Institute of Problems of Chemical Physics.

10.1021/cr0306642 CCC: $48.50
Published on Web 10/09/2004

Rimma P. Shibaeva was born in the Vladimir region of Russia and was educated at the University in Nizhnii Novgorod (the former Gor'ky). She received her Ph.D. degree in 1962 under supervision of academician N. Belov (Institute of Crystallography, Moscow). Her doctoral work dealt with the crystal structures of silicates. From 1962 to 1990, she was a Research Scientist at the Institute of Chemical Physics (Chernogolovka), where she carried out X-ray studies of the organic paramagnetics, stable nitroxyl radicals. From the end of the sixties, she was involved in the team of Prof. I. Schegolev for investigating low-dimensional organic conductors. Many of the crystal structures of the radical anion salts of TCNQ and the radical cation salts of TTT, TSeT, DBTTF, BEDT-TTF, etc. have been studied by Rimma Shibaeva. She received her Doctor of Sciences from the Institute of Crystallography (Moscow) in 1978. In 1991, she moved to the Institute of Solid State Physics, Russian Academy of Sciences (Chernogolovka), where she is working now as a Lieder Scientific Researcher. She has held visiting positions at the Laboratoire de Physique des Solides of the University of Paris XI (Orsay), with the research group of Prof. P. Batail (1994), and at the Graduate School of Science, Kyoto University, Japan, with the research group of Prof. G. Saito (1998). Her research interests include molecular materials, in particular, multifunctional materials based on radical ion salts, and understanding the relationship between their crystal structures and physical properties.

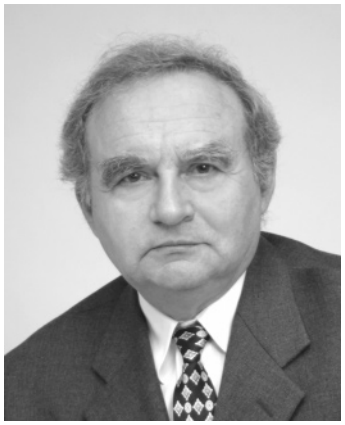

Eduard B. Yagubskii was born in Donetsk, USSR, in 1939. He received his M.Sci. (Organic Chemistry) at Moscow Institute of Fine Chemical Technology in 1962 and his Ph.D. and Dr.Sci. at the Branch of Moscow Institute of Chemical Physics (Chernogolovka) of the USSR Academy of Sciences in 1973 and 1986, respectively. His Ph.D. work under the supervision of Professor M. Khidekel dealt with the synthesis and characterization of the TCNQ conducting complexes with cyanine dyes and arenchromium compounds. His Dr.Sci. work concerned the synthesis and study of low-dimensional molecular metals and superconductors based on the radical cation salts of tetrachalcogenotetracenes and BEDT-TTF. He synthesized the first quasi-two-dimensional organic superconductor at ambient pressure, β-(BEDT-TTF)$_2$I$_3$. He became a Senior researcher, Principal researcher, and Head of Laboratory at the Branch of Institute of Chemical Physics in Chernogolovka in 1974, 1986, and 1987, respectively. Currently, he is a Head of Laboratory of Synthetic Metals at the Institute of Problems of Chemical Physics (Chernogolovka) of the Russian Academy of Sciences. He was awarded an JSPS fellowship in 1994 and a fellowship of the Italian Ministry of Foreign Affairs in 1999 for research in Japan and Italy. His current research interests include low-dimensional molecular metals and superconductors, multi-functional molecular materials with electrical, magnetic, and photochromic properties, as well as endohedral metallofullerenes.

slight chemical modification of their charge-compensating anions. Besides, these systems exhibit many interesting phenomena, including phase transitions and mutual polymorphic transformations. Such structural transitions are often accompanied by drastic changes in the electronic subsystem. Thereby, one can study structure−property relationships on the same crystal. Additionally, there could be transitions in the electron subsystem itself that in turn can cause minute changes in the atomic structure and vice versa. An example of such coupled behavior of electronic and atomic structures gives the M−I phase transition at 135 K in α-(ET)$_2$I$_3$.[16−18]

Furthermore, ET analogues with different heteroatoms (selenium and oxygen) or with different "bridge" groups instead of the ethylene ones in terminal cycles as well as metal complex analogues, in which the central C=C bond is replaced with a metal atom, can also form many charge-transfer salts with trihalide anions. It was found that some of them exhibit unconventional structural properties. Thus, a stable organic metal β''-(BEDO)$_{2.4}$I$_3$ appears as a composite material; there are two incommensurate sublattices in its crystal structure.[19]

The series of radical cation salts based on ET and its analogues with linear trihalide anions were abundantly studied by many research teams, and a variety of data was accumulated. This review endeavorers to summarize the data on the salts, which were structurally characterized for determining a structure−property relationship in this class of low-dimensional organic conductors. This review does not treat in detail the corresponding data on electronic band structures, which were surveyed in review papers by Mori[20−22] and recently have been generalized for some types of the radical cation salts in the works by Canadell.[23,24]

The review describes the (ET)$_2$X family, where X = I$_3$, I$_2$Br, IBr$_2$, (IBr$_2$)$_{0.7}$(I$_3$)$_{0.3}$, ICl$_2$, and BrICl, focusing on synthesis, structural aspects, the donor-layer types, polymorphism, and a genetic connection of polymorphic phases, as well as their transport properties and phase transformations, followed by the discussion of their physical properties. Special consideration is devoted to β_L- and β_H-(ET)$_2$I$_3$, including the structural features under various conditions and methods of preparing β_H. In this connection, other ET polyiodides are described as precursors of β_H-(ET)$_2$I$_3$. Additionally, the radical cation salts of some ET analogues with trihalide anions are reviewed.

The structural formulas of the basic donor molecules are illustrated in Figure 1, which also involves the list of abbreviations used in the text.

2. (ET)$_2$X Family, Where X Is a Linear Trihalide Anion, I$_3$, IBr$_2$, ICl$_2$, etc.

2.1. Crystal Structures

Unit-cell parameters of all salts of the (ET)$_2$X family with linear trihalide anions structurally char-

Table 1. Unit-Cell Parameters of the Basic Phases of $(ET)_2X$ at Room Temperature

no.	compound	a (Å)	b (Å)	c (Å)	α (deg)	β (deg)	γ (deg)	V (Å^3)	space group	Z	properties	references
1	α-$(ET)_2I_3$	10.785	9.172	17.389	82.08	96.92	89.13	1690.3	$P\bar{1}$	2	T_{M-I} = 135 K	16, 25
2	β-$(ET)_2I_3$	6.609	9.083	15.627	85.63	95.62	70.22	852.2	$P\bar{1}$	1	T_c = 1.5−8 K	9−12
3	θ-$(ET)_2I_3$	10.076	33.853	4.964	90	90	90	1693	Pnma	2	T_c = 3.6 K	26
		9.928	10.076	34.220	90	98.39	90	3386.9	$P2_1/c$	4		27
4	κ-$(ET)_2I_3$	16.387	8.466	12.832	90	108.56	90	1687.6	$P2_1/c$	2	T_c = 3.6 K	28
5	α-$(ET)_2I_2Br$	9.142	10.818	17.370	96.98	97.97	90.81	1687.9	$P\bar{1}$	2	T_{M-I} = 245 K	29
6	β-$(ET)_2I_2Br$	6.612	9.024	15.192	94.16	95.23	110.12	842.4	$P\bar{1}$	1	M	30, 31
7	α′-$(ET)_2IBr_2$	12.005	8.898	16.410	88.71	85.15	70.76	1649.1	$P\bar{1}$	2	Sm	32, 33
8	β-$(ET)_2IBr_2$	6.593	8.975	15.093	93.79	94.97	110.54	828.7	$P\bar{1}$	1	T_c = 2.7 K	34
9	β-$(ET)_2(IBr_2)_{0.7}(I_3)_{0.3}$	6.603	8.996	15.152	94.05	95.15	110.22	836.2	$P\bar{1}$	1	M	35
10	β'-$(ET)_2ICl_2$	6.638	9.760	12.906	87.11	100.93	98.62	811.5	$P\bar{1}$	1	Sm	36−38
11	β''-$(ET)_2ICl_2$	5.734	8.979	16.66	82.18	76.59	76.43	808.2	$P\bar{1}$	1	M	39, 40
12	α′-$(ET)_2BrICl$[a]	16.307	12.373	8.871	113.44	91.50	93.60	1636.3	$P\bar{1}$	2	Sm	41
13	β'-$(ET)_2BrICl$[a]	6.642	9.816	12.975	87.29	101.11	98.28	821.3	$P\bar{1}$	1	Sm	36
14	α‴-$(ET)_2BrICl$[a]	17.116	8.956	16.338	88.09	84.22	81.22	2462.1	$P\bar{1}$	3	Sm	42

[a] Really, these phases contain a combination of different trihalide anions.

Table 2. Parameters of Transformed Unit Cells for the Basic Phases of $(ET)_2X$

no.	compound	a' (Å)	b' (Å)	c' (Å)	α′ (deg)	β' (deg)	γ' (deg)	V (Å^3)	space group	Z	transformation
1	α-$(ET)_2I_3$	10.785	9.172	19.326	97.61	116.72	89.13	1690.3	$P\bar{1}$	2	$a' = -a, b' = -b, c' = a + c$
7	α′-$(ET)_2IBr_2$	12.365	8.898	18.490	117.47	104.52	66.44	1649.1	$P\bar{1}$	2	$a' = a - b, b' = -b, c' = b - c$
14	α‴-$(ET)_2BrICl$	18.066	8.956	18.368	117.25	103.97	69.44	2462.1	$P\bar{1}$	3	$a' = a - b, b' = -b, c' = b - c$
2	β-$(ET)_2I_3$	6.609	9.249	18.961	127.19	105.39	67.53	852.2	$P\bar{1}$	1	$a' = -a, b' = b - a, c' = a - b - c$
10	β'-$(ET)_2ICl_2$	6.638	10.950	16.330	127.97	99.62	61.80	811.5	$P\bar{1}$	1	$a' = -a, b' = -a - b, c' = a + b + c$
11	β''-$(ET)_2ICl_2$	5.734	8.979	18.17	116.32	102.64	76.43	808.2	$P\bar{1}$	1	$a' = a, b' = b, c' = c - a - b$

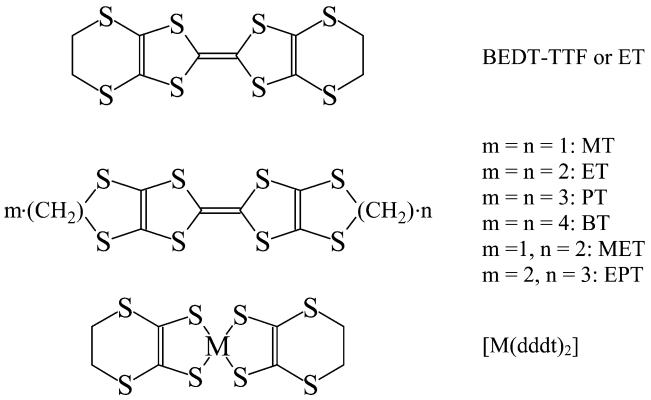

Figure 1. π donors as components of the radical cation salts discussed in the text: ET (or BEDT-TTF), bis(ethylenedithio)tetrathiafulvalene; MT (or BMDT-TTF), bis(methylenedithio)tetrathiafulvalene; PT (or BPDT-TTF), bis(propylenedithio)tetrathiafulvalene; BT (or BBDT-TTF), bis(buthylenedithio)tetrathiafulvalene; MET (or MDTEDT-TTF), methylenedithioethylenedithiotetrathiafulvalene; EPT (or EDTPDT-TTF), ethylenedithiopropylenedithiotetrathiafulvalene; M(dddt)$_2$, M = Pt, Pd, and Au; dddt, 5,6-dihydro-1,4-dithiin-2,3-dithiolate. Abbreviations: BETS, bis(ethylenedithio)tetraselenafulvalene; BEST, bis(ethylenediseleno)-tetrathiafulvalene; BEDO, bis(ethylenedioxo)tetrathiafulvalene. Solvents: TCE, 1,1,2-trichloroethane; BN, benzonitrile; CB, chlorobenzene; NB, nitrobenzene; THF, tetrahydrofuran.

acterized by now are listed in Table 1. Mori summarized the structural genealogy of ET-based organic conductors in three excellent review articles,[20−22] and we hold on to his classification in our paper. Note that in the case of the θ salt the unit-cell parameters correspond to twinning domain crystals. Later,[27] the parameters of the monodomain crystal were reported as $a_m = 2c_o$, $b_m = a_o$, $c_m = b_o - c_o$, where a_o, b_o, and c_o are those of the orthorhombic cell (Table 1), with a_m = 9.928 Å, b_m = 10.076 Å, c_m = 34.220 Å, β = 98.39°, and space group = $P2_1/c$. The orthorhombic symmetry of the averaged structure originates from the twin structure. The authors of ref 43 reported on so-called β_d- and λ_d-$(ET)_2I_3$ crystals with the lattice parameters, a = 6.646 Å, b = 9.257 Å, c = 15.273 Å, α = 98.28°, β = 89.75°, γ = 108.91°, and V = 854.9 Å^3 for β_d and a = 10.086 Å, b = 9.947 Å, c = 34.31 Å, β = 98.51°, and V = 3404.4 Å^3 for λ_d. We suppose that β_d parameters correspond to the twinned crystal of **2** (Table 1), and λ_d parameters really correspond to a monoclinic lattice of θ-$(ET)_2I_3$.[27] It was also reported on the superconducting γ-$(ET)_3(I_3)_{2.5}$ phase with $T_c \approx$ 2.5 K (a = 13.76 Å, b = 14.73 Å, c = 33.61 Å, V = 6812 Å^3, space group = $Pbnm$, and Z = 4).[11] However, the crystals of this phase suitable for complete X-ray analysis were not obtained. Occurrence of these crystals is doubtful. There is no assurance that the structural and superconducting data came from a uniphase single crystal.

The crystal structures of all phases are characterized by the presence of the radical cation layers of ET, alternating with those of linear trihalide anions along the longest lattice axis (parts a−l of Figure 2, parts a and b of Figure 3, and parts a and b of Figure 4). It should be noted that to compare the phases adequately we chose a nonstandard lattice setting, namely, in such a way that the long ET molecular axis would approximately be parallel to the largest period of the cell and the ET stacks in the radical cation layer would run along the b direction. The figures for the α and β salts are given in that very lattice setting. New unit-cell parameters together with the transformation matrixes are listed in Table 2, and they are different from published ones presented in Table 1.

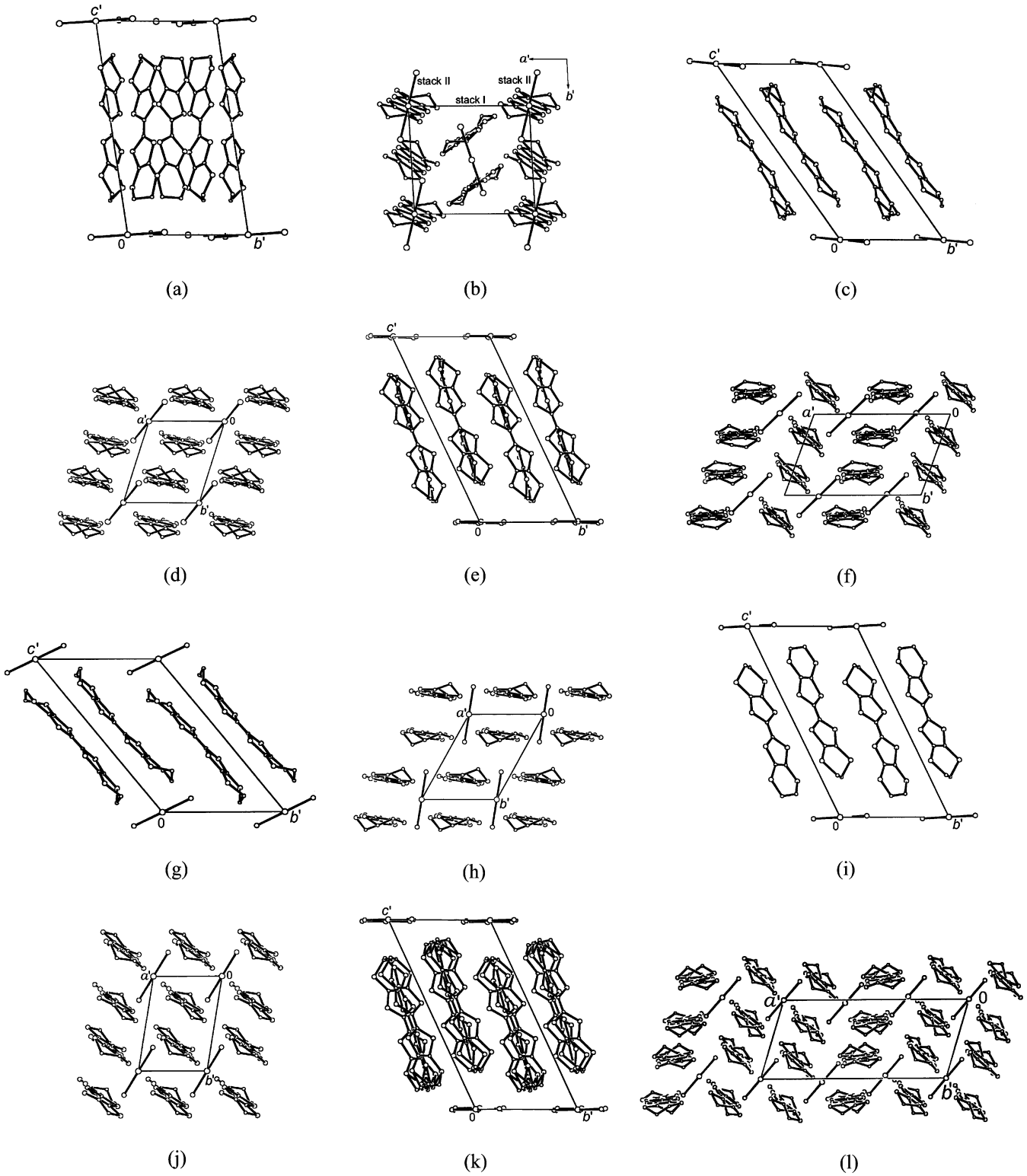

Figure 2. Projections of the crystal structure of α-$(ET)_2I_3$ along a (a) and c' (b) axes; β-$(ET)_2I_3$ along a' (c) and c' (d) axes; α′-$(ET)_2IBr_2$ along a' (e) and c' (f) axes; β'-$(ET)_2ICl_2$ along a' (g) and c' (h) axes; β''-$(ET)_2ICl_2$ along a' (i) and c' (j) axes; and α‴-$(ET)_2BrICl$ along a' (k) and c' (l) axes.

It is seen from Figures 2−4 that the crystals of the $(ET)_2X$ family are quasi-2D systems in which conducting radical cation layers are separated by insulating anion ones. They can essentially differ by the type of an internal structure of a conducting layer, which is shown in section 2.2. It is seen from Table 1 and Figures 2−4 that a radical cation layer can involve a different number of the ET molecules even in the case of triclinic symmetry of crystals, and the ET molecules can occupy the positions of different symmetry in a lattice. Anion layers are composed of parallel linear trihalide anions in all phases except α and κ ones (Figures 2−4).

2.2. Types of Donor Layers

The ability of the ET donor to form a 2D electronic structure was demonstrated, for the first time, in the $(ET)_2ClO_4(C_2H_3Cl_3)_{0.5}$[44] and $(ET)_2PF_6$[45] radical cation

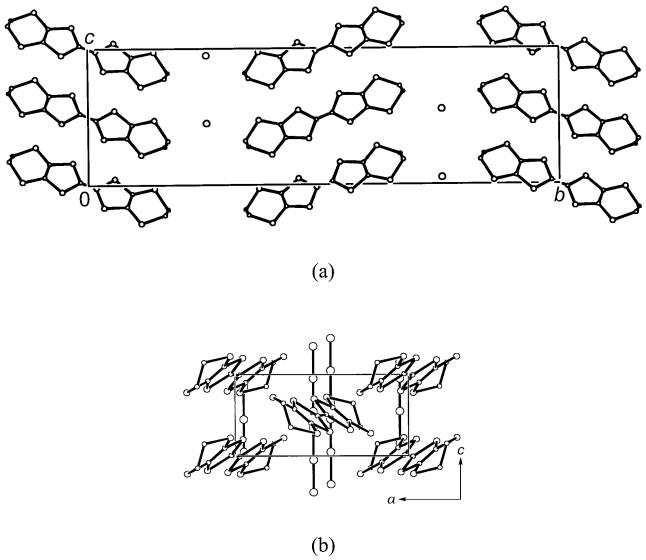

Figure 3. θ-$(ET)_2I_3$, projections of the crystal structure along a (a) and b (b) axes.

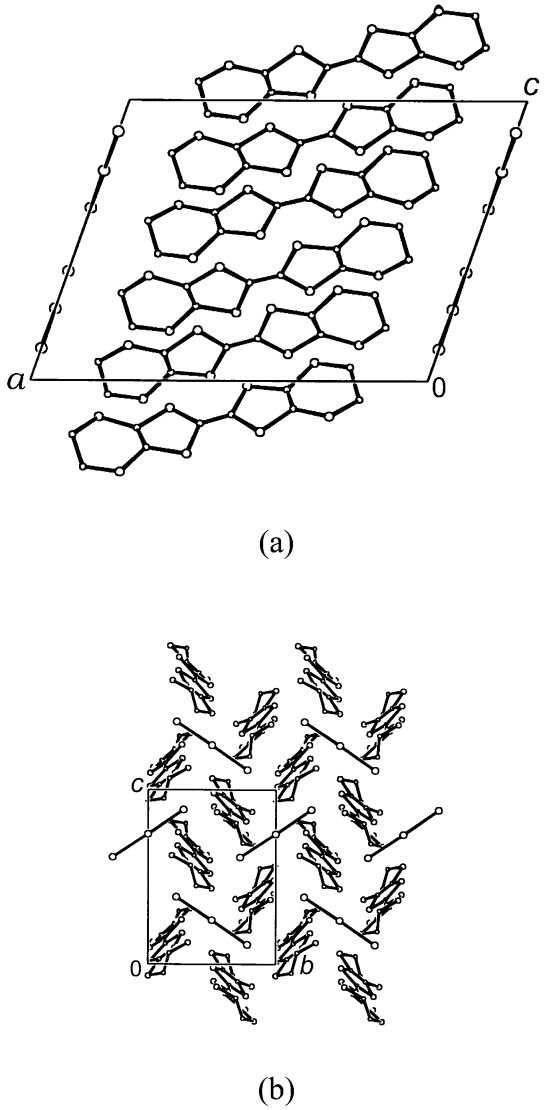

Figure 4. κ-$(ET)_2I_3$, projections of the crystal structure along b (a) and a (b) axes.

salts. At present, this donor is a main building brick for constructing conducting layers of organic metals and superconductors. The ET molecule contains eight sulfur atoms and saturated nonplanar CH_2CH_2 groups. The S atoms promote the formation of multiple side−side S···S contacts in radical cation layers, and the ethylene groups create some steric hindrances for face−face π-intermolecular interactions providing the increment of electronic dimensionality in the ET salts. The ET molecule has some conformational degree of freedom of terminal ethylene groups, which are basic units of a hydrogen-bond network linking ET and counterion species. These two terminal groups can adopt either eclipsed (e) or staggered (s) configurations (Figure 5). The e and s configurations are energetically equal for the isolated ET molecule. In the ET-based radical cation salts, one of conformations may become preferable if there is a cation−anion interaction. In most of the ET salts, some disordering pattern is observed at room temperature because of the presence of both conformations. However, only the e conformation of ET exists in the radical cation salts: β-$(ET)_2IBr_2$,[34] θ-$(ET)_2I_3$,[26,27] and κ-$(ET)_2I_3$.[28] In the crystal structure of α'-$(ET)_2IBr_2$,[32,33] two of three independent ET molecules have an e conformation and the third one has a s conformation. This molecular feature of the ET donor may be a predominant reason for some specific physical properties of ET-based conductors.

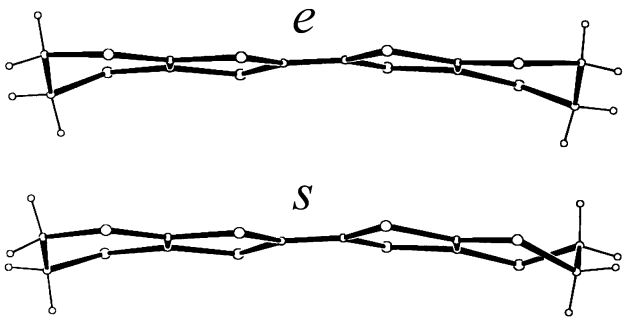

Figure 5. Two conformations of ET: eclipsed (e) and staggered (s).

Because the ET molecule is long and approximately flat, the resulting electronic properties will depend strongly on the way in which these molecules are arranged with respect to each other in the donor layer. The main arrangements are labeled as α, β, and θ phases, when the ET radical cation layers are formed by stacks, and κ phase, if the ET dimers are oriented approximately in an orthogonal manner (parts a−h of Figure 6).[20−22] The ET molecules in the adjacent stacks are parallel to each other in the β-type donor layer (parts a−c of Figure 6); in the α and θ phases, they are arranged at an angle to each other (parts d−f and g of Figure 6, respectively). Besides, more subtle changes are possible within a particular layer type: they can differ in a number of stacks in a repeating unit of lattice, mutual arrangement, and internal structure of a radical cation stack (overlapping mode for adjacent donors in stack and interplanar ET−ET distances). Thus, there are β', β'' and α', α''' phases (parts b and c and parts e and f of Figure 6, respectively). Specific features of structures and properties of particular radical cation salts of the $(ET)_2X$ family are considered in terms of this classification of donor layers.

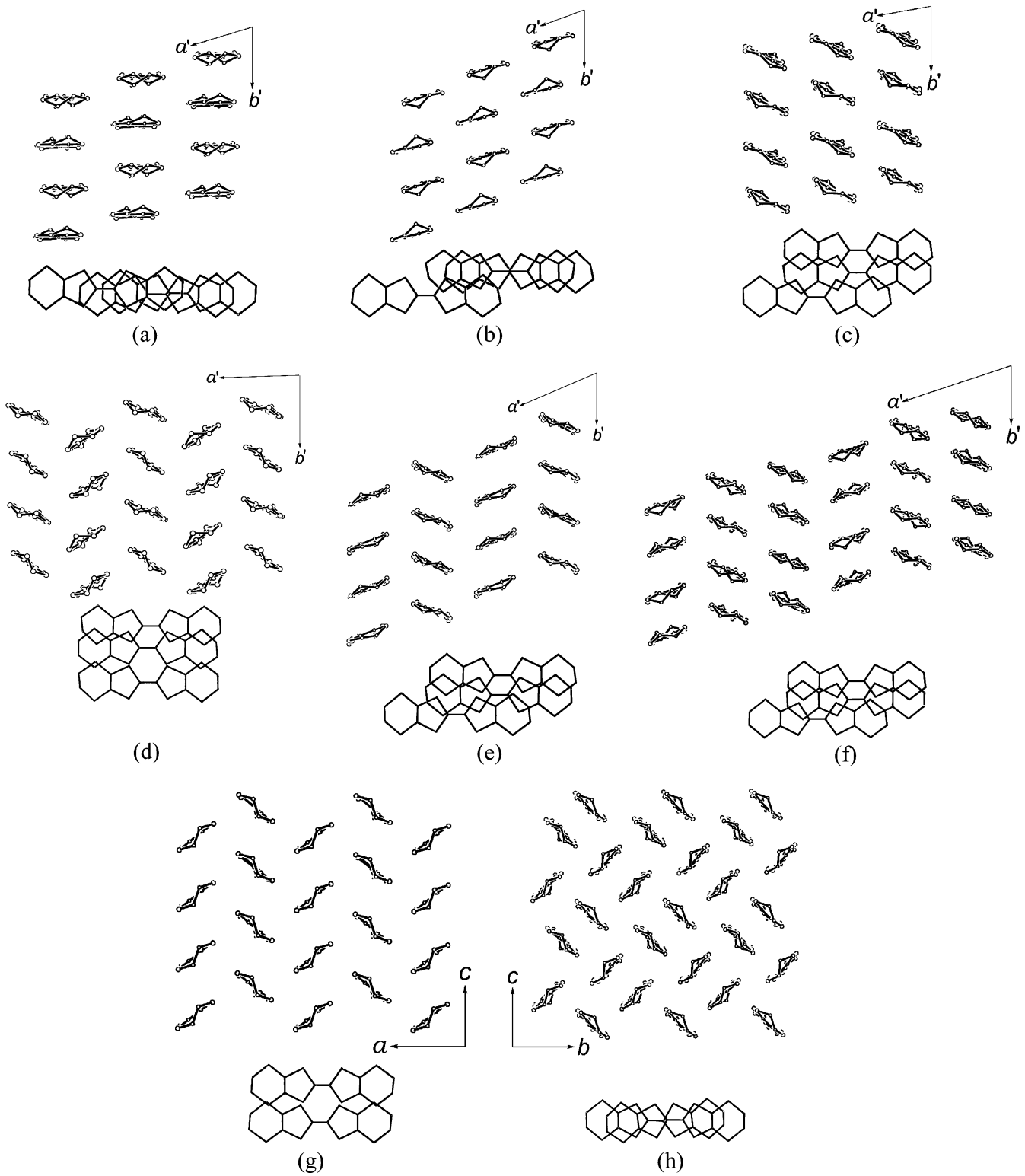

Figure 6. View of radical cation layers along the longer axis of ET and overlap modes in the stacks for β-$(ET)_2I_3$ (a), β'-$(ET)_2ICl_2$ (b), β''-$(ET)_2ICl_2$ (c), α-$(ET)_2I_3$ (d), α'-$(ET)_2IBr_2$ (e), α'''-$(ET)_2BrICl$ (f), θ-$(ET)_2I_3$ (g), and κ-$(ET)_2I_3$ (h).

2.3. Synthesis, Structure, and Properties of the Phases in the $(ET)_2X$ Family

2.3.1. α-$(ET)_2X$

The crystals of the $(ET)_2I_3$ α phase are prepared usually together with β-$(ET)_2I_3$ by electro-oxidation of ET in TCE, BN, CB, NB, or THF on the Pt anode in galvanostatic conditions with (n-$Bu_4N)I_3$, as an electrolyte.[9,10,46,47] The crystals of α and β phases look noticeably different; the α crystals look as either regular rhombuses or large thin shapeless plates, and the β crystals appear as needles, hexagons, and plates. Chemical oxidation of ET by an excess of (n-$Bu_4N)I_3$ in TCE at elevated temperature also affords crystals of the α and β phases,[12,48] while a microcrystalline powder of α-$(ET)_2I_3$ is formed in almost quantitative yield as a result of oxidation of ET with a stoichiometric amount of iodine in anhydrous CB at ambient temperature.[49]

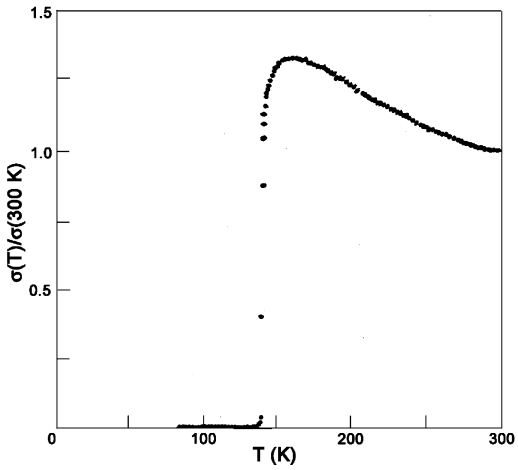

Figure 7. Temperature dependence of normalized conductivity for an α-$(ET)_2I_3$ single crystal.

The radical cation layers in the α phase, α of $(ET)_2I_3$, consist of two nonequivalent stacks with the ET molecules in each stack inclined at about 80° with respect to each other (α-type packing), and no inversion centers are located between the stacks (Figure 6d).[46,50] Under ambient pressure, α-$(ET)_2I_3$ undergoes a metal−insulator (M−I) phase transition at 135 K (Figure 7),[16,25] which can be suppressed by external pressure of >9 kbar.[51] For a long time, the origin of this M−I transition remained a problem to be clarified. Several experiments allow one to conclude that this M−I transition is of the first order and slight changes in the structure were observed in X-ray experiments.[52−54] Spin susceptibility of α-$(ET)_2I_3$ showed an abrupt drop at T_{M-I}, which indicated a nonmagnetic insulating state.[55] These results are close to the behavior of a band insulator. However, structural anomaly observed at the transition is not large enough to lead to any real gap opening. A calorimetric study suggested a purely electronic nature of this phase transition, because the magnitude of the entropy change is comparable to the phase transition from a metal to an antiferromagnetic insulator in quasi-1D conductors.[56,57] On the basis of this finding, a possible rearrangement of a charge distribution was proposed[56] at temperatures below T_{M-I}. Recently, the ^{13}C NMR measurements on a single crystal of α-$(ET)_2I_3$ have been made to clarify the origin of the M−I transition at 135 K.[17,58] Below T_{M-I}, the observed relaxation rate T_1^{-1} has two components. The temperature dependence of the spectra indicates the existence of two differently charged ET molecules. One of them is almost neutral, and the other one has a higher charge density. Above T_{M-I}, T_1^{-1} has only a single component, implying all molecules have a similar charge density.[58] Thus, the NMR experiments showed the transition to be associated with charge disproportionation in the ET layers, as it was predicted theoretically.[59,60] The Raman studies of α-$(ET)_2I_3$ also indicated the presence of the charge poor 0.5e−δ and charge rich 0.5e+δ ET molecules below T_{M-I}.[18,61] The deviation (δ) from average 0.5e on ET is 0.3. Above T_{M-I}, small deviations of δ = 0.05e from the uniform charge distribution were found.[61] However, it should be noted that there is a contradiction between the data of ^{13}C NMR and Raman spectroscopy, on one hand, and those of the X-ray analysis of α-$(ET)_2I_3$ crystals, on the other hand. The unit cell of α-$(ET)_2I_3$ contains three crystallographically independent ET molecules forming two nonequivalent stacks (I and II) alternating along the *a* direction (Figure 2b). The stack I consists of the molecules related by an inversion center, while the adjacent stack II is formed by two other centrosymmetric ET molecules, which are not parallel (a dihedral angle is 10.6°[47]). This particular packing of donor molecules opens the possibility of a different fractional charge on every ET molecule.[56] The analysis of the X-ray data[52,53] showed that below T_{M-I} bond lengths for all ETs are consistent with $\rho \approx +0.5$ on each cation, while at room temperature,[47,52] the charge state of the ET molecules from the stack II is closer to the neutral ones. Thus, according to the X-ray data, the charge distribution in α-$(ET)_2I_3$ below the metal−insulator transition is more uniform than at room temperature. This is in contrast to the ^{13}C NMR and Raman studies. The reason for the discrepancies between the results in evaluating the ET charge state remains not quite clear so far.

It was mentioned above that the M−I transition in α-$(ET)_2I_3$ is suppressed by pressure.[51] It was found that the temperature dependence of the resistance remains qualitatively similar at pressure between 15 and 20 kbar.[62,63] It is nearly constant between 300 and 1.5 K. Usually, temperature-independent resistivity is observed in dirty metals. However, the study of mobility and density of carriers revealed unique features of constant resistance in this system. It was found that carrier mobility increases by about 6 orders of magnitude up to $\sim 10^5$ $cm^2/(V\ sec)$ at low temperatures that compensates for a decreasing carrier density. This quasimetallic state is called a "narrow gap semiconducting" state.[62] The band gap is about 1 meV. The mechanism that gives rise to a correlated temperature dependence of carrier density and mobility has not been clarified yet. It should be noted that similar astonishing transport phenomena under high pressure have recently been observed in three more tri-iodides: α-$(BETS)_2I_3$, α-$(BEST)_2I_3$, and θ-$(ET)_2I_3$.[63] It was suggested that the works[62,63] conclusively clarified the nature of the high-pressure electronic state in α-$(ET)_2I_3$ crystals. However, the recent ^{13}C NMR studies of the narrow gap semiconducting state of α-$(ET)_2I_3$ under pressure showed that the temperature dependence of the relaxation rate seems to contradict with a rapid drop of the carrier density determined by Hall effect measurements at low temperatures.[64] This may require a serious reconsideration of the nature of high-pressure phases.

It should be mentioned that superconductivity has recently been found in α-$(ET)_2I_3$ at temperatures below 7 K under a moderate uniaxial strain along the *a* axis.[65]

In 1984, it was found that the α-phase crystals doped by iodine reveal a metallic behavior of resistance below the insulator phase transition at 135 K, followed by a transition to a superconducting state near 3.2 K.[25] However, superconductivity was not a bulk effect of the crystals. The X-ray analysis re-

vealed that the unit-cell parameters remain unchanged after doping by iodine. Although the appearance of superconductivity in the α crystals treated by iodine vapor was not clear, this result encouraged the study of the effect of heat treatment on conducting properties of the α phase. It was found that tempering the α-$(ET)_2I_3$ crystals resulted in a structural phase transition to the β phase, with $T_c \sim 6-8$ K.[66] The details of $\alpha \rightarrow \beta$ transformation are considered in section 2.3.2.1.

There is only one more α phase known among the ET-based salts with linear trihalide anions in addition to α-$(ET)_2I_3$. This is a ET salt with an unsymmetrical anion I_2Br, α-$(ET)_2I_2Br$, which is isostructural to α-$(ET)_2I_3$.[29] The single crystals of the salt were prepared by ET electro-oxidation in BN solution containing (n-Bu_4N)I_2Br as a supporting electrolyte. Room-temperature conductivity in the plane of the ET layers usually ranges between 2 and 10 Ω^{-1} cm^{-1}, with anisotropy in this plane ≤2, while in the direction perpendicular to the ab plane, the conductivity value is at least 1000 times smaller. The temperature dependence of conductivity shows that in the range between 245 and 300 K the crystal behaves as a 2D metallic conductor and a metal−insulator transition occurs at 245 K.[29] It should be noted that this salt has been studied poorly so far.

2.3.2. β-$(ET)_2X$; X = I_3, IBr_2, I_2Br, and $(IBr_2)_{0.7}(I_3)_{0.3}$

Four isostructural radical cation salts with X = I_3 (**2**), IBr_2 (**8**), I_2Br (**6**), and $(IBr_2)_{0.7}(I_3)_{0.3}$ (**9**) have the β-type conducting layers. The first single crystals (**2**) were grown by electro-oxidation of ET in BN using (n-Bu_4N)I_3 as a supporting electrolyte.[9,67] Conductivity measurements showed that the crystals retained a metallic behavior down to helium temperatures and underwent a superconducting transition at ambient pressure near 1.5 K (Figure 8). One of the criteria usually used to estimate perfection of metallic crystals is a ratio of the low-temperature residual resistance to the room-temperature one, $R_{4.2K}/R_{300K}$. This ratio is $(1-2) \times 10^{-3}$ for the most perfect crystals of β-$(ET)_2I_3$, obtained by electrocrystallization.[9,68] Later, the β crystals were also prepared by chemical oxidation of ET in different solvents (BN, NB, TCE, and CB) at elevated temperatures using I_2, (n-Bu_4N)I_3, (Et_4N)ClI_4, and (Et_4N)I_5 as oxidizers.[69] The oxidation of ET by I_2 in NB and BN at a reagent molar ratio of 1:0.5 and 1:1, respectively, yields β-$(ET)_2I_3$ crystals only, which grow as plates, needles, rulers, and bars (Figure 9). The ruler-shaped crystals are the most perfect ones, with $R_{4.2K}/R_{300K} = (1.4-1.5) \times 10^{-3}$, $T_c = 1.4$ K, and $\Delta T_c = 0.3$ K (curve 1 of Figure 10). For the plate- and bar-shaped crystals, some "steps" are usually observed on the $R(T)$ curves at temperatures near 7.5 K (curve 2 of Figure 10). These "steps" indicate the presence of a small volume fraction of a so-called high-T_c β_H-$(ET)_2I_3$ phase with $T_c = 7-8$ K (see section 2.3.2.1.). Recently, it has been reported on the synthesis of β phase with a 90% yield as a microcrystalline powder by the chemical oxidation of ET with a stoichiometric amount of iodine in THF, CB, or TCE at 85 °C (β_{CO}-$(ET)_2I_3$).[70,71] *Ac* susceptibility measurements of the β_{CO}-phase showed a T_c onset

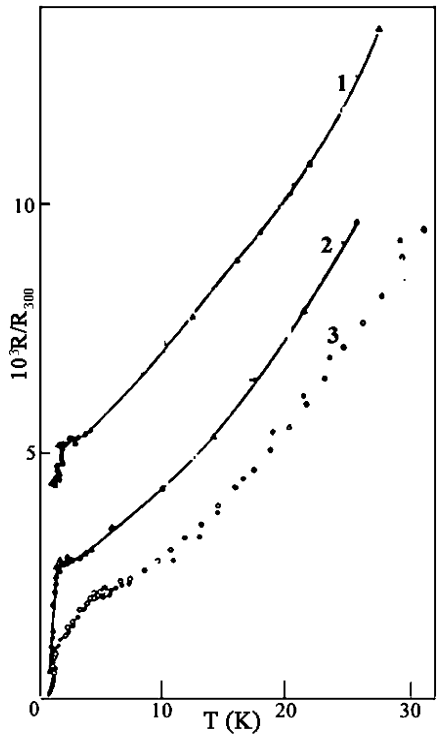

Figure 8. Temperature dependence of resistance for β-$(ET)_2I_3$ single crystals. (1 and 2) crystals as plates, and (3) two crystals as needles.

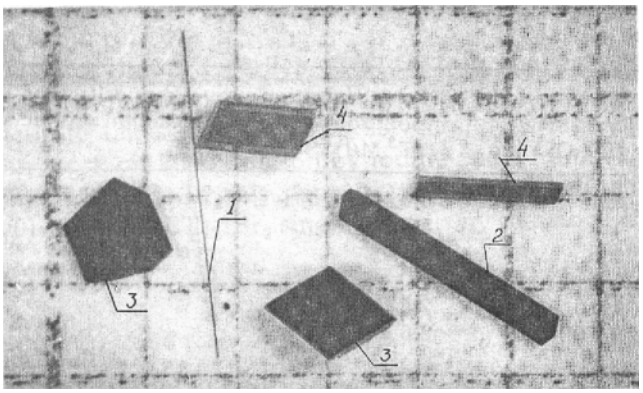

Figure 9. Photograph of β-$(ET)_2I_3$ crystals obtained using ET oxidation by iodine in BN (ET: I_2 = 1:0.5 and 1:1) or in NB (ET: I_2 = 1:0.5). (1) Needle, (2) ruler, (3) plates, and (4) bars. Cell 1 × 1 mm^2. Reprinted with permission from ref 69. Copyright 1989 Elsevier.

at 8 K followed by a broad transition and a second superconducting transition near 2 K.[71]

Single crystals of β-$(ET)_2IBr_2$ (**8**) and β-$(ET)_2I_2Br$ (**6**) were prepared by the electrochemical oxidation of ET in the presence of (n-Bu_4N)IBr_2 or (Et_4N)IBr_2 for the former[32,33] and (n-Bu_4N)I_2Br for the latter,[30,31] with THF or BN as the solvents. The crystals (**8**) were also obtained, together with those of the α′-$(ET)_2IBr_2$ phase by the chemical oxidation of ET in NB with a 5-fold molar excess of (Et_4N)IBr_2 or (n-Bu_4N)IBr_2.[69] The β-phase crystals have a ruler, plate, and bar shape, while those of the α′ phase grow only as rulers (Figure 11). The crystal shape is quite perfect, and the α′-phase crystals may be distinguished from the β-phase ones. All angles determining the shape of the β-phase crystals are obtuse, while one of the α′-phase crystal angles is acute and equal to ≈42° (Figure 11).

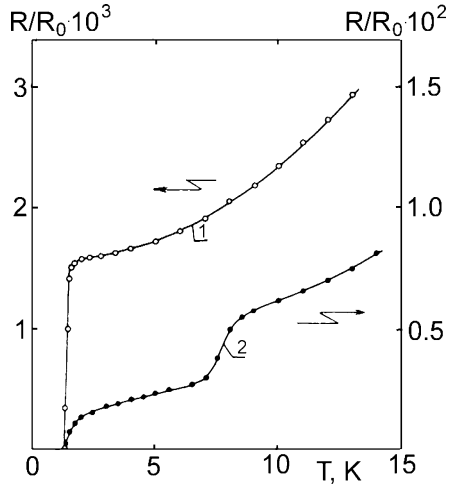

Figure 10. Typical curves of superconducting transition for β-$(ET)_2I_3$ crystals of different shapes grown in BN (see text). Reprinted with permission from ref 69. Copyright 1989 Elsevier.

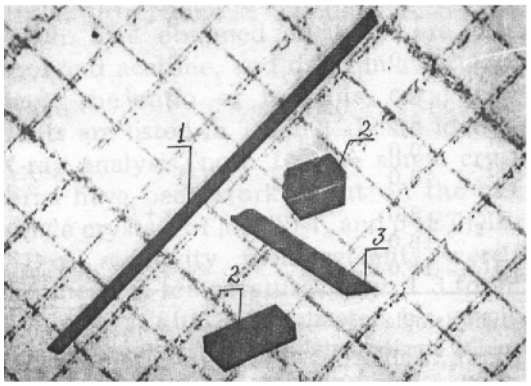

Figure 11. Photograph of β-$(ET)_2IBr_2$ (1−2) and α′-$(ET)_2IBr_2$ (3) crystals obtained using ET oxidation by $(Et_4N)IBr_2$ or $(n\text{-}Bu_4N)IBr_2$ in NB. (1 and 3) Rulers, and (2) plates. Reprinted with permission from ref 69. Copyright 1989 Elsevier.

The ruler-shaped crystals of β-$(ET)_2IBr_2$ obtained by chemical oxidation are the highest quality single crystals of organic superconductors known so far. The best crystals have $R_{4.2K}/R_{300K} = 2.5 \times 10^{-4}$, $T_c = 2.8$ K, and $\Delta T_c = 0.1$ K[69] (Figure 12).

The single crystals (**9**) were obtained by the chemical oxidation of ET with IBr in NB at the ratio ET/IBr = 1:0.5 and 1:1.[35] The composition of the β-$(ET)_2(IBr_2)_{0.7}(I_3)_{0.3}$ crystals was proposed from the X-ray analysis and EDX results.[35] However, the recent studies of low-frequency Raman spectra of these crystals revealed the presence of a ternary mixture of I_3, Br−I−Br, and I−I−Br anions.[72−74] The crystals of the β crystals containing another combination of trihalide anions (I_3 and I_2Cl) were obtained by the chemical oxidation of ET by ICl in NB solution.[74] It should also be noted that the data of Raman spectroscopy indicate the presence of the I_3 anion in addition to I_2Br in the crystals of β-$(ET)_2I_2Br$ obtained by electrocrystallization and chemical oxidation.[72]

Parts c and d of Figure 2 show two projections of the crystal structure (**2**). The ET radical cations are packed in the crystal face−face, which is typical for all quasi-1D organic metals. However, the radical cation stacks are not arranged along the shortest

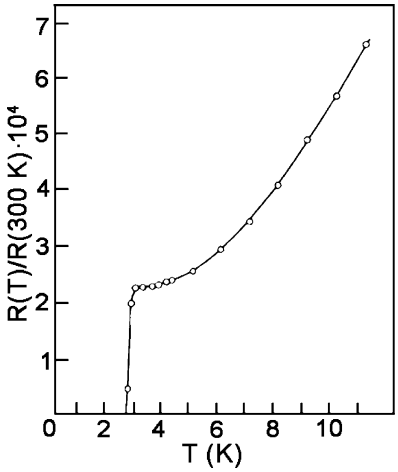

Figure 12. Typical curve of superconducting transition for ruler-shaped β-$(ET)_2IBr_2$ crystals grown in BN. Reprinted with permission from ref 69. Copyright 1989 Elsevier.

period of the crystal, $a = 6.609$ Å, but along $b' = 9.249$ Å (Table 2). It should be noted that all S···S distances in the stacks are much larger than the sum of the van der Waals radii of 3.70 Å. This gives rise to the minimum Coulomb repulsion between radical cations. The mutual arrangement of the cation radical stacks in the crystal is such that the layers are formed parallel to the *ab* plane, and the linear centrosymmetric anions I_3 are located in the channels between these layers. The projection of the ET radical cation layer along the longer ET molecular axis is shown in Figure 6a. It is evident that there is an appreciable coupling between the stacks, which is manifested by a specific orientation of the ET molecules (sulfur atoms from the neighboring stacks are oriented toward each other) and the presence of a number of slightly shortened S···S contacts in the range of 3.568−3.688 Å.

Under ambient conditions, the crystal structure β-$(ET)_2I_3$ is characterized by the presence of internal disorder caused by a random orientation of one of the terminal ethylene groups of the ET radical cation; the ET molecule exists in two approximately equally probable conformations, s and e ones (Figure 5). At ambient pressure, an incommensurate modulation of the structure resulting in almost sinusoidal displacements of ET molecules and tri-iodide ions as well as a variation of ethylene group configurations was observed below 175 K.[75] Whereas, the ET radical cations in **2** were completely ordered at room temperature under a pressure of 9.5 kbar[76] and had the s conformation.

Despite nearly identical structural features of the four strictly isostructural salts **2**, **8**, **6**, and **9**, their transport properties are different; β-$(ET)_2I_3$ (**2**) and β-$(ET)_2IBr_2$ (**8**) are ambient pressure organic superconductors, and β-$(ET)_2I_2Br$ (**6**) and β-$(ET)_2(IBr_2)_{0.7}(I_3)_{0.3}$ (**9**) have metallic properties without a transition to a superconducting state. It was found that down to 120 K no structural modulations occurred in the **8** crystals, in which the ethylene groups of ET were ordered and characterized by the e conformation.[30,33] The ET molecules in the **9** crystals were in two conformations of ethylene groups at a ratio of s/e =

0.26:0.74.[35] The complete ordering of the ethylene groups with the e conformation was observed at T = 130 K. Thus, the phase transition at 135 K observed by DSC can be interpreted as that of the order−disorder type.[35] Room-temperature conductivity of the **9** crystals along the ET layer was measured to be 5 Ω^{-1} cm^{-1}, while the mean value of conductivity in the direction perpendicular to the conducting layer is 500 times less. The temperature dependence of resistivity demonstrates the metal-like behavior within the range studied (1.3−293 K). The overall decrease of the resistance R_{295K}/R_{4K} was found to be ∼300−400, which is close to the residual resistance ratio for the β-$(ET)_2I_3$ crystals (about 500) and much less than that for β-$(ET)_2IBr_2$ (2000−3000).[69]

It could possibly be suggested that a low-temperature-specific feature of the transport properties and a lack of a superconducting transition are most likely related to the disorder in the $[(IBr_2)_{0.7}(I_3)_{0.3}]^-$ anion layer. The absence of superconductivity in the **6** crystals even under modest pressure also appears to be a result of the disordering in the unsymmetrical I_2Br^- anion.[30]

The value of room-temperature conductivity of **2** is about 30 Ω^{-1} cm^{-1}.[9] For the **2** crystals with T_c ∼ 1.5 K, the anisotropy of resistivity in the *ab* plane is ∼1.5−2, while in the orthogonal plane, this value is high enough and equal to 500.[77] Nearly the same values of the anisotropy of resistivity are characteristic of the β-$(ET)_2IBr_2$ crystals. The **2** crystals are also specified by strong anisotropy of upper critical magnetic fields, $H_{c2} \approx$ 20:20:1.[78,79]

2.3.2.1. β_L- and β_H-$(ET)_2I_3$. It is noteworthy that, among all organic superconductors known so far, β-$(ET)_2I_3$ is the most puzzling one, giving much to be thought about. At present, it is well-defined that the quasi-2D organic metal β-$(ET)_2I_3$ has two superconducting phases: β_L with T_c of 1.4−1.5 K[9] and β_H (or β^*) with T_c of 7−8 K.[12,80−82] Moreover, in some crystals there are typical pretransition phenomena observed as if notifying the presence of phases with the T_c values ranging from 1.5 to 8 K.[12,82] Some of these phases were really isolated. There are numerous experimental data obtained, which characterize the formation conditions for β_L and β_H phases.

While studying the effect of electrocrystallization conditions on conducting properties of the crystals, it was found that some crystals of β-$(ET)_2I_3$ exhibited the acceleration of the resistivity fall starting from ∼4 and/or ∼8 K (Figures 13 and 14).[12,82] The application of magnetic field suppressed this fall that indicated the existence of one and/or two more superconducting phases of $(ET)_2I_3$ with higher T_c. The behavior of the β-$(ET)_2I_3$ crystals under pressure was studied, and a drastic change in superconductivity was found, with the increase of T_c to 8 K at a low pressure (Figure 15).[80,81] The T−P phase diagram was investigated and it was established that the β-$(ET)_2I_3$ crystals can exist in two superconducting states: a low-temperature one (β_L) with T_c of 1.5 K under ambient pressure and a high-temperature one (β_H) with T_c of 8 K at $P \approx$ 400 bar.[83−86] The limits of stability of both phases were determined. The β_H phase can be retained at ambient pressure by cooling

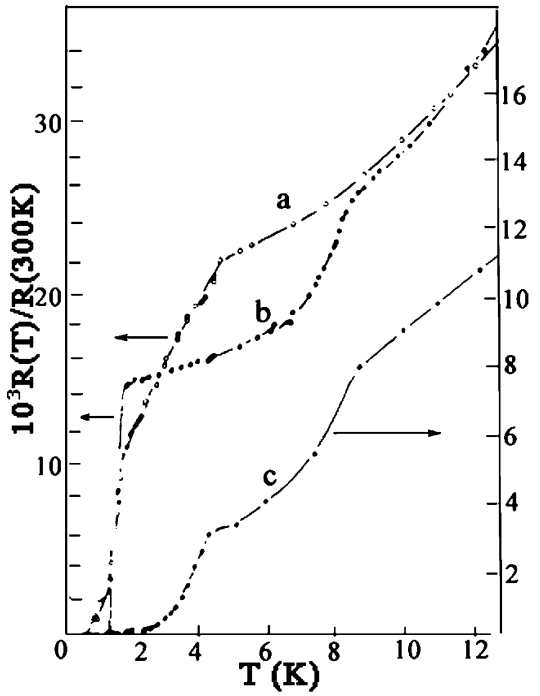

Figure 13. Examples of resistance behavior in β-$(ET)_2I_3$ crystals with acceleration (A) of resistance falling in the pretransitional temperature range. (a) A from ∼4 K; (b) A from ∼8 K; (c) A from ∼4 and 8 K.

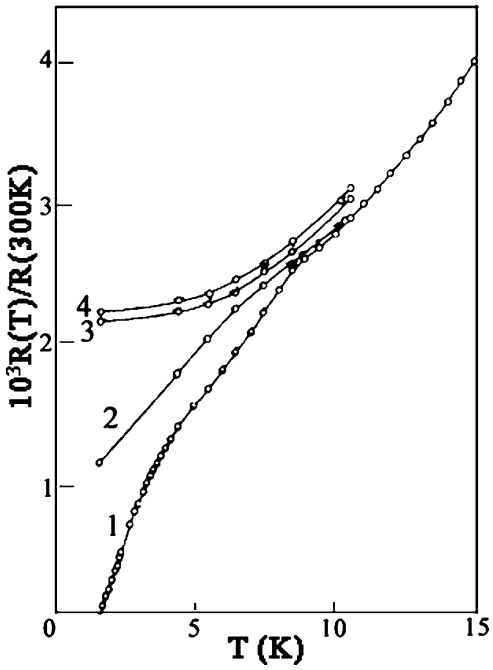

Figure 14. Temperature dependence of resistance of a crystal with a broad superconducting transition (from ∼8 K) in different magnetic fields. $H \parallel c$ = 1:0, 2:6, 3:34, and 4:50 kOe.

the sample under pressure (P > 400 bar) followed by the pressure release at low temperatures.[87,88] On such a treatment, the β_H phase exists at atmospheric pressure at T < 150 K, above which it converts to the β_L phase (Figure 16).[83−86] It was asserted in ref 89 that the high-T_c state in β-$(ET)_2I_3$ cannot be accessed by only hydrostatic pressure but requires, in addition, a substantial shear component. When pure hydrostatic pressure was applied to a sample

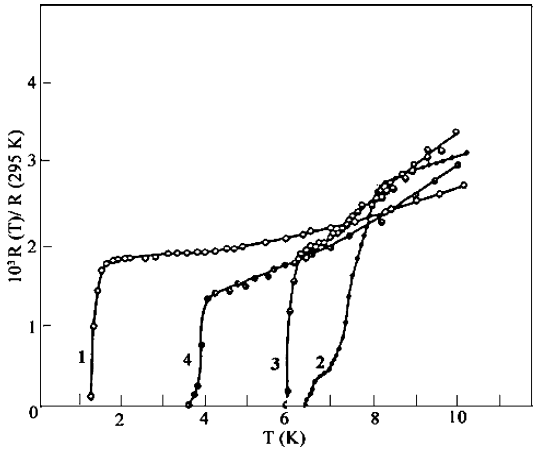

Figure 15. Pressure-induced displacement of superconducting transition in β-$(ET)_2I_3$: 1−1 bar, 2−1.2 kbar, 3−1.9 kbar, and 4−3.3 kbar.

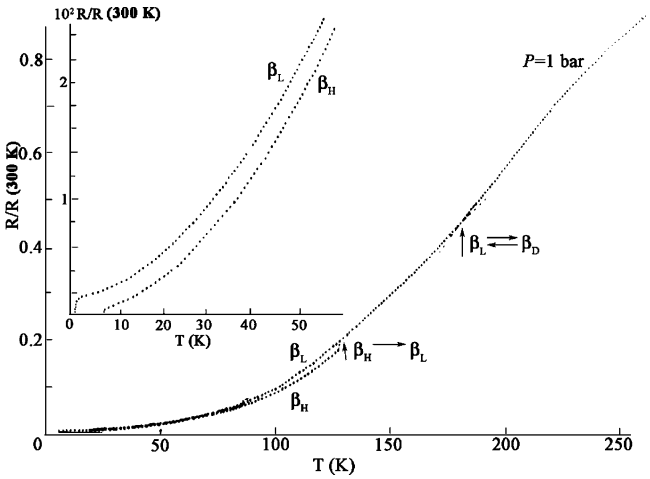

Figure 16. Temperature dependence of resistance along the *a* axis for β_L and β_H phases of $(ET)_2I_3$ at ambient pressure. Low-temperature portions of curves are shown in the inset.

through careful isobaric freezing of He,[4] a high-T_c state was not observed. On the other hand, fast freezing of liquid He^4 or solidification of pressure-transmitting liquid produces a shear component in pressure applied to the crystal, and under these conditions, the high-T_c state was produced.[89] No reasonable explanation has been found so far for the role of shear stress in superconductivity or the lattice modulation.

It was a great deal of interest and excitement to study the interplay between β_H and β_L states. Internal and external factors of the $\beta_L-\beta_H$ crossover in β-$(ET)_2I_3$ were extensively investigated to understand its nature. Thus, the key impulses were the observation of the phase transition in β-$(ET)_2I_3$ at $T \approx 175$ K under ambient pressure, resulting in incommensurate structure modulation,[75,90,91] and the X-ray study of β-$(ET)_2I_3$ at high pressure, which showed its structure to be completely ordered under pressure of 9.5 kbar.[76] Structural analysis utilizing a four-dimensional space group and complete (fundamental and satellite) reflection data collected at 120 K was carried out. It was found that structural modulation results in long-range ordering of one of the two ethylene groups in each ET molecule, which is

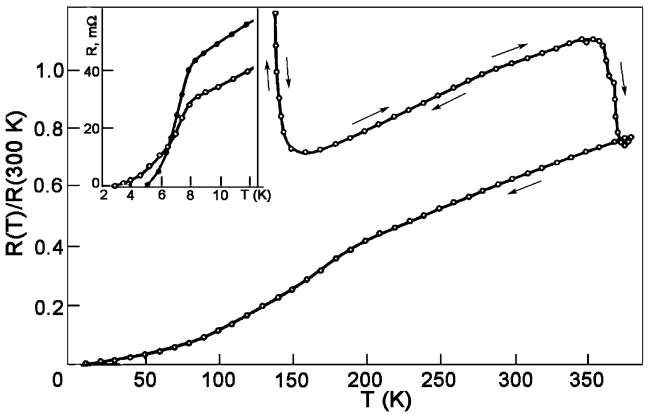

Figure 17. Temperature dependence of resistivity of an α-$(ET)_2I_3$ single crystal during the cooling−heating−cooling cycle accompanied by the transformation to the β phase. The inset shows a low-temperature portion of the curve in the range of the superconducting transition (○) and the superconducting transition in the sample of the β phase resulting from tempering of the α-$(ET)_2I_3$ crystal at 100 °C for 6 h (●).

otherwise disordered above the phase-transition point.[75,90] The origin of structural modulations appears to be the cation···anion (−CH_2···I) interactions. The ET molecules with disordered ethylene groups in the s and e conformations would involve unfavorable H···I contacts; a combination of two configurations in a modulated fashion is required to achieve a favorable packing arrangement in the crystal, provided complementary displacements of the ET molecules and I_3^- anions.[75,90] A neutron diffraction study of the β-$(ET)_2I_3$ crystals at 4.5 K and 1.5 kbar showed that they are completely ordered and have no modulated structure.[92]

A key question is that of the origin of a 5-fold increase of T_c in the β_H phase as compared to that in the β_L phase (8 versus 1.5 K). Such a large increase of T_c is not due to the changes in electronic density of states on transforming from β_L to β_H because, according to the magnetic susceptibility measurement data, electronic densities of states of the β_L and β_H phases differ not more than by 15−20%.[55,93,94] The difference in T_c of the β_L and β_H phases can be explained in terms of the suppression of superconductivity by a random scattering potential, which arises in the β_L phase because of an incommensurate structure-induced lattice distortion.[95,96]

Additionally to the pressure application discussed above, there are several physical and chemical methods known now to enhance T_c to ≈8 K in β-$(ET)_2I_3$. Some of them are considered in detail. It is known that tempering the α-$(ET)_2I_3$ crystals results in a structural phase transition to the β phase with $T_c \sim$ 6−8 K.[66,97,98] The X-ray control of the samples of the α phase after heating showed the presence of reflections characteristic of the β phase in Weissenberg photographs.[66] The transformation process is noticeably fast even at 70 °C and essentially accelerates with the temperature increase. For example, the time needed for the transformation at 80 °C amounts to 10−15 h and is equal to 5−6 h at 100 °C, somewhat varying depending on the sample. Figure 17 shows the temperature dependence of resistance for the α

crystal during a cooling−heating−cooling cycle accompanied by the transformation to the β phase. The features related to the $\alpha \rightarrow \beta$ transformation are manifested in the temperature dependence of resistance at $345 < T < 370$ K. A slow (~5 h) temperature increase in this range results in the appearance of a portion of essential (up to 40%) drop of resistance in the $R(T)$ curve for a crystal of the α phase, which is then replaced by a portion of the resistance growth. With the following cooling of the sample, one observes a monotonic decrease in its resistance, which is completed below 8 K by a rather broad superconducting transition (Figure 17). The study of the DSC spectra showed that the $\alpha \rightarrow \beta$ transition is accompanied by an endothermic effect (~8 J/g).

The highest critical temperature, $T_c \cong 7$ K, determined from the midpoint of a superconducting transition was reported in ref 66 for the crystals heated at 100 °C for 6 h (inset in Figure 17). Later on, more prolonged tempering α crystals (for several days) at lower temperature (75 °C) allowed one to prepare β crystals with a sharp superconducting transition at 8 K.[97] The transition was completed by 6.5 K, and its onset temperature lied near 9 K. The β-$(ET)_2I_3$ samples obtained by a thermal treatment of the α phase are usually denoted as α_t-$(ET)_2I_3$.[97] It should be noted that they exhibit a superconducting transition near 8 K even on pressed pellets. The X-ray analysis of the α_t crystals showed that they are twinned and mosaic ones. Although no detailed crystal structure of the α_t samples is available so far, the similarities of the T_c values, the unit-cell dimensions, and the symmetrical stretching modes of the I_3^- ions in the Raman spectra[97,98] strongly suggest that β_H-$(ET)_2I_3$ and α_t-$(ET)_2I_3$ are probably very similar in structure. The emergence of 8 K superconductivity in the tempered crystals indicates that the β_H-$(ET)_2I_3$-like structure retains in them to low temperatures without adopting incommensurate lattice modulation. The suppression of the latter one is probably associated with local strains equivalent to external pressure, which arise in the crystals under their solid-state conversion upon heating. In this context, it should be noted that the inhomogeneous compression of the β crystals with low T_c (~1.5 K) at 50 kbar and room temperature followed by pressure release gives rise to 8 K superconductivity at ambient pressure[99] (see below).

The $\alpha \rightarrow \beta$ transformation was successfully used for the preparation of superconducting composite films containing a network of oriented nanocrystals of β-$(ET)_2I_3$ in a surface layer of an inert polymer matrix.[100,101] Additionally, to the α phase, some dielectric ET polyiodides are also transformed upon heating to β-$(ET)_2I_3$ with T_c near 7−8 K. The conversions of the ET polyiodides to the β phase are considered in the next section.

The effect of plastic deformation on T_c of the β crystals was studied at uniaxial (along the a axis) and isotropic but nonhydrostatic compression to pressures of several ten kbar at $T \approx 295$ and 78 K.[99] Isotropic nonhydrostatic compression was performed in high-pressure chambers of either "piston-cylinder" or "toroid" type in conditions when the pressure-transmitting liquid solidifies either upon cooling to 78 K or as a result of the generation of high enough pressure (~50−60 kbar) at room temperature. After pressure was fully released, the samples in the chamber were heated to room temperature, the crystals were drawn out and washed off, and the temperature dependence of conductivity was measured. Such a deformation was found to be accompanied by the appearance of a surface-striped structure characteristic of twinning (Figure 18) with different orientation and stripe density depending on the conditions of twinning. The presence of twins was justified by the X-ray analysis. The β-$(ET)_2I_3$ crystals turned out to be easily deformed by twinning remaining undestroyed at both room and low temperature. However, one did not observe twinning in the β-$(ET)_2IBr_2$ and β-$(ET)_2AuBr_2$ crystals upon uniaxial compression up to high enough pressure values resulting even in sample destruction.[99] The twins in these crystals with a characteristic striped structure formed only at low temperature (≈78 K) as a result of pressure application.

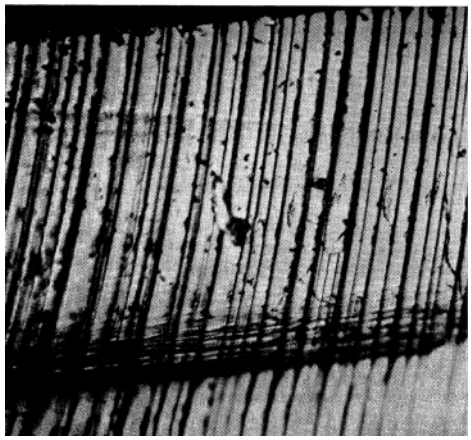

Figure 18. Photograph of the ab plane of the β-$(ET)_2I_3$ crystal deformed by uniaxial compression along the a axis at $T = 295$ K.

Figure 19 shows typical curves of a transition to a superconducting state for the β-$(ET)_2I_3$ crystals before and after various treatments with nonuniform pressure.[99] It is seen that, for the sample manifesting a conventional superconducting transition in an initial state at $T_c \approx 1.3$ K (curve 1), a step appears near 6−7 K after uniaxial compression (curve 2). With the sample saturation by twins, the step is more pronounced and shifts to higher temperatures, and the share of the β_L phase decreases (curve 3). Finally, high-pressure (≈50 kbar) deformation affords samples with a very high concentration of twins differently oriented and undergoing a full superconducting transition at $T_c \approx 8$ K (curve 4). It should be noted that a 2D character of properties of the β-$(ET)_2I_3$ crystals retains upon twinning, $H_{c2}^{(b')} \approx H_{c2}^{(a')} \gg H_{c2}^{(c^*)}$. For the crystal deformed under pressure of ~50 kbar, the values of $(dH_{c2}/dT)_{T_c}$ are equal to 20 and 2.7 kOe/K for the b′ and c* directions, respectively,[99] and close to similar characteristics of the β_H phase.[102] Thus, one could suggest that a drastic increase in a transition temperature from 1.3 to ≈8 K in deformed β-$(ET)_2I_3$ crystals is due to the appearance and stabilization of the β_H phase as a result

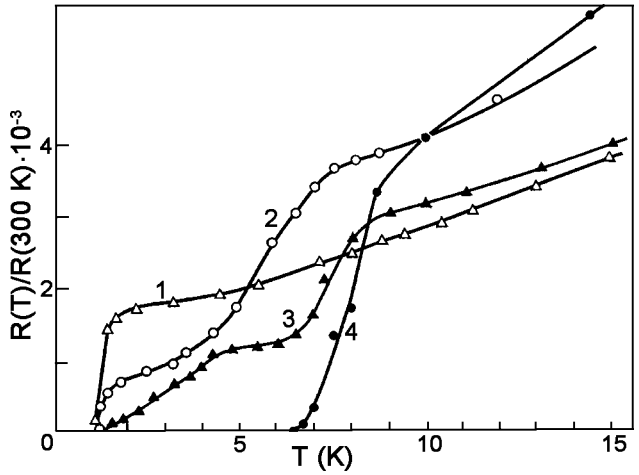

Figure 19. Superconducting transition curves for starting and deformed samples of β-$(ET)_2I_3$. (1) Starting sample; (2) sample after uniaxial compression at 295 K; (3) sample after inhomogeneous deformation at $P = 15$ kbar and $T = 78$ K; and (4) sample after inhomogeneous deformation at $P = 50$ kbar and $T = 295$ K.

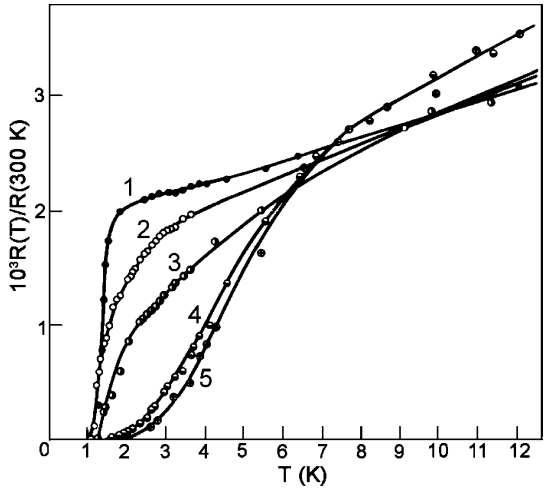

Figure 20. Curves of superconducting transitions of the same β-$(ET)_2I_3$ crystal obtained in five cycles (1−5) of cooling−heating.

of local strains occurring at plastic deformations. In this context, it should be noted that only $P \approx 500$ bar is enough to provide the formation of the β_H phase with $T_c \approx 7.5$ K.[87] As to the effect of twinning on T_c, the increase of T_c is 20−30% for the β-$(ET)_2IBr_2$ and β-$(ET)_2AuBr_2$ crystals because of the formation of twins,[99] as it was observed in Nb.[103] Mechanical twins appearing at deformation even in the β_H phase result in the increase in the temperature of the onset of a superconducting transition of the β_H phase from 8 to ~9 K.[99]

A series of works reported on the study of effects of temperature cycling and annealing on T_c of the β phase.[12,78,82] The curves of superconducting transitions obtained on the same single crystal during the five cycles of cooling are shown in Figure 20.[78] The sample was heated to room temperature between two successive experiments. It is seen that after each cooling cycle T_c grows from 1.3 K in the first cycle to 4.5 K (a midpoint) in the fifth one, a superconducting transition being observed starting from ~7 K.[78] Note, however, that such a behavior is not intrinsic to all

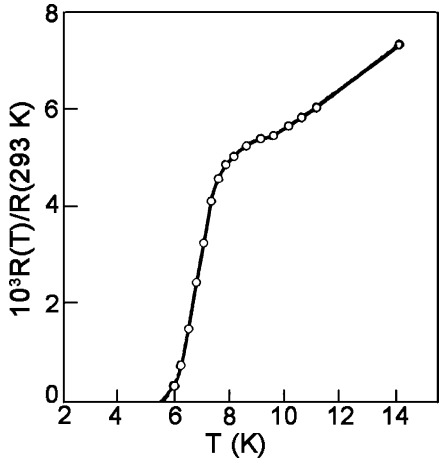

Figure 21. Superconducting transition in the β_H-$(ET)_2I_3$ crystal prepared by electro-oxidation of ET in NB in the presence of $(n\text{-}Bu_4N)I_3$, KSCN, CuSCN, and 18-crown-6.

crystals of the β phase. The resistance of many of them does not change greatly with temperature cycling. The cycling of the crystals with two superconducting transitions in the combinations 1.5 K + 4 K, 1.5 K + 7 K, and 4 K +7 K (Figure 13) gives rises to a considerable growth of the 7.5 K phase.[12,82] The β crystals annealed at 100−120 K at ambient pressure for 20−40 h exhibit two superconducting transitions at 2 and 7.5 K.[104−107] The authors suggested that the 2 K phase is different from the β_L phase with $T_c = 1.5$ K. During an X-ray diffraction study of the structure in relation to the $P-T$ phase diagram, it was found[105,107] that the wave vector of incommensurate superstructure changes from $Q_0 =$ (0.075, 0.275, and 0.205)[91,108] to $Q' =$ (0.067, 0.248, and 0.187) when the sample is kept at 100−120 K and ambient pressure for a long time, e.g., 24 h. The change in the wave vector was considered to be due to the repositioning of the ethylene groups in the ET molecules.

Besides the application of special temperature−pressure procedures, the following techniques turned out to be successful to prepare the crystals of β-$(ET)_2I_3$ with $T_c > 1.5$ K: (i) doping via a cation part by introducing ET derivatives, e.g., PT and MET, into the reaction of electrocrystallization;[109,110] and (ii) doping via an anion part using supporting mixed $(n\text{-}Bu_4N)I_3 + KSCN + Cu(SCN)_2 +$ 18-crown-6 electrolyte in TCE or NB.[111] The resulting β crystals exhibited superconducting transitions with $T_c \approx 4.6$ and 6.5 K (Figure 21), respectively. Note, however, that X-ray structural studies of the salt synthesized in the condition of MET doping gave no direct evidence for the presence of the MET donor, but they showed that the phase possessed the prototype structure of the perfectly ordered β_H-$(ET)_2I_3$ phase, the only difference being a slight (~2%) disorder in the I_3^- anions.

Now there are numerous experimental data on the elevated temperatures of superconducting transition in β-$(ET)_2I_3$. However, the question of a more than 5-fold increase in T_c of β-$(ET)_2I_3$ remains open because of the lack of detailed structural information. Nevertheless, we made an attempt to analyze scarce experimental structural data available at present.

Table 3. Main Crystal Data for β-$(ET)_2I_3$ (Space Group = $P\bar{1}$, and $Z = 1$) at Different T and P Conditions

	P = 1 bar				P = 1 bar					P = 1.5 kbar	P = 9.5 kbar
parameters	T = 293 K	T = 293 K	T = 293 K	T = 293 K	T = 200 K	T = 125 K	T = 120 K	T = 20 K	T = 4.5 K	T = 4.5 K	T = 293 K
β_{T_c}[a]	$\beta_{1.5}$	$\beta_{6.5}$	$\beta_{2\text{ and }8}$	$\beta_{4.6}$	$\beta_{2\text{ and }8}$	$\beta_{4.6}$	$\beta_{1.5}$	$\beta_{1.5}$	$\beta_{1.5}$	$\beta_{1.5}$	$\beta_{1.5}$
a (Å)	6.609(1)	6.609(1)	6.613(2)	6.600(2)	6.585(2)	6.503(2)	6.561(1)	6.543(2)	6.519(2)	6.449(3)	6.392(4)
b (Å)	9.083(1)	9.092(1)	9.092(2)	9.090(3)	9.038(2)	9.064(2)	9.013(2)	8.968(3)	8.920(6)	8.986(4)	8.897(3)
c (Å)	15.267(2)	15.273(2)	15.270(3)	15.268(5)	15.205(2)	15.113(4)	15.173(3)	15.114(7)	15.052(15)	15.034(1)	15.020(6)
α (Å)	94.37(2)	94.37(2)	94.42(1)	94.33(2)	94.90(1)	94.51(2)	95.07(2)	95.34(3)	95.32(8)	94.79(4)	94.26(4)
β (Å)	95.62(2)	95.56(2)	95.54(1)	95.57(3)	95.74(1)	96.28(2)	95.93(2)	96.05(3)	96.09(6)	96.57(3)	96.85(9)
γ (Å)	109.78(2)	109.76(2)	109.75(1)	109.76(2)	110.00(1)	110.93(2)	110.28(2)	110.30(3)	110.44(4)	111.29(3)	111.07(3)
V (Å^3)	852.2(2)	853.8(2)	852.9(4)	852.1(5)	839.1	820.4(4)	829.2(3)	819.1(8)	807.6(16)	799.1(9)	785.0(6)
s/e	0.5:0.5	0.43:0.57	0.43:0.57	0.5:0.5	0.50:0.50	1.0:0.0	0.56:0.44			1.0:0.0	1.0:0.0
modulation						no	yes	yes	yes	no	
reference	10, 113	this paper	112	110	112	110	75	92	92	92	76

[a] T_c (K) is given for the *as grown* crystals.

Table 4. Shortened S···S Contacts ($r \leq 3.70$ Å) between ET Radical Cations in the Structure β-$(ET)_2I_3$ at Different Conditions

	P = 1 bar		P = 1 bar		P = 1.5 kbar	P = 9.5 kbar
contact[a]	T = 293 K	T = 293 K	T = 200 K	T = 120 K	T = 4.5 K	T = 293 K
β_{T_c}[b]	$\beta_{1.5}$	$\beta_{6.5}$	$\beta_{2\text{ and }8}$	$\beta_{1.5}$	$\beta_{1.5}$	$\beta_{1.5}$
A	3.620	3.628	3.582	3.547	3.480	3.442
B	3.602	3.599	3.571	3.533	3.420	3.411
C	3.648	3.650	3.611	3.578	3.526	3.438
D	3.568	3.570	3.558	3.553	3.538	3.489
E	3.594	3.595	3.573	3.550	3.451	3.415
F	3.589	3.593	3.565	3.552	3.548	3.489
G	3.689	3.691	3.643	3.626	3.610	3.560
H					3.671	3.606
a				3.695	3.646	3.700
b					3.640	3.668
c					3.643	3.630

[a] A−H = interstack contacts, and a−c = intrastack contacts (see Figure 22). [b] T_c (K) is given for the *as grown* crystal.

It should be noted that in the case of β_{CO}-$(ET)_2I_3$ obtained by chemical oxidation[70,71,112] synchrotron radiation diffraction data were collected at 293, 200, 130, 100, and 35 K on a microscopic single crystal (a powder grain) of the compound. As it is evidenced from *ac* susceptibility and *dc* magnetization measurements, the compound exhibits two superconducting transitions near 2 and 8 K, respectively ($\beta_{2\text{ and }8}$). The compound was found to be slightly iodine-deficient and better described as β-$(ET)_2I_{3-x}$ (x = 0.014), and the authors[70,71,112] yielded to temptation to consider anion deficiency as a possible reason for enhanced T_c. In this context, note that in the case of $\beta_{6.5}$[111] and $\beta_{4.6}$[110] the occupancy of the anion sites was refined and no deviation from ideal stoichiometry was found.

Table 3 shows the main crystallographic parameters for the β-$(ET)_2I_3$ crystals with different T_c values under different conditions. Table 4 shows the changes in shortened S···S contacts under certain conditions. These contacts are marked by dashed and dotted lines in Figure 22.

Actually, the analysis of the structural data listed in Tables 3 and 4 provides the possibility to compare the structure of organic metal β-$(ET)_2I_3$ for its different phases, including the superconducting state.

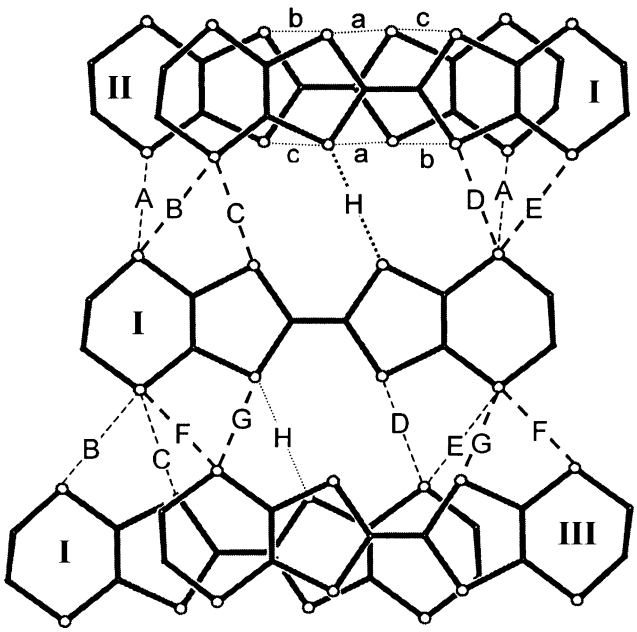

Figure 22. Intermolecular overlaps and short S···S contacts of ET in β-$(ET)_2I_3$.

Thus, the X-ray data obtained at T = 4.5 K and P = 1.5 kbar correspond to the structure of β-$(ET)_2I_3$ in the superconducting state. Although the starting β-$(ET)_2I_3$ crystal had T_c = 1.5 K, it converted to the β_H phase after cooling to 4.5 K under a pressure of 1.5 kbar.[92] T_c of such a β_H phase was estimated to be ~6 K, taking into account the T_c−pressure dependences.[89] Thus, the structure of an organic conductor was determined below the superconducting transition point.

Under ambient conditions, all β-$(ET)_2I_3$ crystals have the same unit-cell parameters and are characterized by the presence of internal disorder caused by a random orientation of one of the terminal ethylene groups of the ET radical cation. ET exists in the crystal with two approximately equally probable conformations, s/e = 0.5:0.5 or 0.43:0.57. The ordering of the ethylene groups at ambient pressure occurs at the temperature decrease, probably resulting in the modulated structure at $T \sim 175$ K.[75] However, in this case, ET again exists in the crystal in two conformations, s and e, both at 125 and 4.5 K.

Table 5. Conditions of Synthesis of Different Phases in the System ET−I

conditions of crystallization	ratio of reagents ET/I_2							
	benzonitryl					nitrobenzene		
ET/I_2	1:0.5	1:1	1:2	1:5	1:10	1:0.5	1:1	1:2
$T = 80$ °C		η	η			β		
20 °C < T < 80 °C	β	β	η	ζ	ζ	β	$\epsilon + \eta$	ζ
V^a= 0.5°/h								
20 °C < T < 80 °C	β	β	ϵ	ζ	ζ	β	$\epsilon + \eta$	ζ
V^a= 1.5°/h								

[a] V = the rate of cooling.

Upon cooling the β_{CO} crystals to 130 K and lower, about 60% of the ethylene groups adopt a staggered conformation, thus providing evidence for a temperature-induced, partial-ordering process.[71] The sets collected at $T \leq 130$ K, exhibited weak diffraction spots, which could not be indexed by the average unit cell but could be fitted exactly with the Q vector of an incommensurate modulated structure in single crystals of β-$(ET)_2I_3$.[91] Disordered β-$(ET)_2I_3$ phase ($T_c \approx 2$ K) with modulated structure and ordered β_H-$(ET)_2I_3$ phase ($T_c \approx 8$ K) probably coexist in β_{2-8}-$(ET)_2I_3$.

The pressure application leads to the complete positional ordering of the ethylene groups and, hence, to the only s conformation in ET. Such a structure is typical for β-$(ET)_2I_3$ at $P = 9.5$ kbar ($T = 293$ K) and $P = 1.5$ kbar ($T = 4.5$ K) (Table 3). However, it was shown that at 125 K the modulated structure is not present in β_H with $T_c = 4.6$ K and all ET molecules in the crystal have a s conformation, typical for high pressure. The question arises as to the structural differences in the β crystals with $T_c \cong 4.6$, 6.5, and 8 K. There has been no unambiguous answer to this question so far.

A comparison of the interstack S···S contacts of $\beta_{1.5}$-$(ET)_2I_3$ and $\beta_{6.5}$-$(ET)_2I_3$ (ambient conditions) with those of β_H ($T = 4.5$ K and $P = 1.5$ kbar) (Table 4 and Figure 22) reveals a significant shortening upon cooling and compression only for A, B, C, and E ($\Delta = -0.140$, -0.182, -0.122, and -0.143 Å, respectively), whereas all other S···S contacts decrease significantly less. Moreover, one observes shortened intrastack $a-c$ contacts. Depending on the mode of adjacent ET molecules overlapping in radical cation stacks in β-$(ET)_2I_3$ (Figure 22), the stacks are divided into pairs with different overlapping modes inside, I−II, and between the pairs, I−III (Figure 22). Thus, below the point of the phase transition, the interaction between the stacks in a radical cation layer becomes stronger in β_H and dimerization in the stack increases as well. Nevertheless, these structural changes should be considered as natural and subtle ones. The structural data together with the $T-P$ phase diagram of β-$(ET)_2I_3$[86] indicate that the main difference between the β_L and β_H phases is directly related to whether the lattice is modulated incommensurately. The pressure application and different ways of deformations as well as chemical doping promoting the appearance of local tension similar to the pressure effect suppress a superstructural transition.

2.3.2.2. Polyiodides of ET as Precursors of β_H-$(ET)_2I_3$. During the study of the effect of the ET/I_2 ratio, solvent nature, and crystallization conditions

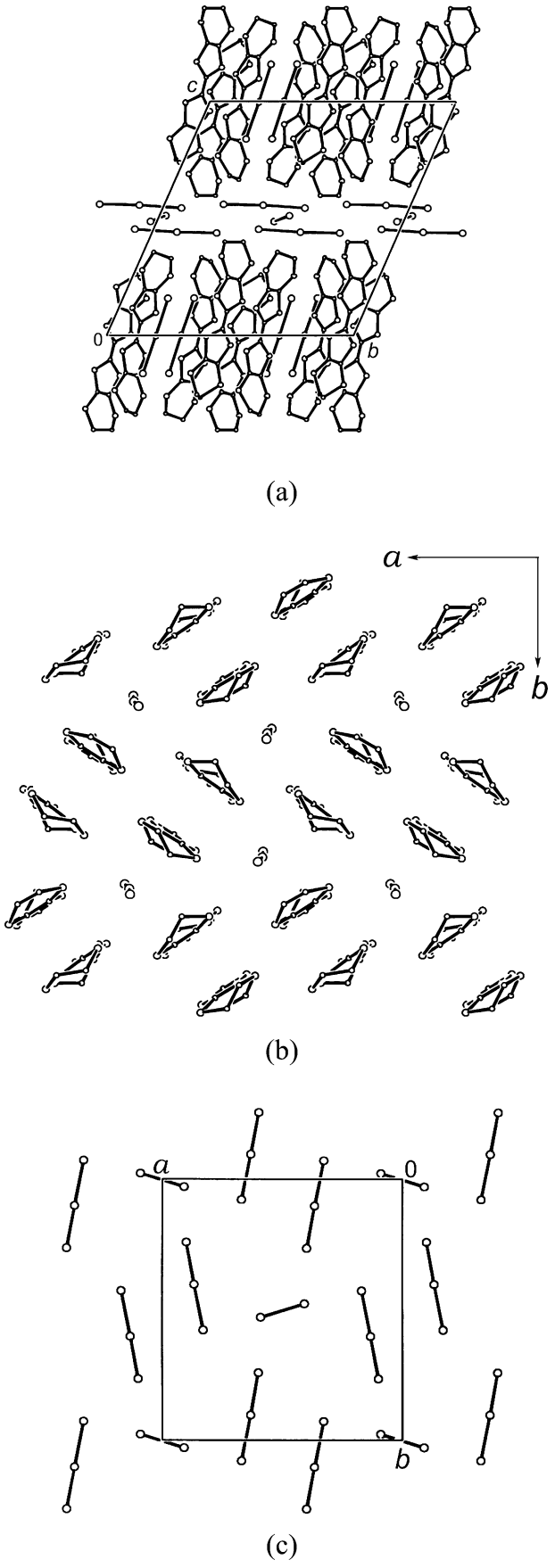

Figure 23. ϵ-$(ET)_2I_7$. (a) Projection of crystal structure along the a direction. (b) View of complex cation−anion layer along the long molecular axis of ET. (c) Projection of anion layer along the c direction.

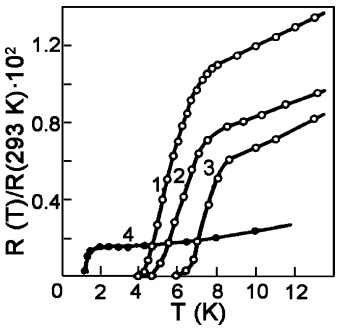

Figure 24. Examples of superconducting transitions in the β-$(ET)_2I_3$ crystals obtained at different conditions of the $\epsilon \rightarrow \beta$ conversion (1−3). Superconducting transition in the crystal $\beta_{1.5}$ (4) is showed for comparison.

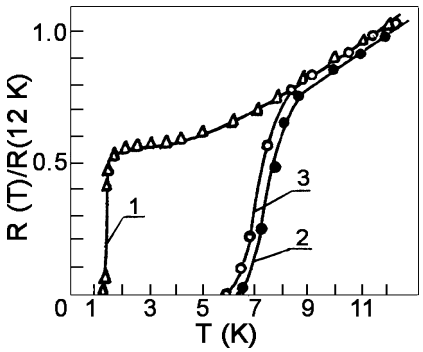

Figure 25. Curves of superconducting transitions of the β crystals, obtained by electrocrystallization (1) and solid-state transformation of $\epsilon \rightarrow \beta_H$ (2) and $\zeta \rightarrow \beta_H$ (3).

on the yield and phase composition of reaction products, four new ET polyiodides in addition to the α and β phase were found: ϵ-$(ET)_2I_7$, η-$(ET)I_3$, ζ-$(ET)_2I_{10}$, and η'-$(ET)_2(I_3)(I_5)$.[69,114,115] The conditions for the formation of the ϵ, η, and ζ phases are given in Table 5. All of these phases were identified by the X-ray structural analysis.[115−118] The structure of the ϵ phase is characterized by the presence of mixed cation−anion layers of the $(ET)_2I_3$ composition, which are separated by anion sheets consisting of flat z-shaped I_8^{2-} anions[116] (parts a−c of Figure 23). The crystals of the ζ phase are built of strongly dimerized ET stacks and complex I_{10}^{2-} anions ($I_8^{2-} + I_2$).[118] The structure of the η phase is composed of ET stacks separated by I_3^- anions.[117] In addition to the ET tri- and polyiodides considered above, two more salts were found in the ET−I system: δ-$(ET)I_3(TCE)_{0.333}$[119] and $(ET)I_3C_{60}$.[120] The former salt was synthesized by electrocrystallization in TCE at high current density (~65 μA/cm^2), and the latter one was prepared by the oxidation of ET by iodine in the presence of C_{60}.

The ϵ, η, and ζ phases have low room-temperature conductivity (~10^{-4} Ω^{-1} cm^{-1}) and are semiconductors. However, upon heating (50−90 °C), the ϵ and ζ phases easily lose a part of iodine and transform to the β phase of $(ET)_2I_3$ with T_c near 7−8 K.[114,121,122] It should be noted that the conversion of these phases to the β phase is accompanied not only by iodine loss but also the change in the ET charge state, namely, by the reduction of a part of cations because the ET charge in ϵ and ζ phases is equal to +1, while it is +0.5 in the β phase. ET^+ is likely reduced by the I^- anion formed as a product of the decomposition of the I_3^- anion in the process of solid-phase transformations. This suggestion is supported by the fact that ET does not form salts with I^- anion in contrast to I_3^-.

The $\epsilon \rightarrow \beta$ conversion was monitored by observing X-ray diffraction on a single crystal of the ϵ phase during the process of heat treatment.[121] Integral intensities of 14 strong reflections of the ϵ phase were measured at room temperature at the end of each cycle of crystal heating at 70 °C for 1.5−2 h. After heating for 5.5 h, the intensity of reflections became ~20 times lower, and their halfwidth increased from 0.22° to 1.24°. Crystal orientation therefore remained almost unchanged. After heating for 8.5 h, reflections of the ϵ phase were not registered and new reflections were observed. All of them were attributed to reflections of the β phase, assuming the crystal to be a twin with a 2-fold axis, which coincides with the 2_1 axis of the starting ϵ phase. The volume ratio for two domains in a twin was equal to 3:2. The twin plane is (001) and coincides with the (001) plane of the starting ϵ phase. Orientation of the a_1, b_1, and c_1 and a_2, b_2, and c_2 axes of unit cells of the resulting β phase with respect to the a, b, and c axes of the unit cell of the ϵ phase is defined by the following ratios:

$$a_1 = 0.339a + 0.263b + 0.004c$$
$$a_2 = 0.339a - 0.263b - 0.004c$$
$$b_1 = 0.583a - 0.114b + 0.002c$$
$$b_2 = 0.583a + 0.114b - 0.002c$$
$$c_1 = 0.017a + 0.229b - 0.872c$$
$$c_2 = 0.017a - 0.229b + 0.872c$$

A small number of reflections and their broadening (halfwidth is ~5°) are evidence of the formation of low perfect mosaic crystals as a result of $\epsilon \rightarrow \beta$ conversion. The averaged value of room-temperature conductivity of these crystals is 15 ± 5 Ω^{-1} cm^{-1}, i.e., a bit lower than that of β crystals with T_c = 1.5 K (~30 Ω^{-1} cm^{-1}), and the drop of resistance down to 10 K is characterized by the values $R_{300}/R_{10} \approx 150-200$ rather than 350−460.

It should be noted that the width of a superconducting transition is essentially dependent on the temperature and time of $\epsilon \rightarrow \beta$ conversion. However, the transition almost always starts at 8−8.5 K (Figure 24). When thermolysis conditions of ϵ and ζ phases were varied, the superconducting β-$(ET)_2I_3$ crystals with the value of T_c = 7.5 K (determined from the midpoint of the curves 2 and 3 of Figure 25) were obtained.[114,121] By 6 K, the superconducting transitions are complete and resistivity is zero within the experimental possibilities. The *ac* susceptibility measurements showed superconductivity in the β crystals obtained by $\epsilon \rightarrow \beta$ conversion to be a bulk effect.[123] The thermolized crystals manifest specific 2D anisotropy of the upper critical fields H_{c2}, at which $H_{c2}^{(a)} \approx H_{c2}^{(b^*)} > H_{c2}^{(c^*)}$ (Figure 26). The values of the derivative $(dH_{c2}/dT)_{T_c}$ in the a, b^*, and c^* directions are equal to 27.5, 25, and 3.4 kOe/K, respectively.[121] The transition temperature and the values of $(dH_{c2}/dT)_{T_c}$ for crystals are very close to the similar characteristics for the β_H state existing in β-$(ET)_2I_3$

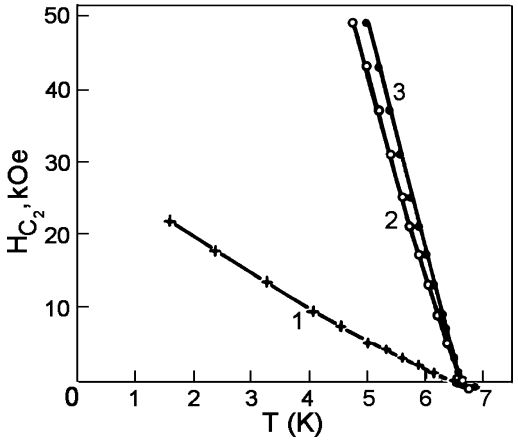

Figure 26. Temperature dependence of upper critical fields $H_{c2}{}^{a}$, $H_{c2}{}^{b*}$, and $H_{c2}{}^{c*}$ for one of the β_H-$(ET)_2I_3$ crystals prepared by $\epsilon \rightarrow \beta$ conversion. (●) $H \parallel a$, (○) $H \parallel b^*$, and (×) $H \parallel c^*$.

under pressure. According to measurements reported in ref 102, $(dH_{c2}{}^{(c^*)}/dT)_{T_c} = 2.9$ kOe/K and $(dH_{c2}{}^{(a)}/dT)_{T_c} = 33$ kOe/K for the β_H state at $P = 1.6$ kbar.

The weight loss of the sample on $\epsilon \rightarrow \beta$ conversion accounts for ~30% because of iodine evolution. The thermal vacuum treatment of ϵ crystals at different temperatures indicated thermolysis to be complete at 70−90 °C ($\Delta m/m_0 \sim 30\%$).[114] However, with the further temperature increase (≥100 °C), the weight loss is again observed because of a partial decomposition of the resulting β phase. The β crystals with $T_c = 7.5$ K can be obtained by thermolysis of ET polyiodides only if the rate of the β-phase formation is much higher than that of its decomposition. The optimal conditions for $\epsilon \rightarrow \beta$ and $\zeta \rightarrow \beta$ conversions are as follows: $70 < t < 90$ °C, the duration of the process is 100 h, and $50 < t < 80$ °C, for 70 h, respectively.[114] Under other conditions, superconducting transitions in crystals are broadened and complete only at 1−2 K. It was reported at the initial stage of investigations of ϵ crystals that they undergo a superconducting transition near 2.5 K at ambient pressure.[11,93] Actually, the ϵ crystals are dielectrics, and the appearance of superconductivity is a result of the insertion of the β phase formed either at partial loss of iodine upon storage or during vacuum sputtering of gold contacts on the crystals for conductivity measurements.

Unlike the ϵ and ζ phases, the η phase is more thermally stable and begins to lose iodine extensively at $T \geq 130$ °C. The β crystals obtained by the $\eta \rightarrow \beta$ conversion have broad superconducting transitions with $T_c = 3-4$ K.[114]

The β-$(ET)_2I_3$ samples obtained by thermal treatment of the ET polyiodides are usually denoted as β^* or β_t-$(ET)_2I_3$. As in the case of α_t crystals obtained as a result of $\alpha \rightarrow \beta$ phase transition, the X-ray analysis of the β_t crystals showed that they are twinned and mosaic ones. Although no detailed crystal structures of the β_t samples are available, the similarities of the T_c values and the values and anisotropy of the upper critical fields as well as the unit-cell parameters strongly suggest that the β_t state is probably very similar to the β_H state of $(ET)_2I_3$, which usually arises under pressure. As it is known, the increase of T_c up to 8 K in a high-pressure phase is due to a suppression of incommensurate structure modulation in the β crystals.[86,96] It was shown[99] that internal strains can stabilize the β_H state in the β-$(ET)_2I_3$ crystals at ambient pressure. The occurrence of the β_H state in thermolized crystals is probably associated with internal strains arising in crystals during the $\epsilon \rightarrow \beta$ and $\zeta \rightarrow \beta$ conversions.

2.3.3. α′-(ET)$_2$X

This type of conductor involves the following radical cation salts: α′-$(ET)_2IBr_2$ (**7**),[32,33,34] α′-$(ET)_2BrICl$ (**12**),[41] and α′-$(ET)_2Br_{1.3}I_{1.1}Cl_{0.6}$.[42,124] Single (**7**) crystals were formed together with single (**8**) crystals (Table 1) as a result of electrocrystallization of ET in THF with supporting electrolyte $(n\text{-}Bu_4N)IBr_2$ or in BN with $(Et_4N)IBr_2$.[32,34] The crystals were also prepared by chemical oxidation of ET in NB with a 5-fold excess of $(Et_4N)IBr_2$.[125] The α′-$(ET)_2BrICl$ crystals were described in ref 41 as those comprising the linear BrICl anion. In reality, they probably contain a mixture of three anions: IBr_2, ICl_2, and BrICl, similar to that shown for the β′ phase of $(ET)_2BrICl$.[36] Recently, it has been reported on the preparation of the α′ phase with $(ET)_2Br_{1.3}I_{1.1}Cl_{0.6}$ composition, containing a set of four trihalide anions: nonpolar $(Br-I-Br)^-$ and $(Cl-I-Cl)^-$ and polar $(Br-I-I)^-$ and $(Br-I-Cl)^-$ anions, which was justified by X-ray analysis and energy dispersion X-ray (EDX) and Raman spectroscopy.[42,124] These α′ crystals were formed as black plates together with those of the α‴ phase of the same composition upon chemical oxidation of ET in NB by $(n\text{-}Bu_4N)Br_{0.6}I_{1.4}Cl$ at elevated temperatures. The initial tetrabuthylammonium salt was obtained by addition of IBr to a solution of $(n\text{-}Bu_4N)Cl$ in ethanol at a reagent ratio of 1:0.5.[42] Composition of the anion in this salt was established by EDX. It was determined from the Raman spectra that the anion consists of the IBr_2^-, I_2Br^-, $BrICl^-$, and ICl_2^- trihalide anions. In contrast to chemical oxidation, only single crystals of the α′ phase were obtained when the room-temperature electrocrystallization method, employing $(n\text{-}Bu_4N)Br_{0.6}I_{1.4}Cl$ as an electrolyte and nitrobenzene as a solvent, was used.

The crystal structure of α′-$(ET)_2IBr_2$ is characterized by layers of radical cations and anions alternately along the c direction (Figure 2e).[33] The radical cation layers (Figure 2f) contain two crystallographically nonequivalent stacks, and a dihedral angle between the planes of ET from neighboring stacks is 48°; i.e., on the whole, the layer is formed by nonparallel molecules. The overlapping of adjacent radical cations in the stacks (Figure 6e) differs from that in α-$(ET)_2I_3$ (Figure 6d), in which there is only a transverse displacement of the radical cations relative to one another.

The value of room-temperature conductivity of crystals (**7**) along the a direction is equal to ~1 Ω^{-1} cm^{-1} and has a semiconducting behavior with $E_a = 0.25$ eV.[32]

It was found that the α′-$(ET)_2IBr_2$ crystals could be prepared by applying high pressure to the β-$(ET)_2IBr_2$ crystals[125] (Figure 27). The resulting α′ phase remains unchanged under ambient conditions

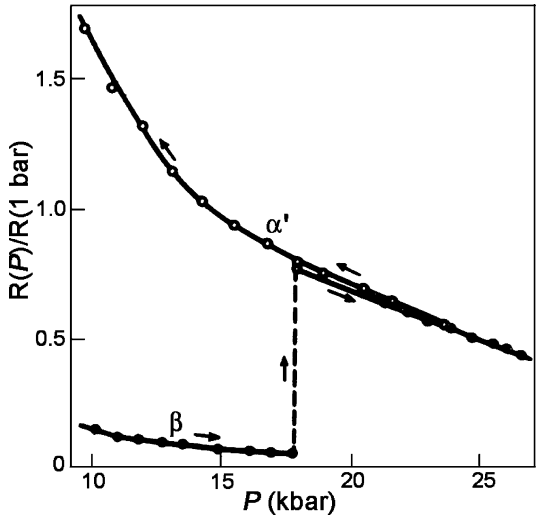

Figure 27. Pressure dependence of resistivity near the $\beta \rightarrow \alpha'$ phase transition in $(ET)_2IBr_2$.

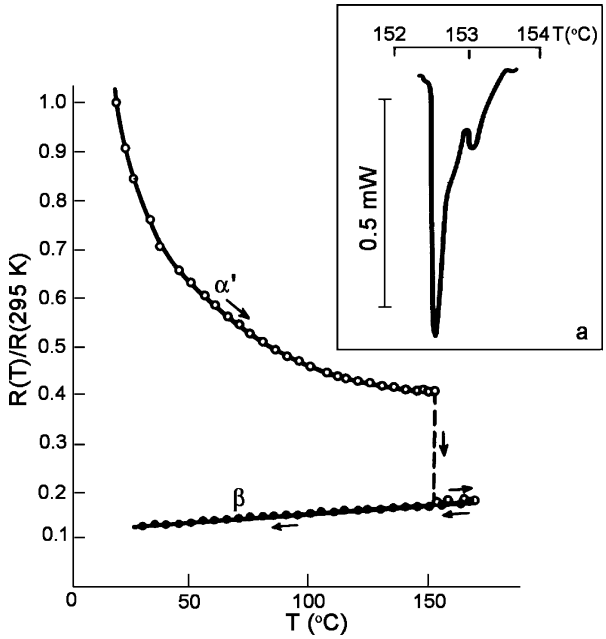

Figure 28. Temperature dependence of resistivity near the $\alpha' \rightarrow \beta$ phase transition in $(ET)_2IBr_2$. (a) Thermogram of the $\alpha' \rightarrow \beta$ phase transition.

for an infinitely long time. To transform the crystals back from the α' to the β phase, one should heat them up to 153−155 °C at ambient pressure[125,126] (Figure 28). It is seen that there is a reverse jump of resistance, and a semiconducting temperature dependence of resistance changes to a metallic one. The β crystals are still close enough to perfect after such a phase transition: $R_{295K}/R_{3.5K} \approx 1000$, $T_c \approx 2.8$ K to $\Delta T_c \approx 0.5$ K. These crystals afford X-ray photographs rich in well-pronounced reflections, which were not observed in the case of the $\alpha \rightarrow \beta$ transition for the β-$(ET)_2I_3$ crystals.[66] The reversible $\alpha \rightleftharpoons \beta$ phase transitions have a giant hysteresis that allows either a superconducting β or semiconducting α' phase to remain in a metastable state under ambient conditions for an infinitely long time (the field of a stable existence of the α' phase is at high pressures and that of the β phase is at $T \geq 155$ °C). The $\alpha' \rightarrow \beta$ phase transition is accompanied by heat absorption; latent heat $\Delta H \approx 0.5 \pm 1$ J/g is an order of magnitude lower than that for the $\alpha \rightarrow \beta$ transition in $(ET)_2I_3$.[66] Moreover, in contrast to $(ET)_2I_3$, the $\alpha' \rightarrow \beta$ conversion in $(ET)_2IBr_2$ is very drastic and seems to have a martensite character. The reverse $\beta \rightarrow \alpha'$ conversion manifests a similar behavior. The value of a bulk effect of the $\beta \rightleftharpoons \alpha'$ transition in $(ET)_2IBr_2$ calculated from the X-ray data is $\Delta V/V_0 \approx 0.5\%$, while $\Delta V/V_0 \approx 0.8\%$ for the $\alpha \rightarrow \beta$ transition in $(ET)_2I_3$.

It should be noted that in a structure of cation and anion layers the α' and β phases of $(ET)_2IBr_2$ are closer to each other than the α and β phases of $(ET)_2I_3$ (parts e, a and c, a of Figure 2, respectively). On the $\beta \rightarrow \alpha'$ transition, the period a becomes almost twice as much, the direction of cation stacks [110] with a period of 8.777 Å turns the direction $b = 8.898$ Å (Table 1), and the adjacent stacks become nonequivalent. All IBr_2^- anions are parallel in the anion layers of both α' and β phases. Such similarities cannot be found by comparing the structures of the α and β phases of $(ET)_2I_3$. Thus, it is possible to use them to interpret the fact that β-$(ET)_2IBr_2$ can transform to α'-$(ET)_2IBr_2$ at high pressure, and upon heating, α' transforms to β with a lower bulk effect and latent heat is an order of magnitude lower than that for the $\alpha \rightarrow \beta$ transition in $(ET)_2I_3$.[66] Because of this reason, one does not observe the $\beta \rightarrow \alpha$ transition in $(ET)_2I_3$ under high pressure; even the pressure of up to 60 kbar does not result in the formation of the α phase but stabilizes the β_H phase with $T_c \approx 8$ K.[99]

For α'-$(ET)_2BrICl$ (**12**),[41] which is isostructural to α'-$(ET)_2IBr_2$, the following feature should be noted. Although linear $(BrICl)^-$ anions occupy general positions in crystal, similar to IBr_2^- anions in crystals (**7**), and in principle could have an ordered structure, thermal parameters of the Br and Cl anions indicate the existence of orientational disorder. The structure was refined with varying an atomic population of these atoms. The ratio of the preferred orientation to the inverted orientation is about 0.65:0.35, and the mean bond length of I−Br and I−Cl is 2.65 Å, which is shorter than the I−Br length in β-$(ET)_2IBr_2$ (2.70 Å)[34] but longer than the I−Cl distance in β'-$(ET)_2ICl_2$ (2.57 Å).[36−38] We noted above the possibility of a mixture of ICl_2^-, IBr_2^-, and $BrICl^-$ anions in α'-$(ET)_2$-BrICl that may explain the existence of orientational disorder in this salt. Similar disorder takes place in the salt α'-$(ET)_2Br_{1.3}I_{1.1}Cl_{0.6}$ containing a combination of four trihalide anions.[42,124] It is interesting to note that this salt undergoes a structural phase transition to α'''-$(ET)_2Br_{1.3}I_{1.1}Cl_{0.6}$ polymorph upon heating[124] (see section 2.3.6), unlike α'-$(ET)_2IBr_2$, which transforms to β-$(ET)_2IBr_2$ upon heating.

2.3.4. β'-$(ET)_2X$

The first ET trihalide salts with β' packing of the radical cation layer, β'-$(ET)_2ICl_2$ (**10**) and β'-$(ET)_2BrICl$ (**13**), were obtained by electrocrystallization in THF with supporting electrolyte $(n\text{-}Bu_4N)ICl_2$ or $(n\text{-}Bu_4N)$-BrICl, respectively.[36−38] To characterize the $(BrICl)^-$ anion in **13**, the IR and Raman spectra of polycrystalline samples of initial electrolyte $(n\text{-}Bu_4N)BrICl$ were analyzed. It was found that $(n\text{-}Bu_4N)BrICl$ contains both IBr_2^- and ICl_2^-. Consequently, β'-

$(ET)_2BrICl$ used in the X-ray analysis may contain a mixture of the three IBr_2^-, ICl_2^-, and $BrICl^-$ anions.[36] Recently, two new β'-ET trihalides containing the different sets of various trihalide anions have been synthesized, β'-$(ET)_2Br_{0.5}I_{1.0}Cl_{1.5}$ and β'-$(ET)_2I_{1.1}Cl_{1.9}$.[74,127] The former salt in the shape of needles is formed together with its β'' polymorph (plates) on chemical oxidation of ET in NB solution by a large excess of tetramethylammonium trihalide $(Me_4N)Br_{0.5}I_{1.0}Cl_{1.5}$ containing a mixture of IBr_2^-, $BrICl^-$, and ICl_2^- anions. The latter salt was obtained, together with β-$(ET)_2I_{2.3}Cl_{0.7}$ and β''-$(ET)_2I_{1.2}Cl_{1.8}$ phases, by oxidation of ET with ICl in NB. Composition of the anions and the character of trihalide particles in these salts were established by EDX and Raman spectroscopy.[74,127]

The crystal packing motif (parts g and h of Figure 2) of the isostructural ET salts with small anions ICl_2^- and $BrICl^-$ is significantly different from that of the isostructural salts **2**, **6**, **8**, and **9** with large anions (parts a and b of Figure 2). According to the overlapping modes in the stacks (parts a and b of Figure 6), the ET molecule pairs of β'-type salts are significantly more dimerized than those of β-type salts. As a consequence, short interstack S···S contacts in β'-type salts were found only along the crystallographic a axis, in contrast to β-type salts, which contain short S···S contacts more or less uniformly in the ab plane. Unlike the β-type salts with a 2D electronic structure, anisotropy of the intermolecular overlap integrals of HOMO of ET in β' suggests the 1D character of the electronic structure.[37] Low-temperature X-ray study of the **10** and **13** single crystals showed that there is complete ordering of ET molecules with e conformation of the ethylene groups.[36]

In the β'-$(ET)_2ICl_2$ salt, some phase transition was observed by ESR at $T \sim 22$ K. Axial rotation photographs of the X-ray diffraction about the a, b, and c axes at $T \sim 15$ K (i.e., at a temperature below its phase transition) revealed no evidence of superlattice formation.[36] Later,[128] this phase transition was interpreted as a transition from the Mott insulator to antiferromagnetic ordering below $T_N = 22$ K. Recently, some surprising results have been reported.[14] It was demonstrated that an organic Mott insulator, β'-$(ET)_2ICl_2$, was metallized under extremely high pressure and became a superconductor with the maximum $T_c = 14.2$ K at 8.2 GPa.

2.3.5. β''-$(ET)_2ICl_2$

The β''-$(ET)_2ICl_2$ crystals (**11**) were prepared by the electrochemical oxidation of ET in THF with $(Et_4N)ICl_2$ as a supporting electrolyte.[39] This salt also forms on a slow cooling of BN solution of ET and $(Et_4N)ICl_2$ taken at a 1:2 molar ratio from 78 °C to room temperature. The β''-$(ET)_2ICl_2$ crystals also grew in both electrochemical and chemical syntheses. Parts i and j of Figure 2 show the projections of the crystal structure of **11** along the a and c directions. The projection of a radical cation layer along the longer axis of the ET molecule is shown in Figure 6c. The radical cation layer is formed by equivalent ET stacks with interplanar ET−ET distances of 3.85 and 3.59 Å. All S···S distances inside the stack are longer than interstack distances and are not less than the sum of the van der Waals radii (3.70 Å). However, there is a number of shortened S···S contacts between the stacks within the 3.335−3.660 Å range. The ET molecule occupies a general position. There is a certain positional disordering of one of the ethylene groups of ET, which is justified by high thermal parameters of corresponding carbon atoms. The linear ICl_2 anions are located in the centers of symmetry, an interatomic I−Cl distance is 2.536(3) Å. It was shown above that linear I_3, I_2Br, and IBr_2 anions are close in size and form isostructural radical cation salts with ET. The conducting layer is the β-type layer (parts c and d of Figure 2). However, the use of essentially the smaller ICl_2^- anion (Table 6) results in noticeable structural changes: (1) significantly decreased cell volume, with the period a being strongly shorter; and (2) the changes in the overlapping mode for adjacent ET molecules in a stack. In contrast to the β-type radical cation layer in which adjacent ET molecules are only longitudinally shifted with respect to each other (Figure 6a), there is a longitudinal-transverse shift in the β''-type radical cation layer (Figure 6c) as it is observed in the α'-type radical cation salts (Figure 6e).

Table 6. Crystal Phases in the $(ET)_2X$ System

X phase	I_3	I_2Br	IBr_2	BrICl	ICl_2
anion lengths (Å)	10.1	9.7	9.4	9.0	8.7
κ	+	−	−	−	−
θ	+	−	−	−	−
α	+	+	−	−	−
β	+	+	+	−	−
α'	−	−	+	+	−
α'''	−	−	−	+	−
β'	−	−	−	+	+
β''	−	−	−	−	+

The conductivity of crystals (**11**) along the a axis, $\sigma_{293K} \sim 3 \times 10^{2-3}$ Ω^{-1} cm^{-1},[39,40] is an order of magnitude higher than that of the β-$(ET)_2I_3$ crystals. The temperature dependence of conductivity shows a metallic behavior; however, no superconducting transition is observed down to 1.3 K. It should be noted that the value of room-temperature conductivity of the β''-$(ET)_2ICl_2$ crystals is close to that of the β-$(ET)_2I_3$ crystals at a pressure of ~8 kbar,[80] possibly because of a strong shortening of interstack S···S contacts: 3.335−3.660 Å in β''-$(ET)_2ICl_2$ and 3.411−3.606 Å in β-$(ET)_2I_3$ at $P = 9.5$ kbar,[76] as compared to 3.568−3.689 Å in β-$(ET)_2I_3$ at ambient pressure.[10,113] The ESR spectrum of **11** exhibited a Dysonian line. The intensity of spin susceptibility abruptly decreased at 17 K, although electrical resistivity and the Bragg diffraction intensity showed no discontinuous changes, indicating the occurrence of a magnetic phase transition.[40]

Additionally to β''-$(ET)_2ICl_2$, the β''-type packing of a cation layer was also found in some ET trihalides containing a mixture of various trihalide anions: β''-$(ET)_2Br_{0.5}I_{1.0}Cl_{1.5}$ and β''-$(ET)_2I_{1.2}Cl_{1.8}$, which were mentioned in section 2.3.4. The room-temperature conductivity of these β'' salts in the ab plane is ~1 order of magnitude less than that of β''-$(ET)_2ICl_2$. Their temperature dependence of the resistance is

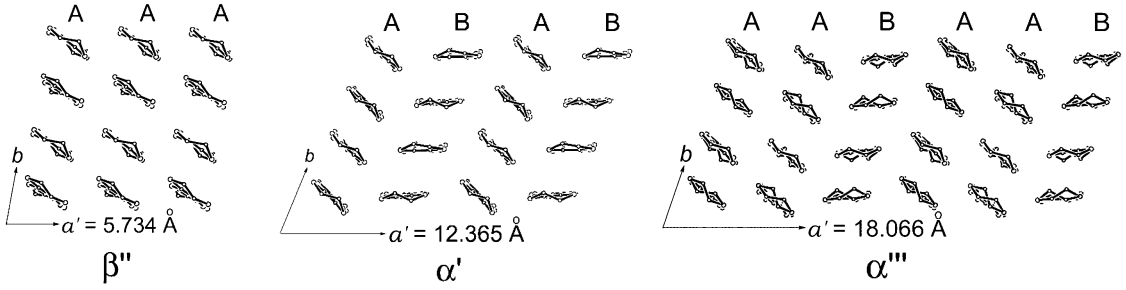

Figure 29. Genealogy of the β'', α', α''' structures. View along the molecular long axis. Crystallographic axes are depicted for a new choice of the unit cells (Table 2). Courtesy of S. S. Khasanov.

metal-like within the 15−300 K temperature range. Below 10 K, the resistance slightly increases, most likely resulting from a localization of carriers, which can be provoked at low temperature by the disorder in the anion layers.[74,127] The X-ray analysis of β''-$(ET)_2Br_{0.5}I_{1.0}Cl_{1.5}$ crystals also revealed the existence of disorder in the ET layers associated with both terminal ethylene groups and one of the S atoms located in the six-membered rings of ET. It should be noted that localization of carriers was not observed for β''-$(ET)_2ICl_2$ down to 1.5 K.[38]

2.3.6. α'''-$(ET)_2BrICl$

The crystals of the α''' phase were synthesized by the chemical oxidation of ET with $(n\text{-}Bu_4N)Br_{0.6}I_{1.4}Cl$, containing a combination of the I_2Br^-, IBr_2^-, $BrICl^-$, and ICl_2^- anions.[42,124] In the synthesis the crystals of the α''' phase crystallized together with α' crystals (a = 12.348 Å, b = 8.865 Å, c = 16.317 Å, α = 91.41°, β = 93.66°, γ = 113.44°, V = 1635.7 Å^3, and $P\bar{1}$), it was determined from the EDX data that the crystals of both types have the same composition $(ET)_2Br_{1.3}I_{1.1}Cl_{0.6}$. According to Raman data, the anion part contains in fact the mixture of four types of trihalide anions: I_2Br^-, IBr_2^-, $BrICl^-$, and ICl_2^-. The $(ET)_2BrICl$ formula is used below for simplicity.

Like all known ET trihalides, the crystals of α'''-$(ET)_2BrICl$ contain layers of the ET radical cations separated by anion layers. The ET layers in the crystal alternate with anion layers along the c direction (Figure 2k). The packing motif of the ET radical cations (Figure 6f) is significantly different from the packing modes of other ET salts. In contrast to the α and α' phases of the ET trihalides, in which the organic layers contain two stacks in the unit cell, the radical cation layer of the α''' crystals has three stacks (Figure 2l). The overlap mode of adjacent radical cations in the stacks is identical to that in the α'- and β''-type salts. Thus, the ET layers of the α''' crystals can be described as those formed by fragments of the β'' and α' phases (Figure 29). There are no intermolecular S···S contacts shorter than the van der Waals distance (3.70 Å) between the ET molecules within the stacks, but there is a large number of short S···S contacts between the stacks.

A projection of the α'''-crystal structure along the c direction is shown in Figure 2l. There are two crystallographically nonequivalent anions; one of them occupies a center of symmetry, whereas the other one is located in a general position. The anions have a linear shape (Br−I−Cl) with bond angles of 180° and 179.41(3)°. The I−Br and I−Cl bond lengths are 2.626(1) Å (anion at a center of symmetry), and 2.670(1) and 2.675(1) Å (anion in general position). This difference in bond lengths implies that the anion compositions are different for centrosymmetric and general positions, with the anion in the general position being slightly polar. These bond lengths are shorter than the I−Br lengths in α'-$(ET)_2IBr_2$ [2.709(1) and 2.715(1) Å][32,33] but longer than the I−Cl distances in $(ET)_2ICl_2$ [2.539(1) and 2.552(1) Å].[36−40] Note that the values of the anion bond lengths in α'''-$(ET)_2BrICl$ are close to those (2.65 Å) found in α'-$(ET)_2BrICl$,[41] which implies that the latter has a mixed anion composition too. All interanion distances are longer than 4.20 Å.

The ESR parameters, especially the anisotropy of the ESR signal, of the α''' crystals were studied in comparison with those of α'- and β''-phase crystals.[124] The observed difference between the ESR parameters of the α''' crystal and those of the α' and β'' phases enables one to identify the crystal samples obtained in one or different syntheses. The line width and g factor slightly changed when the magnetic field was rotated in the ab plane that indicated an isotropic electronic structure in the ab plane for the α''' phase.

The values of room-temperature conductivity of single crystals of the α''' phase (elongated plates) are very close to those of α' crystals and amount approximately to 4 Ω^{-1} cm^{-1} (in plane) and 5 × 10^{-3} Ω^{-1} cm^{-1} (interplane), demonstrating a quasi-2D electronic nature of both phases.

The temperature dependences of conductivity (Figures 30 and 31) and ESR parameters reveal pronounced discontinuities, which indicate phase transitions in the α''' crystals near 180 and 400 K.[42,124] A sudden drop of resistance and its change to a metal-like behavior were observed at both low and high temperatures (see Figures 30 and 31). Both transitions are reversible and of the first order with a noticeable hysteresis. Because the conducting layers of the α''' phase (see above) contain fragments of both α' and β'' types of structure and the β''-type phases have metal-like behavior, it was proposed[42] that the structural $\alpha''' \rightarrow \beta''$ transition takes place at both low and high temperatures. Figure 32 demonstrates this low-temperature transition. Unit-cell parameters of β''-$(ET)_2Br_{1.3}I_{1.1}Cl_{0.6}$ at 175 K are a = 5.674 Å, b = 9.021 Å, c = 16.340 Å, α = 92.79°, β = 97.56°, γ = 103.41°, and V = 803.7 Å^3.

It was also found that both polymorphs (α''' and α') can transform to each other.[124] The $R(T)$ depen-

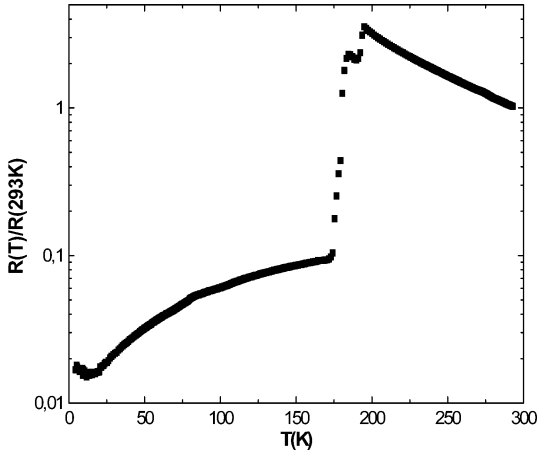

Figure 30. Temperature dependence of normalized resistance for an α‴-$(ET)_2Br_{1.3}I_{1.1}Cl_{0.6}$ single crystal at low temperatures. Reprinted with permission from ref 42. Copyright 2000 Wiley−VCH.

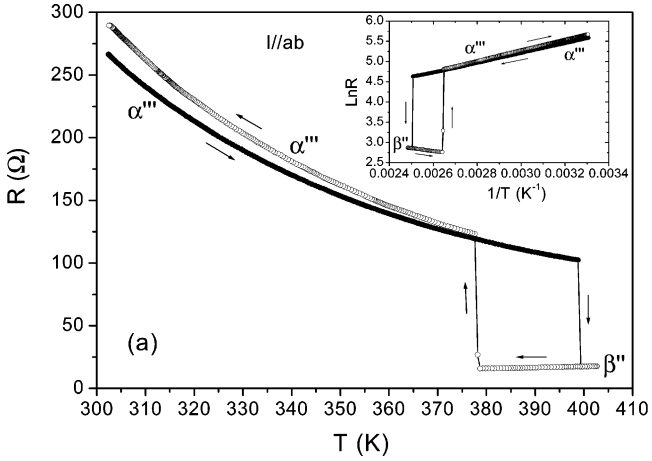

Figure 31. Temperature dependence of resistivity for an α‴-$(ET)_2Br_{1.3}I_{1.1}Cl_{0.6}$ single crystal at high temperatures. Reprinted with permission from ref 124. Copyright 2003 American Chemical Society.

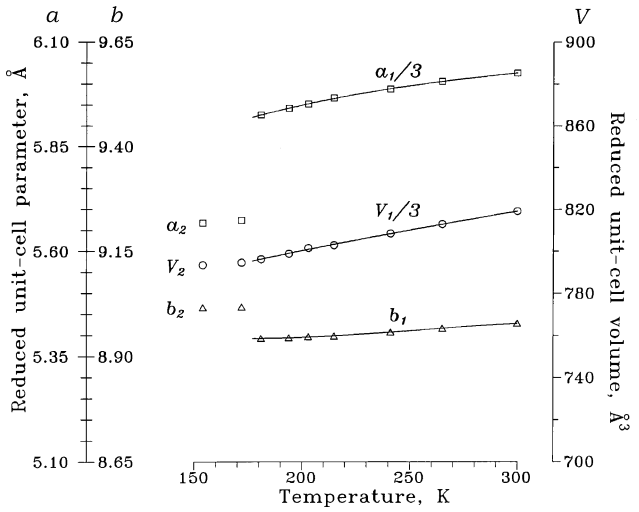

Figure 32. Low-temperature behavior of lattice parameters for an α‴-$(ET)_2Br_{1.3}I_{1.1}Cl_{0.6}$ single crystal. Courtesy of S. S. Khasanov.

dence for α′ polymorph shows a semiconductor-like behavior upon heating to 330 K with an activation energy $E \approx 135$ meV (Figure 33), which differs from that for the α‴ phase ($E \approx 95$ meV). Further heating

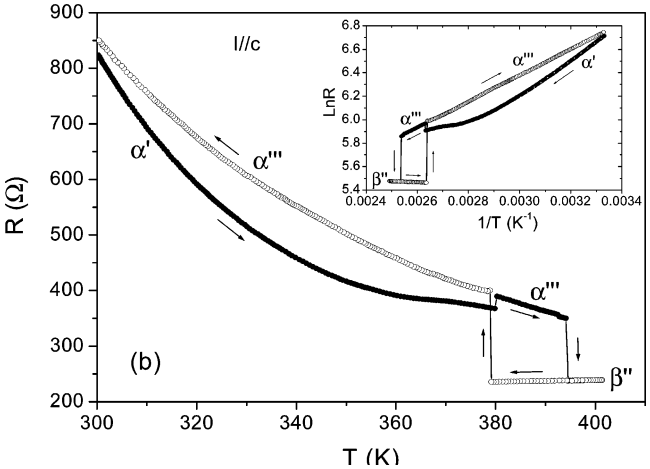

Figure 33. Temperature dependence of resistivity for an α′-$(ET)_2Br_{1.3}I_{1.1}Cl_{0.6}$ single crystal. Reprinted with permission from ref 124. Copyright 2003 American Chemical Society.

of α′ polymorph results in some upward deviation from the Arrhenius fit (see inset in Figure 33) and a subsequent small sharp rise of the resistance at ~380 K. The estimation of the activation energy at temperatures lower than 380 K yields the value characteristic of the α‴ phase. The following changes in the $R(T)$ behavior (a dramatic drop of the resistance) are similar to those observed for the α‴ phase, occurring in the same temperature range (see Figures 31 and 33). The X-ray diffraction analysis of the initial α′ phase from room temperature up to 430 K and then back down to 130 K with a step of ca. 1−3 K was carried out.[124] It was shown that at high temperatures the unit-cell parameters of the initial α′ crystal change, adopting consecutively the values characteristic of the α‴ structure ($a = 17.251$ Å, $b = 9.020$ Å, $c = 16.353$ Å, $\alpha = 87.97°$, $\beta = 84.28°$, $\gamma = 81.38°$, and $V = 2502.8$ Å^3 at 386 K) and the β'' structure ($a = 5.918$ Å, $b = 9.136$ Å, $c = 16.282$ Å, $\alpha = 92.07°$, $\beta = 96.48°$, $\gamma = 105.30°$, and $V = 841.7$ Å^3 at 398 K). Reverse transitions to the α‴ phase below 375 K and β'' phase below 183 K were observed upon cooling. Thus, the X-ray studies definitely indicate that spectacular changes in transport properties are related to the α′ → α‴→ β'' → α‴ → β'' phase transitions. Furthermore, the X-ray and ESP studies showed that at room temperature the α‴ phase, obtained as the result of these transformations, converts back to the α′ polymorph at room temperature with time (over a few days), while the original α‴ phase is stable at room temperature.

2.3.7. θ- and κ-$(ET)_2I_3$

Unlike the polymorphous α and β modifications of $(ET)_2X$, which contain different trihalide anions, θ and κ phases of $(ET)_2X$ were formed only in the case of the tri-iodide anion. These phases were originally synthesized in 1986 as mixed-anion salts of the $(ET)_2(I_3)_{1-x}(AuI_2)_x$ composition in an attempt to change the structural modulation in β-$(ET)_3I_3$ by the introduction of crystallographic disorder in the anion.[26,28,129−131] The electro-oxidation of ET was carried out in THF in the presence of a mixed

supporting electrolyte (TBA·I_3 and a small amount of TBA·AuI_2). X-ray microanalysis of the θ-phase salt indicated the presence of Au in concentrations too small for precise determination.[26] Similar analysis of the κ-phase salt indicated that the Au content was below the limits of detection ($x < 0.006$).[28] Later, the θ and κ phases were also prepared from THF solution without adding TBA·AuI_2 to the TBA·I_3 electrolyte.[132−134] As a rule, the crystals of the θ and κ phases are minor products among other types of crystals, such as α- and β-$(ET)_2I_3$.[133] Nevertheless, in the literature, there is information on preparation of a large (4.47 mg) single crystal of κ-$(ET)_2I_3$, which was used in high-resolution specific heat measurements.[135]

Most of the θ-$(ET)_2I_3$ crystals are twinning and originally identified as having a pseudo-orthorhombic structure.[26] Parts a and b of Figure 3 show the orthorhombic average structure (Table 1). The ET molecules are on the centrosymmetric sites and form a 2D network of sulfur interactions. The dihedral angle between the planes of the neighboring molecules connected by short S···S contacts is about 80°.[26] Each I_3 anion occupies one of the two independent positions on the mirror plane m in a tunnel formed by the ET molecules with the occupancy probability of 50%. In a real monoclinic structure, the period of the anion arrangement becomes $a_m = 4.964 \times 2$ Å, twice that of the average structure (Table 1).[27] Owing to the ordered arrangement of I_3 in the monoclinic lattice, the molecular arrangement of ET is slightly modified from that of the orthorhombic average structure. A tight binding band calculation gives a cylindrical energy spectrum with the Fermi surface open in the b and a directions.[27] Two dimensionality is ascertained experimentally through the optical[136] and conductivity measurements.[131,137,138] The conductivity ratio of $\sigma_{\parallel} \cong 10^2\ \Omega^{-1}\ cm^{-1}$ (parallel to the ab-conductive plane) to $\sigma_{\perp}$ (normal to the plane) is about 1000 at room temperature, while the anisotropy of conductivity in the conductive plane is less than 2. Upon cooling, the resistivity decreases monotonically down to 3.6 K, where the crystals undergo a superconducting transition. It should be noted that not all of the θ-phase specimen crystals exhibit superconducting transitions, which suggests that the crystals are very sensitive to lattice defects and crystal imperfections.[131,138] The θ-$(ET)_2I_3$ crystals were investigated in high magnetic fields and the semiclassical angle-dependent oscillations of magnetoresistance as well as the magnetoquantum oscillations, the de Haas−van Alphen (dHvA) and the Shubnikov−de Haas (SdH) effects, were found.[139−141] Cyclotron resonance was also observed in θ-$(ET)_2I_3$.[142] The study of this phase under hydrostatic pressure showed it to transform to a narrow gap semiconductor at about 5 kbar.[63] The character of the carrier system varies drastically when entering into the high-pressure state. Carrier density decreases by several orders of magnitude from 300 to 1.5 K. However, mobility increases with decreasing temperature. Such a behavior is similar to that observed in α-$(ET)_2I_3$ under high hydrostatic pressure (see section 2.3.1).

Unlike the crystal structure of θ-$(ET)_2I_3$, the structure of κ-$(ET)_2I_3$ has no segregated stacks of ET molecules but consists of dimers units $(ET)_2^+$. The κ-$(ET)_2I_3$ salt was the second, after $(ET)_2Hg_3Cl_8$,[143,144] organic superconductor with the κ-type packing of the ET layer.

The first determination of the lattice constants and the collection of the X-ray intensity data for κ-$(ET)_2I_3$ was made on a weakly twinned crystal.[28] Later, the crystal structure was determined at 295, 150, and 10 K.[132] The structure of κ-$(ET)_2I_3$ is shown in parts a and b of Figure 4. Only one ET is crystallographically independent, and the I_3 anions are on the inversion centers. The donor and anion sheets alternate along the a direction. The radical cation layer is shown in Figure 6h. It is composed of paired molecules. The shortest S···S contact in the dimer is 3.66 Å. The neighboring ET dimers are oriented almost perpendicular to each other (the dihedral angle is 87°). The proximity of dimeric units in all directions is sufficient to yield a 2D sulfur network in the plane of the ET donor molecule layer.

It should be noted that the unit-cell parameters of κ-$(ET)_2I_3$ determined from three independent experiments are (i) $a = 16.433(1)$ Å, $b = 8.500(3)$ Å, $c = 12.871(3)$ Å, $\beta = 108.51(1)°$, and $V = 1704$ Å^3 using a crystal grown from the mixed anion (I_3^- and AuI_2^-) solution of THF;[133] (ii) $a = 16.453(5)$ Å, $b = 8.506(3)$ Å, $c = 12.888(5)$ Å, $\beta = 108.53(2)°$, and $V = 1710$ Å^3 using a crystal grown from THF solution without AuI_2^- anion;[133] and (iii) $a = 16.429$ Å, $b = 8.504$ Å, $c = 12.876$ Å, $\beta = 108.50°$, and $V = 1706$ Å^3 using a crystal also prepared from THF solution without AuI_2^-.[132,134] The unit-cell parameters of (i)−(iii) are almost identical to each other. However, they are slightly larger than those in ref 28 (Table 1). One of the authors of ref 133 found that this difference was caused by an insufficient adjustment of the four-circle diffractometer used in the work.[28]

The κ-$(ET)_2I_3$ crystals showed a superconducting transition around 3.5−4.3 K.[28,132−134,138,145] Resistivity exhibited an anomaly around 170 K, which was coupled with the structural phase transition accompanied by the change of the space group ($P2_1/c \rightarrow P2_1$).[133] The temperature dependence of thermopower in three directions of a single crystal indicated a broad structural transition between 170 and 210 K as well as another possible phase transition at about 25 K.[132] The low-temperature crystal structure analysis showed a conformational change in the ethylene groups.

The single crystals of κ-$(ET)_2I_3$ exhibit a large anisotropy of resistivity, $\rho_{\perp}/\rho_{\parallel} > 10^3$,[138] and a large anisotropy of the upper critical magnetic field around 30.[138,145] κ-$(ET)_2I_3$ is an electronically extreme two-dimensional organic metal with a supercoducting transition, and this makes it an interesting and promising model system for investigation of the effects of two dimensionality onto normal and superconducting state properties.[27,134,145−149] In particular, recently measured dHvA and SdH oscillations in κ-$(ET)_2I_3$ exhibit a dramatic appearance at low temperatures of a significant oscillatory structure cor-

responding to doubling of the fundamental frequency, which is a consequence of two dimensionality.[146−148]

It should be noted that bulk superconductivity is also observed in pressed polycrystalline pellets of κ-$(ET)_2I_3$ (a broad transition with an onset at 5.2 K and zero resistivity at 2 K) in contrast to polycrystalline pressed samples of the other superconducting κ salts of the ET family, κ-$(ET)_2Cu(NCS)_2$ and κ-$(ET)_2Cu[N(CN)_2]Br$.[132] Annealing the single crystals as well as the polycrystalline pressed samples of κ-$(ET)_2I_3$ at 75 °C for a few days results in the structural transformation with an increase in the transition temperature for superconductivity (~8 K for the crystals and ~6 K for the polycrystalline samples). The IR spectra of the tempering samples indicated a transformation into the structure identical to that of β_H-$(ET)_2I_3$,[132] as often as this takes place during annealing the samples of α-$(ET)_2I_3$ (see section 2.3.2.1.) It is conceivable that the pressing κ-$(ET)_2I_3$ specimens are accompanied by a partial structural transformation into the β_H-$(ET)_2I_3$ phase, and therefore superconductivity in pressed polycrystalline pellets of κ-$(ET)_2I_3$ arises.

2.3.8. Polymorphism and Structural Phase Transitions in $(ET)_2X$

Various polymorphous transitions in the $(ET)_2X$ family were described above when considering the $(ET)_2X$ phases. It would be natural that such transitions are of a general character. In this section, we try to summarize experimental data and reveal general regularities.[150]

The structural data listed in Table 1 can be given more pictorially as presented in Table 6. This diagram appears as a simplified phase diagram upon composition in the $(ET)_2X$ system. It is seen that there is a change of phases from α to β'' in the $(ET)_2X$ salts upon varying the X anion from I_3 to ICl_2, with each phase having a certain range of stability in composition. More correctly, this diagram depicts the ranges of phase existence depending on the X anion size. (The effect of the X anion size on structure and properties of the $(ET)_2X$ salts was one way or another considered by numerous research groups. Experimental data were generalized in the books[1,2]). Providing higher dimensionality of the diagram by adding the data on the temperature−pressure axes, we would be able to obtain the full pattern of the behavior of these phases depending upon the composition, temperature, and pressure, i.e., a classical P−T−x (x = composition) phase diagram. However, even from Table 6, one can predict general tendencies of phase behavior with temperature and pressure.

Because of high compressibility of cation sublattices of the $(ET)_2X$ salts, applied pressure results in decreasing in-plane unit-cell parameters of the cation sublattice relative to the anion size. Such compression should give the same effect as the increase of the anion size; i.e., the phase change from β'' to α should be realized upon a pressure increase (Table 6). Similarly, a reverse sequence of transitions from α to β'' is expected with the temperature increase that causes the expansion of in-plane unit-cell parameters of the cation sublattice relative to the anion size. Here, one could speak about general tendencies forced by interactions between cations and anions, resulting from their efficient sizes. The details of a phase diagram are dependent upon additional factors and features of an interaction in a cation−anion system.

The phase transitions described above are considered again below.

1. α → β Transition. In $(ET)_2I_3$, the α → β transition takes place in accordance with the diagram tendencies (Table 6). The α phase turns unstable for anions smaller than I_2Br; therefore, no α phase is found for the IBr_2 anion, while the β phase is still stable for the IBr_2. Consequently, the α → β transition is expected with the temperature increase, i.e., with cation sublattice expansion relative to the anion size. A reverse transformation should take place upon a pressure increase. Additionally, there is a thermodynamic factor because of a specific volume difference for these two phases: 845 Å^3/molecule in the α phase versus 852 Å^3/molecule in the β phase at room temperature, $\delta V/V \approx -0.01$. Nevertheless, it seems to be rather difficult to realize such a transition in real experimental conditions.

2. β → α′ Transition. In $(ET)_2IBr_2$, the β → α′ transition with the pressure increase is likely due to a thermodynamic factor as a result of a volume decrease, $\delta V/V \approx -0.005$. In favor of this, there is a reverse transition observed upon a temperature increase. Anion−cation size effect would give a opposite tendency. Then, one could expect a re-entrant β → α′ → β transition with the further pressure increase (>17 kbar, see section 2.3.3.), when a "size" factor could dominate. Such a re-entrant transformation in the IBr_2 salt would correspond to the pathway from the β-$(ET)_2IBr_2$ area in the diagram (see Table 6) to the α′-$(ET)_2IBr_2$ area at moderate pressure and the pathway from the α′ area to the β-$(ET)_2I_2Br$ area at higher pressure.

3. α‴ → β″ Transition. In $(ET)_2IBrCl$, the α‴ → β″ transition with the temperature increase corresponds to the left−upward → right−downward pathway in the diagram. This transition is temperature-reversible. It is natural to expect the β″ → α‴ transition with the pressure increase for the *as grown* β″ phase.

4. α′ → α‴ Transition. The α′ → α‴ transition takes place with the temperature increase. This transition can be considered as a temperature-reversible one. In general, the starting α‴ phase should transform into the α′ phase with the pressure increase or the temperature decrease, in accordance with the diagram. Contradictory, the α‴ → β″ transition observed upon cooling near 180 K[42,124] seems to be forced by mechanical tension appearing in a fixed sample. This transition is accompanied by great shear strains that make it a ferroelastic one. The application of hydrostatic high pressure should force the α‴ → α′ transition, in accordance with general tendencies of the diagram.

5. β′ → β Transition. The assumed β′ → β transition in $(ET)_2ICl_2$ at high pressures (~80 kbar) again corresponds to the right−downward → left−upward

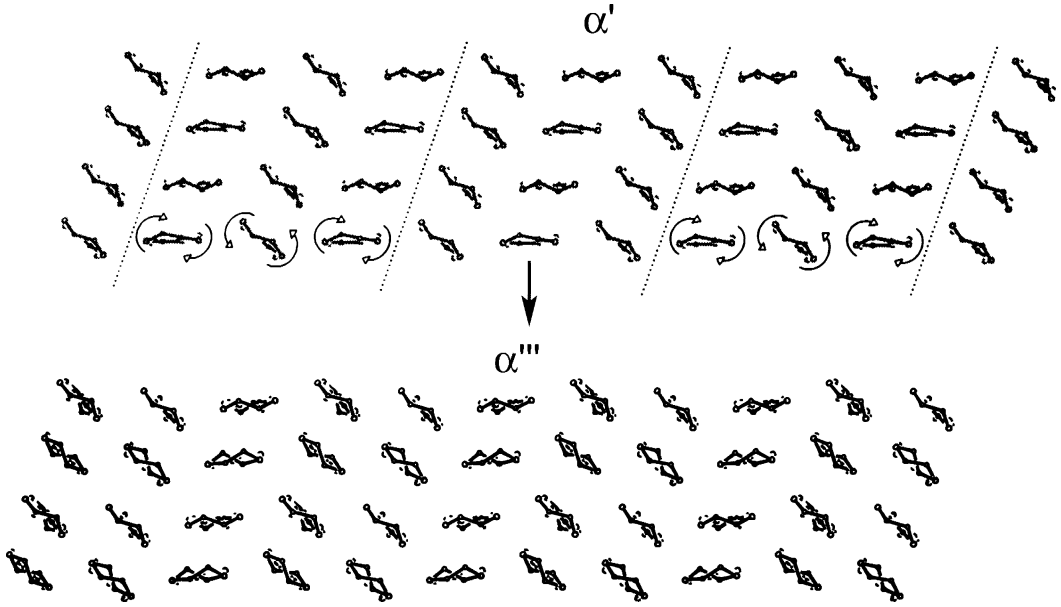

Figure 34. Possible mechanism of the α′ → α‴ phase transition. Courtesy of S. S. Khasanov.

shift in the diagram and, hence, is forced by a size factor.

It is worth paying attention in real experiments to the sequence of transitions that can be dependent on multiple factors including the pressure or temperature change rate because structural transformations are of an activation character. It should also be noted that temperature contraction is not equivalent to pressure contraction, in general.

The most easily realized are α′ → α‴ → β″ transitions; furthermore, they are reversible and can be reasonably interpreted. Figure 29 shows the views of a cation layer along the longer axis of the ET molecules. It is seen that the β″ structure consists of the A-type stacks, the α′ structure consists of alternating stacks of A and B types, and the α‴ structure is composed of the AABAABAAB... sequence. The additional B-type stack in the α′ phase results in the increase of the parameter *a*′ approximately by 6.6 Å as compared to that of the β″ phase. The *a*′ parameter of the α‴ phase is almost equal to the sum of the α′- and β″-phase parameters that correspond to the addition of the A-type stack, i.e., the insertion of the β″ structure into the α′ structure. Then, the modes of molecule overlapping in the stacks are very similar in the three structures (see parts c, e, and f of Figure 6). Therefore, if the molecules are turned synchronously clockwise at an angle of ∼50° in every second or every third stack in the β″ layer, this results in the formation of the α′-type layer or the α‴ phase, respectively. The reverse turns result in reverse transitions. Such a hypothetic possibility was considered in refs 20−22 for α → β transitions on the whole. The problem arises as to what is a mechanism of such a structural reconstraction. In the β″ layer with numerous interstack contacts, such a changeover is not realized easily because of a high-energy barrier. Here, one could expect that with a temperature or pressure change, the in-plane unit-cell parameters and intermolecular distances of the cation sublattice became incommensurate to the anion size. Such incommensurability inevitably leads to a domainlike structure with domain boundaries where intermolecular contacts are weakened. The barrier for switching the stacks is lowered in domain walls (- - -, Figure 34). Then, the triades of coupled stacks can switch synchronously by turning as it is shown in Figure 34; thus, the α′ → α‴ transition is realized.

From this consideration, it is seen that other polytype structures with different combinations of A- and B-type stacks can exist along with the α′, α‴, β″ phases. However, it seems that it is true only for mixed anion salts, where complementarity of the anion sublattice is provided by modulation of the anion composition at crystal growth. As it was noted above in the α‴ phase, there are two crystallographically nonequivalent anions in the structure. Moreover, they are nonequivalent chemically too. As a result, the β″ phase converted from the α‴ phase is not equal to the *as grown* β″ phase. The converted β″ phase has a superstructure with averaged unit-cell parameters close to those of the α‴ phase. This should lead to some peculiarities of its electronic structure.

3. Radical Cation Salts Based on Some ET Analogues

We have already considered radical cation salts of the $(ET)_2X$ family, where X is a single charged linear trihalide anion, which exhibits a rich variety of structural phases and electrical properties. The possibility of tuning the types of conducting layers in these salts by using linear anions of different lengths was demonstrated. A similar tuning of conducting layers is, in principle, possible with the replacement of ethylene bridges in ET by other bridges: methylene (MT), propylene (PT), buthylene (BT), etc., and using the unsymmetrical donors MET, MPT, EPT, etc. However, such an approach was not very productive, and now only some radical cation salts based on these donors with linear trihalide anions are characterized. Only one MT-based salt is known, $MT{\cdot}I_3$[151] (a = 13.185 Å, b = 9.433 Å, c = 7.830 Å,

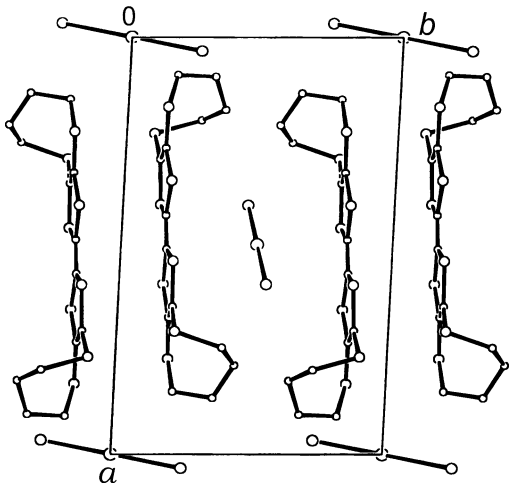

Figure 35. Projection of the crystal structure of BT·IBr_2 along the *c* axis.

α = 102.99°, β = 104.64°, γ = 67.56°, *V* = 861.8 Å^3, *Z* = 2, and *P*$\bar{1}$). The radical cations from eclipsed face−face dimers are connected by side−side S···S contacts of 3.395−3.772 Å rather than isolated from each other. The salt is a diamagnetic semiconductor with $\sigma_{293K} = 10^{-5}$ Ω^{-1} cm^{-1} and $E_a = 0.36$ eV.

A radical cation salt BT·IBr_2 (*a* = 16.64 Å, *b* = 10.143 Å, *c* = 7.198 Å, α = 77.28°, β = 106.11°, γ = 96.01°, *V* = 1137.3 Å^3, *P*$\bar{1}$, *Z* = 2) was also reported.[152] Projection of the crystal structure along the *c* direction is shown in Figure 35. The structure is specified by the presence of mixed cation−anion layers of the $(BT)_2IBr_2$ composition, which alternate with the layers composed of the IBr_2^- anions along the [100] direction. The radical cation−anion layer is formed by centrosymmetrical BT dimers separated by the IBr_2^- anions. Room-temperature conductivity of the BT·IBr_2 crystals is ∼10^{-3} Ω^{-1} cm^{-1}, and its temperature dependence is of a semiconducting character.

3.1. β-$(PT)_2I_3$ and β-$(EPT)_2I_3$

The crystals of radical cation salts β-$(PT)_2I_3$ (*a* = 16.340 Å, *b* = 9.246 Å, *c* = 6.843 Å, α = 111.11°, β = 93.21°, γ = 91.99°, *V* = 962.3 Å^3, *Z* = 1, and *P*$\bar{1}$)[153] and β-$(EPT)_2I_3$ (*a* = 6.716 Å, *b* = 9.185 Å, *c* = 15.795 Å, α = 88.38°, β = 94.57°, γ = 69.22°, *V* = 906.4 Å^3, *Z* = 1, and *P*1)[154] are isostructural to the β-$(ET)_2I_3$ crystals (Table 1). It should be noted that β-$(EPT)_2I_7$[155] was prepared first. The X-ray analysis of this radical cation salt showed that the crystals were isostructural to those of ϵ-$(ET)_2I_7$[116] considered in section 2.3.2.2. Both salts have rather low values of room-temperature conductivity, namely, 10^{-4}−10^{-5} Ω^{-1} cm^{-1}, and the temperature dependence of conductivity is of a semiconducting character. It was found that, similar to ϵ-$(ET)_2I_7$, ϵ-$(EPT)_2I_7$ crystals lose a part of iodine upon heating and convert to β-$(EPT)_2I_3$. However, in contrast to superconducting β_H-$(ET)_2I_3$, which is formed as a result of ϵ → β transformation,[121] β-$(EPT)_2I_3$ is a semiconductor. The crystals of β-$(EPT)_2I_3$ obtained by thermolysis were of low quality and could not be used in the X-ray analysis. Single crystals of the salt were prepared by the chemical oxidation of EPT by molecular iodine at a EPT: I_2 = 1:0.75 ratio in BN. The β-$(EPT)_2I_3$ structure is specified by the presence of radical cation EPT layers alternating with those composed of the I_3^- anions along the *c* direction.[154] Unsymmetrical EPT molecules are packed in a "head−head" manner in the crystal. Therefore, the crystals of β-$(EPT)_2I_3$ have the noncentrosymmetrical space group *P*1 in contrast to those of β-$(PT)_2I_3$[153] and β-$(ET)_2I_3$[9−12] based on symmetrical ET and PT radical cations. The averaged interplanar distances in the radical cation stacks are equal to 3.72 and 3.77 Å. There is a number of shortened contacts some of which are intrastack ones. Room-temperature conductivity of the β-$(EPT)_2I_3$ crystals ranges from 0.2 to 7 Ω^{-1} cm^{-1} for different samples, and the temperature dependence of conductivity is of a semiconducting character. Although the β-$(EPT)_2I_3$, β-$(PT)_2I_3$, and β-$(ET)_2I_3$ salts are isostructural, the former two are semiconductors, whereas the β-$(ET)_2I_3$ crystals are superconductors with T_c = 1.5−8 K.[2] One could suggest that such a strong difference in the properties of these crystals is stipulated by the fact that β-$(ET)_2I_3$ is a quasi-2D system in both structure and physical properties. The anisotropy of conductivity for the β-$(ET)_2I_3$ crystals is ∼1.5−2 in the *ab* plane and ∼400[77] in the perpendicular direction. There are numerous shortened interstack S···S contacts in the radical cation layer; each radical cation layer has 14 such neighboring contacts (3.568−3.688 Å), while there are no intrastack shortened contacts.[10,113]

The β-$(PT)_2I_3$ and β-$(EPT)_2I_3$ crystals are quasi-1D rather than 2D systems. For example, the anisotropy of conductivity for β-$(PT)_2I_3$ is ∼6 in the radical cation plane; the value of conductivity is ∼1.7 Ω^{-1} cm^{-1} along the stacks and ∼0.3 Ω^{-1} cm^{-1} in the orthogonal direction.[153] Similar to the β-$(PT)_2I_3$ crystals, there are shortened intrastack S···S contacts in β-$(EPT)_2I_3$, and a number of shortened interstack contacts are essentially less than that in β-$(ET)_2I_3$: in β-$(PT)_2I_3$, each radical cation has only six contacts (3.44−3.64 Å); in β-$(EPT)_2I_3$, one of the EPT radical cations has five S···S contacts; and the other one has seven S···S contacts (3.38−3.70 Å).

The conductivity of the β-$(PT)_2I_3$ single crystals was studied at room temperature under high quasihydrostatic pressure up to 80 kbar.[156] An unusually high increase in conductivity was observed at high pressure. In some cases, conductivity increased more than 1300 times at 80 kbar, while the conductivity of β-$(ET)_2I_3$ crystals increases not more than 10 times under pressure of 80 kbar (Figure 36). At pressure up to 25 kbar, the β-$(PT)_2I_3$ salt is a semiconductor over the whole temperature range (300−4.2 K). At higher pressures, semiconducting properties occur at low temperature, and at high temperature, the salt transforms to a metallic state and retains this state up to 36 kbar.

3.2. δ-$(PT)_2ICl_2$ and δ-$(EPT)_2ICl_2$, δ′-$(PT)_2ICl_2$ and δ′-$(EPT)_2ICl_2$

Two polymorphic modifications of the PT radical cation salt with the ICl_2^- anion are known: δ-$(PT)_2ICl_2$ (*a* = 6.974 Å, *b* = 16.83 Å, *c* = 31.92Å, α = 94.99°, *V* = 3732 Å^3, *Z* = 4, and *I*2/*c*) and δ′-$(PT)_2ICl_2$ (*a* = 6.955 Å, *b* = 17.200 Å, *c* = 15.999 Å, α = 100.80°,

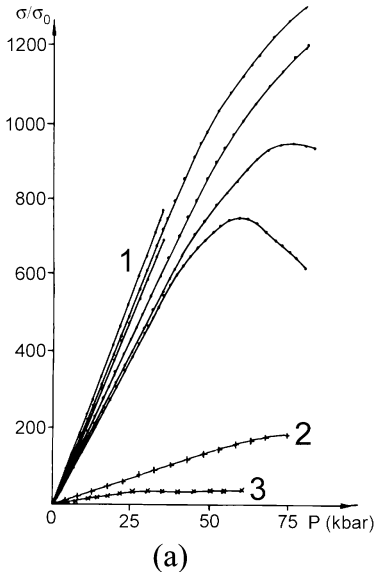

Figure 36. Conductivity versus pressure at room temperature, (1) for different β-$(PT)_2I_3$ crystals, (2) for a pellet of β-$(PT)_2I_3$, and (3) for a crystal of β-$(ET)_2I_3$.

$V = 1880.0$ Å^3, $Z = 2$, and $P2/b$).[157] Both salts were prepared by the chemical oxidation of PT by $(Et_4N)ICl_2$ in TCE at 100 °C and by electrocrystallization in TCE with $(Et_4N)ICl_2$ as a supporting electrolyte. The projections of both structures along the *a* direction and the projections of cation layers and anion sheets along the *c* direction are shown in parts a−d of Figure 37 and parts a−c of Figure 38, respectively. These structures are specified by the presence of radical cation layers parallel to the *ab* plane, which alternate with the anion sheets along the *c* direction. In principle, the radical cation layers are similar in these salts. They are formed by almost noninteracting PT stacks running along the *b* direction. There are only two slightly shortened interstack S···S contacts equal to 3.646 Å. The radical cation stacks consist of centrosymmetrical dimers with an average interplanar distance of 3.65 Å (δ) and 3.59 Å (δ') in the dimer. Centrosymmetrical dimers are turned at an angle of ~30° about the stack axis with respect to each other (Figures 37c and 38c). There are shortened S···S contacts within each stack: the interdimer contacts of 3.484 Å in the δ structure and the intradimer contacts of 3.639 Å in the δ' structure.

The internal structures of anion sheets in the δ and δ' phases are essentially different. In the δ' phase, the anion sheet is formed by parallel ICl_2^- anions (Figure 38b), and in the δ phase, the angle between two anions related by the 2_1 axis is equal to 86° (Figure 37d). Moreover, the anions in these structures occupy positions of different symmetry. The interatomic I−Cl distances in the anions are 2.534(2) Å in the δ phase and 2.552(1) Å in the δ' phase.

The values of room-temperature conductivity for δ and δ' crystals are close and equal to 0.1 and 0.4 Ω^{-1} cm^{-1}, respectively. The lack of short intermolecular S···S contacts and strong dimerization in the PT stack is considered to be a consequence of the crystal packing of relatively bulky propylene groups of PT, resulting in semiconducting transport properties.

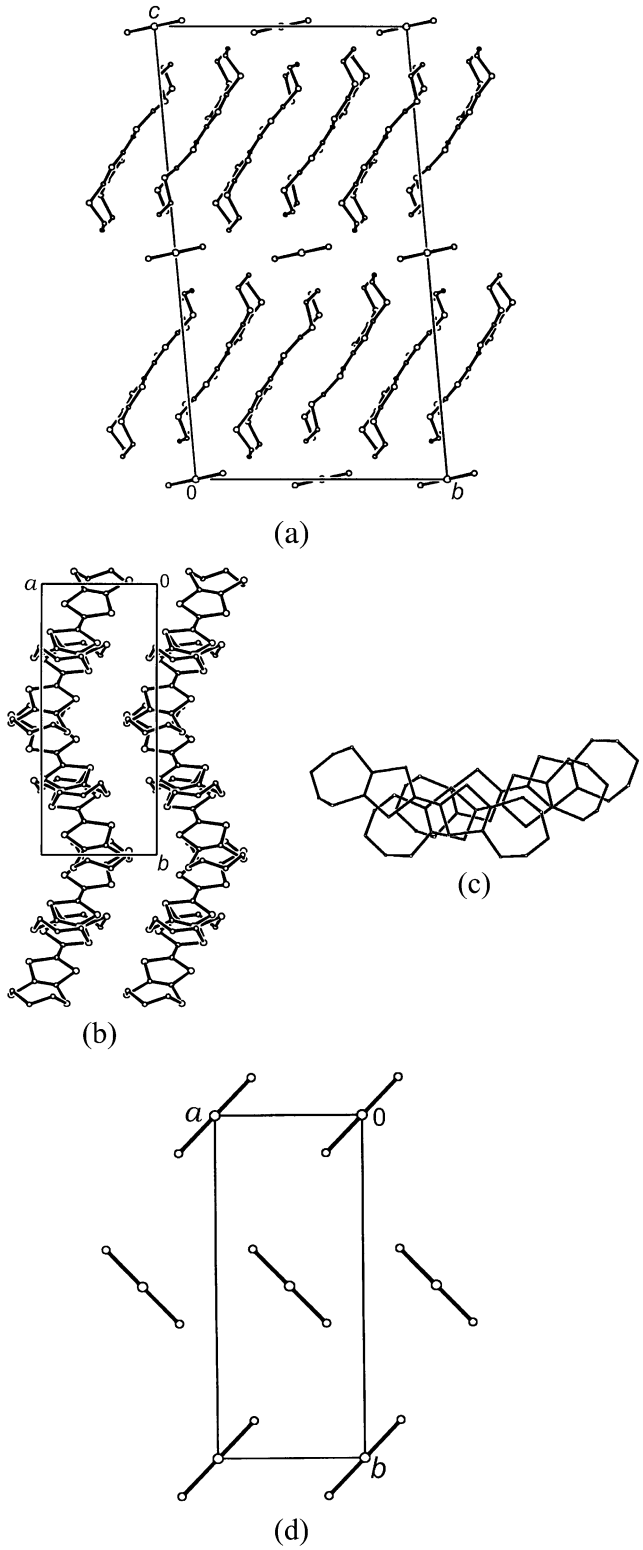

Figure 37. δ-$(PT)_2ICl_2$. (a) Projection of the crystal structure along the *a* direction. (b) Projection of the radical cation layer along the *c* axis. (c) Overlap modes in the radical cation stack. (d) Projection of the anion layer along the *c* axis.

The radical cation salts δ'-$(EPT)_2ICl_2$ ($a = 15.752$ Å, $b = 6.780$ Å, $c = 16.910$ Å, $\beta = 101.34°$, $V = 1771$ Å^3, $P2/c$, and $Z = 2$) and β'-$(EPT)_2ICl_2$ ($a = 6.880$ Å, $b = 10.925$ Å, $c = 12.048$ Å, $\alpha = 87.32°$, $\beta = 100.30°$, $\gamma = 100.54°$, $V = 875.9$ Å^3, $P\bar{1}$, and $Z = 1$) were obtained by electrocrystallyzation of EPT in THF

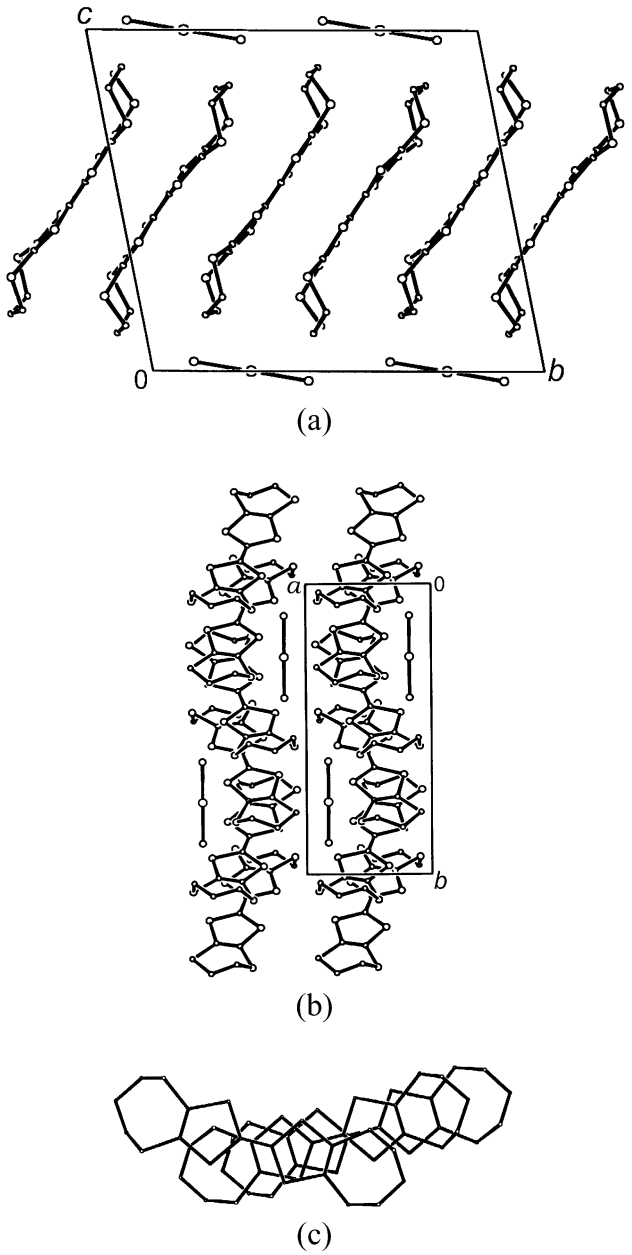

Figure 38. δ'-$(PT)_2ICl_2$. (a) Projection of the crystal structure along the *a* axis. (b) Projection of the crystal structure along the *c* axis. (c) Overlap modes in the radical cation stack.

with $(Bu_4N)ICl_2$ as a supporting electrolyte.[158] The crystals of δ'-$(EPT)_2ICl_2$ are nearly isostructural to those of δ'-$(PT)_2ICl_2$ (Figure 38).[157] The interplanar distance within the dimers is 3.56 Å and between the dimers is 3.99 Å. The EPT donor molecules have a chair conformation. The ICl_2^- anion resides at an inversion center, and the I−Cl distance is 2.531(4) Å. The crystals of δ'-$(EPT)_2ICl_2$ exhibit semiconductor behavior of conductivity with an activation energy of 0.066 eV.[158] The radical cation salt β'-$(EPT)_2ICl_2$ is nearly isostructural to that of β'-$(ET)_2ICl_2$[36−38] (Table 1). It contains dimers of EPT donor molecules with a boat conformation connected side−side to form 1D chains in the *a* direction (parts g and h of Figure 2). The interplanar distance within the dimer is 3.51 Å. The ICl_2^- anions are located at inversion centers with the I−Cl distance of 2.553(1) Å. The crystals have semiconducting properties with E_a = 0.282 eV.[158]

3.3. $[M(dddt)_2]_2X$; M = Pt, Pd and Au; X = IBr_2 and ICl_2

The $M(dddt)_2$ bisdithiolene complexes are inorganic analogues of ET, in which the central C=C bond is formally substituted by a metal (M) ion. Like ET, the $M(dddt)_2$ complexes (M = Ni, Pt, Pd, and Au) form conducting cation salts in a partially oxidized state.[159] Although the crystal structures of the $M(dddt)_2$ and ET salts are similar and neutral $Au(dddt)_2$ and ET are isostructural, their electronic band structures and some properties are essentially different.

For the $M(dddt)_2$ complexes, the energy gap between the highest occupied molecular orbital (HOMO) and the lowest unoccupied molecular orbital (LUMO) is small (∼0.4 eV), while in ET, LUMO lies considerably higher in energy than HOMO (∼2 eV).[160] Only HOMO of ET contributes to the conduction bands of its salts, whereas both HOMO and LUMO of the $M(dddt)_2$ complexes can be involved in the conduction bands of their salts.

As compared to ET, neutral $M(dddt)_2$ complexes are very low soluble in organic solvents, thus causing difficulties in the preparation of crystals of the their salts by electrocrystallization. Low solubility of the complexes is probably associated with the intermolecular $\pi-d$ interaction between S and metal atoms.

Oxidation potentials for neutral $M(dddt)_2$ complexes (∼0.9 V) are considerably higher than that for the ET molecule (∼0.5 V), which limits a number of anions to be used as counterions in the synthesis of $M(dddt)_2$ cation salts.

Polymorphism characteristic of the ET salts is not observed in the $M(dddt)_2$ cation salts, which is probably associated with a stiffer nature of the lattice of these salts as compared to the ET ones.

About 30 salts based on $M(dddt)_2$ cationic complexes with anions of various origin and size have been synthesized by now. Their conducting properties range from almost insulating to stable metallic ones.[159] The present review considers the structures and properties of the $M(dddt)_2$ salts with only linear trihalide anions, whose number is rather limited. These salts involving the ICl_2 and IBr_2 anions were synthesized by electro-oxidation of $M(dddt)_2$ (M = Pt, Pd, and Au) neutral complexes in NB solution on Pt-anode under galvanostatic conditions (1−5 $\mu A/cm^2$).[161−164] (n-$Bu_4N)ICl_2$ and (n-$Bu_4N)IBr_2$ were used as the electrolytes. The attempts to prepare the $M(dddt)_2$ salts with I_3^- using the same method were unsuccessful probably because of high oxidation potentials of $[M(dddt)_2]^0$. The Pt(Pd)$(dddt)_2$ salts with ICl_2 and IBr_2 are isostructural and have 2:1 stoichiometry similarly to the ET salts with these anions. The unit-cell parameters for $[Pt(dddt)_2]_2IBr_2$ (a = 6.352(1) Å, b = 8.543(2) Å, c = 15.993(4) Å, α = 88.76(2)°, β = 84.43(2)°, γ = 67.80(2)°, V = 810.6 $Å^3$, and space group = $P\bar{1}$)[161] are close to those for β-$(ET)_2IBr_2$ (Table 1),[34] and their structures are similar.

The projection of the structure of $[Pt(dddt)_2]_2IBr_2$ along the *a* direction is shown in Figure 39. There is

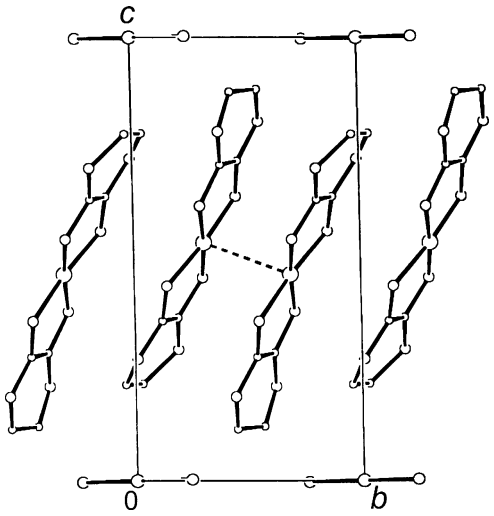

Figure 39. Projection of the crystal structure of [Pt(dddt)$_2$]$_2$IBr$_2$ along the *a* axis.

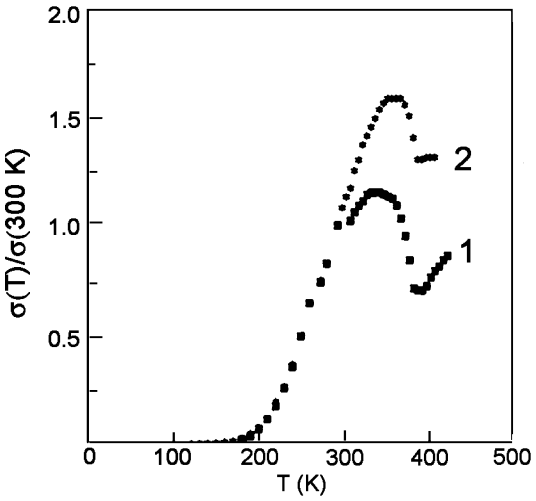

Figure 40. Temperature dependence of normalized conductivity for [Pt(dddt)$_2$]$_2$ICl$_2$ (1) and [Pt(dddt)$_2$]$_2$IBr$_2$ (2).

one symmetrically independent Pt(dddt)$_2$ cation in a general position and one linear IBr$_2$ anion in a special position. The Pt(dddt)$_2$ cation is not fully planar. The maximum atomic deviation from the mean plane of all of the cation atoms except the terminal carbon atoms is equal to 0.4 Å.

The analysis of bond lengths in chelate Pt−S−C=C−S−Pt fragments showed that elongated C=C and shortened (Pt)S−C bonds were observed in the Pt(dddt)$_2$ cation salts as compared with the Et$_4$N[Pt(dddt)$_2$] anion salt, whereas the Pt−S bond lengths remained almost unchanged.[161] These facts are evidence of the fact that the oxidation of the Pt(dddt)$_2$ complexes takes place mainly on a dithiolate ligand rather than on metal ions. The Raman spectra for the M(dddt)$_2$ complexes in different charge states justify this conclusion.[165]

The cations in the [Pt(dddt)$_2$]$_2$IBr$_2$ crystals are packed face−face, similar to the cations in β-(ET)$_2$IBr$_2$, forming stacks along the *b* axis (Figure 39). However, the internal structure of the stacks in the Pt(dddt)$_2$ salt essentially differs from that in β-(ET)$_2$IBr$_2$. Unlike the latter one, the stacks in [Pt(dddt)$_2$]$_2$IBr$_2$ consist of well-formed dimers with shortened S···S (<3.65 Å) and Pt···Pt (3.36 Å) distances. The cations in dimers are arranged over each other with almost no shift, whereas some transverse and longitudinal displacement equal to ~1/4 of the Pt(dddt)$_2$ molecular length exists between the dimers. Similar to ET stacks in β-(ET)$_2$IBr$_2$, the Pt(dddt)$_2$ stacks in [Pt(dddt)$_2$]$_2$IBr$_2$ form layers in the *ab* plane because of the presence of numerous shortened side−side S···S contacts. The cation layers alternate with those of centrosymmetrical linear IBr$_2$ anions along the *c* axis.

Room-temperature conductivity of [Pt(dddt)$_2$]$_2$X (X = IBr$_2$ and ICl$_2$) crystals is 5−10 Ω^{-1} cm^{-1} and decreases upon cooling, demonstrating a semiconducting behavior. At higher temperatures (300−423 K), the conductivity of crystals has a nonmonotonic character; at T ~ 350 K, it passes through a maximum followed by a minimum at about 390 K (Figure 40).[161] A similar nonmonotonic behavior of conductivity with a maximum at low temperature (~170 K) was also observed for the crystals of Au(dddt)$_2$ salt with the IBr$_2$ anion.[166]

Although room-temperature conductivities are close for the [Pt(dddt)$_2$]$_2$IBr$_2$ and β-(ET)$_2$IBr$_2$ crystals, their low-temperature states are quite different (semiconducting and metal states with a transition to a superconducting state near 2.8 K, respectively). The difference in conducting properties is associated with the dimerization of the Pt(dddt)$_2$ cations in the stacks, as it is evident from the calculations of electron band structures of M(dddt)$_2$ salts.[160] It should be noted that the dimerization degree depends on the anion. As compared to [Pt(dddt)$_2$]$_2$IBr$_2$, the dimerization of the cations in [Pt(dddt)$_2$]$_2$AuBr$_2$, which is isostructural to the former salt, is stronger (the Pt···Pt distance is 2.983 Å).[161] As a result, conductivity becomes lower by an order for [Pt(dddt)$_2$]$_2$AuBr$_2$ than for [Pt(dddt)$_2$]$_2$IBr$_2$. The ability of Pt and Pd ions to form metal−metal bonds apparently dictates the packing type in [Pt(dddt)$_2$]$_2$ and [Pd(dddt)$_2$]$_2$ cation salts. Therefore, unlike ET salts, the M(dddt)$_2$ (M = Pt and Pd) salts with anions of different geometry (linear, tetrahedral, and octahedral) are isostructural.[161,162,164,167−169] Dimerization characteristic of the Pt(dddt)$_2$ salts and associated with the Pt···Pt interaction was not observed for Ni(dddt)$_2$ ones. The [Ni(dddt)$_2$]$_3$(AuBr$_2$)$_2$ salt containing the Ni(dddt)$_2$ uniform stacks is a quasi-2D molecular metal stable down to 1.3 K.[170,171]

4. Concluding Remarks

The present review is devoted to the analysis of the data of the experimental study of a large family of low-dimensional organic conductors based on trihalides of ET and some its analogues. A particular emphasis was put on peculiarities of crystal structures, which are very important for interpreting transport properties of these materials. It has been shown that the family of radical cation salts (ET)$_2$X, where X is a linear trihalide anion, is characterized by a wide variety of conducting properties, rich polymorphism, and phase transitions. It is suggested that general structure−property correlations revealed in this review are relevant for a wider class

of radical cation salts based on different π-organic donors and having another stoichiometry and anions of diverse geometry.

Although radical cation salts of the $(ET)_2X$ family are widely studied materials, some of their properties have not been fully understood to now and should be studied deeper. Along this line, it is worth noting some of the questions remaining open. One of them is concerned with the nature of a phase transition at 135 K in the α-$(ET)_2I_3$ crystals. As it was mentioned above, the transition is associated with charge disproportionation in the ET radical cations. According to recently published results of NMR[17,58] and Raman spectroscopy,[18,61] three crystallographically independent molecules have a charge of +0.5 at $T > 135$ K and differ in charge below the phase transition point. These results are at some variance with X-ray structural data. The bond-length distribution shows that even at room temperature the ET molecules at the centers of symmetry are closer to neutral ones, while the molecule in a general position is closer to the ET^+ radical cation.[47,52] Below the phase transition point at 120 K, there is the tendency toward a more uniform charge distribution in the ET molecules.[52] The central C=C bond length, which is most sensitive to charge, changes in the three ET molecules from 1.382(9), 1.344(9), and 1.326(9) Å[47] or 1.376(7), 1.358(9), and 1.353(9) Å[52] at room temperature to 1.366(7), 1.358(9), and 1.360(9) Å[52] at 120 K, respectively.

The other problem relates to the organic superconductor β-$(ET)_2I_3$. The matter is that there is no full comprehension of the nature of a superconducting state of β_H so far because of very scarce structural information. It seems that superconducting states are realized in the crystals of this radical cation salt not only with $T_c = 1.5$ and 8 K but also other intermediate values of T_c. Therefore, it is very important to prepare high-quality single crystals of β_H-$(ET)_2I_3$ for a detailed diffraction investigation in a wide temperature range. Such investigation should involve the control of structural modulation and the complete structural analysis with the refinement of occupancy of s and e conformations in the ET molecule, to have an opportunity to trace the history of one sample.

It would be very interesting to study in detail the problems of phase stability in the $(ET)_2X$ salts and, consequently, the problems of phase transitions realized in them. Obviously, the interaction between cations and anions plays a key role in phase stability in the system. Trihalide anions are considered in most structures as noninteracting anions because they are arranged at distances greater than the van der Waals distances. However, it was reported in ref 124 that dipole−dipole interactions should be considered in the case of unsymmetrical anions. Moreover, these materials provide for the unique possibility of a detailed enough comparative analysis of the influence of chemical compression, thermal expansion, and compression under pressure on their structures and properties. On the whole, these phenomena are expected to result in a deeper comprehension of intrinsic causes for the formation of different structures and to make it possible to perform tailoring synthesis.

It was mentioned above that at high pressure β'-$(ET)_2ICl_2$ undergoes a transition from the Mott dielectric to a metallic state with a superconducting transition at $T_c = 14.2$ K.[14] To interpret the appearance of superconductivity in β'-$(ET)_2ICl_2$, Kontani[172] suggested that its structure transforms to the β-type structure under pressure. It should be noted that this suggestion does not contradict the tendencies of the diagram (Table 6). Moreover, if one considers the modes of molecules overlapping in both structures (see parts a and b of Figure 6), the $\beta' \rightarrow \beta$ conversion seems to be the least difficult as compared to the other possible ones. However, there is a confusing aspect; namely, in β phases, T_c decreases with the increase in the structure density as a result of both chemical compression and compression under external pressure. Therefore, one could expect that at high pressure β-$(ET)_2ICl_2$ behaves as a metal without superconducting transition. Probably some other mechanisms of structural changes take place in β'-$(ET)_2ICl_2$ under pressure leading to a superconducting state. Indeed, the other theoretical model has very recently been proposed in ref 173. Thus, the X-ray study of the behavior of β'-$(ET)_2ICl_2$ under pressure is obviously important.

In conclusion, we would like to note that ET trihalide salts have promising applications. They can successfully be produced as a well-oriented nanocrystalline layer on a polymer film surface. This allows one to combine transport and magnetic properties of molecular conductors with advantageous properties of commercial polymers.[73,100]

5. Acknowledgment

The work was supported by INTAS Grant 01-2212. We wish to express thanks and appreciation to our colleagues S. S. Khasanov and L. V. Zorina for many useful discussions and effort in the preparation of the manuscript. The authors would also like to thank their current and former co-workers and numerous collaborators for their contributions to the original works underlying this review article.

6. References

(1) Williams, J. M.; Ferraro, J. R.; Thorn, R. J.; Carlson, K. D.; Geiser, U.; Wang, H. H.; Kini, A. M.; Whangbo, M.-H. *Organic Superconductors (Including Fullerenes). Synthesis, Structure, Properties, and Theory*; Prentice Hall: Englewood Cliffs, NJ, 1992; p 400.
(2) Ishiguro, T.; Yamaji, K.; Saito, G. *Organic Superconductors*, 2nd ed.; Springer-Verlag, Berlin, Heidelberg: New York, 1998; p 522.
(3) Schegolev, I. F. *Jpn. J. Appl. Phys.* **1987**, *26*, 1972.
(4) Schegolev, I. F.; Yagubskii, E. B. *J. Mol. Electron.* **1989**, *5*, 215.
(5) Yagubskii, E. B.; Shibaeva, R. P. *J. Mol. Electron.* **1989**, *5*, 25.
(6) Shibaeva, R. P. *Strukturnaya Kristallografiya*; Nauka: Moscow, Russia, 1992; p 41.
(7) Yagubskii, E. B. *Mol. Cryst. Liq. Cryst.* **2002**, *380*, 15.
(8) Yagubskii, E. B. in *Organic Conductors, Superconductors, and Magnets: From Synthesis to Molecular Electronics*; Ouahab, L., Yagubskii, E., Eds. (Proceedings of NATO ASI, Corfu, Greece, April 29−May 11, 2003); Kluwer Academic Publishers: Dordrecht, The Netherlands, 2003; p 45.
(9) Yagubskii, E. B.; Schegolev, I. F.; Laukhin, V. N.; Kononovich, P. A.; Kartsovnik, M. V.; Zvarykina, A. V.; Buravov, L. I. *JETP Lett.* **1984**, *39*, 12.
(10) Kaminskii, V. F.; Prokhorova, T. G.; Shibaeva, R. P.; Yagubskii, E. B. *JETP Lett.* **1984**, *39*, 17.

(11) Shibaeva, R. P.; Kaminskii, V. F.; Yagubskii, E. B. *Mol. Cryst. Liq. Cryst.* **1985**, *119*, 361.
(12) Schegolev, I. F.; Yagubskii, E. B.; Laukhin, V. N. *Mol. Cryst. Liq. Cryst*. **1985**, *126*, 365.
(13) Kartsovnik, M. V.; Laukhin, V. N.; Nizhankovskii, V. I.; Ignat'ev, A. A. *JETP Lett.* **1988**, *47*, 363.
(14) Kartsovnik, M. V.; Kononovich, P. A.; Laukhin, V. N.; Schegolev, I. F. *JETP Lett.* **1988**, *48*, 541.
(15) Taniguchi, H.; Miyashita, M.; Uchiyama, K.; Satoh, K.; Mori, N.; Okamoto, H.; Miyagawa, K.; Kanoda, K.; Hedo, M.; Uwatoko, Y. *J. Phys. Soc. Jpn.* **2003**, *72*, 468.
(16) Bender, K.; Dietz, K.; Endres, H.; Helberg, H. W.; Hennig, I.; Keller, H. J.; Schäfer, H. W.; Schweitzer, D. *Mol. Cryst. Liq. Cryst*. **1984**, *107*, 45.
(17) Takahashi, T. *Synth. Met*. **2003**, *133*−*134*, 261.
(18) Wojciechowski, R.; Yamamoto, K.; Yakushi, K.; Inokuchi, M.; Kawamoto, A. *Phys. Rev. B* **2003**, *67*, 224105.
(19) Petricek, V.; Maly, K.; Coppens, P.; Bu, X.; Cisarova, I.; Frost-Jensen, A. *Acta Crystallogr., Sect. A* **1991**, *47*, 210.
(20) Mori, T. *Bull. Chem. Soc. Jpn.* **1998**, *71*, 2509.
(21) Mori, T. *Bull. Chem. Soc. Jpn.* **1999**, *72*, 179.
(22) Mori, T. *Bull. Chem. Soc. Jpn.* **1999**, *72*, 2011.
(23) Lee, Y. J.; Nieminen, R. M.; Ordejon, P.; Canadell, E. *Phys. Rev. B* **2003**, *67*, 180505(R).
(24) Rousseau, R.; Gener, M.; Canadell, E. *Adv. Funct. Mater.* **2004**, *12*, 483.
(25) Yagubskii, E. B.; Schegolev, I. F.; Laukhin, V. N.; Shibaeva, R. P.; Kostyuchenko, E. E.; Khomenko, A. G.; Sushko, Yu. V.; Zvarykina, A. V. *Pis'ma v ZhETF* **1984**, *40*, 387.
(26) Kobayashi, H.; Kato, R.; Kobayashi, A.; Nishio, Y.; Kajita, K.; Sasaki, W. *Chem. Lett.* **1986**, 789.
(27) Kobayashi, A.; Kato, R.; Kobayashi, H.; Moriyama, S.; Nishio, Y.; Kajita, K.; Sasaki, W. *Chem. Lett.* **1986**, 2017.
(28) Kobayashi, A.; Kato, R.; Kobayashi, H.; Moriyama, S.; Nishio, Y.; Kajita, K.; Sasaki, W. *Chem. Lett.* **1987**, 459.
(29) Zhu, D.; Wang, P.; Wan, M.; Yu, Zh.; Zhu, N. *Solid State Commun.* **1986**, *57*, 843.
(30) Emge, T. J.; Wang, H. H.; Beno, M. A.; Leung, P. C. W.; Firestone, M. A.; Jenkins, H. C.; Cook, J. D.; Carlson, K. D.; Williams, J. M.; Venturini, E. L.; Azevedo, L. J.; Schirber, J. E. *Inorg. Chem.* **1985**, *24*, 1736.
(31) Kobayashi, H.; Kato, R.; Kobayashi, A.; Saito, G.; Tokumoto, M.; Anzai, H.; Ishiguro, T. *Chem. Lett.* **1985**, 1293.
(32) Yagubskii, E. B.; Schegolev, I. F.; Shibaeva, R. P.; Fedutin, D. N.; Rozenberg, L. P.; Sogomonyan, E. M.; Lobkovskaya, R. M.; Laukhin, V. N.; Ignat'ev, A. A.; Zvarykina, A. V.; Buravov, L. I. *Pis'ma v ZhETF* **1985**, *42*, 167.
(33) Shibaeva, R. P.; Lobkovskaya, R. M.; Simonov, M. A.; Yagubskii, E. B.; Ignat'ev, A. A. *Sov. Phys. Crystallogr.* (English translation) **1986**, *31*, 654.
(34) Williams, J. M.; Wang, H. H.; Beno, M. A.; Emge, T. J.; Sowa, L. M.; Copps, P. T.; Behroozi, F.; Carlson, K. D.; Crabtree, G. W. *Inorg. Chem.* **1984**, *23*, 3839.
(35) Laukhina, E. E.; Narymbetov, B. Zh.; Zorina, L. V.; Khasanov, S. S.; Rozenberg, L. P.; Shibaeva, R. P.; Buravov, L. I.; Yagubskii, E. B.; Avramenko, N. V.; Van, K. *Synth. Met.* **1997**, *90*, 101.
(36) Emge, T. J.; Wang, H. H.; Leung, P. C. W.; Rust, P. R.; Cook, J. D.; Jackson, P. L.; Carlson, K. D.; Williams, J. M.; Whangbo, M.-H.; Venturini, E. L.; Schirber, J. E.; Azevedo, L. J.; Ferraro, J. R. *J. Am. Chem. Soc.* **1986**, *108*, 695.
(37) Kobayashi, H.; Kato, R.; Kobayashi, A.; Saito, G.; Tokumoto, M.; Anzai, H.; Ishiguro, T. *Chem. Lett.* **1986**, 89.
(38) Buravov, L. I.; Zvarykina, A. V.; Ignat'ev, A. A.; Kotov, A. I.; Laukhin, V. N.; Makova, M. K.; Merzhanov, V. A.; Rozenberg, L. P.; Shibaeva, R. P.; Yagubskii, E. B. *Bull. Acad. Sci. USSR* (English translation) **1988**, 1825.
(39) Shibaeva, R. P.; Rozenberg, L. P.; Yagubskii, E. B.; Ignat'ev, A. A.; Kotov, A. I. *Dokl. Akad. Nauk SSSR* **1987**, *292*, 1405.
(40) Ugawa, A.; Okawa, Y.; Yakushi, K.; Kuroda, H.; Kawamoto, A.; Tanaka, J.; Tanaka, M.; Nogami, Y.; Kagoshima, S.; Murata, K.; Ishiguro, T. *Synth. Met.* **1988**, *27*, A407.
(41) Kobayashi, H.; Kato, R.; Kobayashi, A.; Saito, G.; Tokumoto, M.; Anzai, H.; Ishiguro, T. *Chem. Lett.* **1986**, 93.
(42) Laukhina, E.; Vidal-Gancedo, J.; Khasanov, S.; Tkacheva, V.; Zorina, L.; Shibaeva, R.; Singleton, J.; Wojciechowski, R.; Ulanski, J.; Laukhin, V.; Veciana, J.; Rovira, C. *Adv. Mater.* **2000**, *12*, 1205.
(43) Qian, M.-X.; Wang, X.-H.; Zhu, Y.-L.; Zhu, D. *Synth. Met.* **1988**, *27*, A277.
(44) Saito, G.; Enoki, T.; Toriumi, K.; Inokuchi, H. *Solid State Commun*. **1982**, *42*, 557.
(45) Kobayashi, H.; Mori, T.; Kato, R.; Kobayashi, A.; Sasaki, Y.; Saito, G.; Inokuchi, H. *Chem. Lett.* **1983**, 581.
(46) Bender, K.; Hennig, I.; Schweitzer, D.; Dietz, K.; Endres, H.; Keller, H. J. *Mol. Cryst. Liq. Cryst*. **1984**, *108*, 359.
(47) Kaminskii, V. F.; Laukhin, V. N.; Merzhanov, V. A.; Neiland, O. Ya.; Khodorkovskii, V. Yu.; Shibaeva, R. P.; Yagubskii, E. B. *Izv. AN SSSR, Ser. Khim.* **1986**, 342.
(48) Kostyuchenko, E. E.; Yagubskii, E. B.; Neiland, O. Ya.; Khodorkovskii, V. Yu. *Izv. AN SSSR, Ser. Khim.* **1984**, 2834.
(49) Müller, H.; Svensson, S. O.; Fitch, A. N.; Lorenzen, M.; Wanka, S.; Wosnitza, J. *Synth. Met.* **1999**, *102*, 1685.
(50) Hennig, I.; Bender, K.; Schweitzer, D.; Dietz, K.; Endres, H.; Keller, H. J.; Gleitz, A.; Helberg, H. W. *Mol. Cryst. Liq. Cryst.* **1985**, *119*, 337.
(51) Kartsovnik, M. V.; Kononovich, P. A.; Laukhin, V. N.; Khomenko, A. G.; Schegolev, I. F. *Zh. Eksp. Teor. Fiz.* **1985**, *88*, 1447.
(52) Emge, T. J.; Leung, P. C. W.; Beno, M. A.; Wang, H. H.; Williams, J. M. *Mol. Cryst. Liq. Cryst*. **1986**, *138*, 393.
(53) Endres, H.; Keller, H. J.; Swietlik, R.; Schweitzer, D.; Angermund, K.; Krüger, C. *Z. Naturforsch., A: Phy. Sci.* **1986**, *41*, 1319.
(54) Nogami, Y.; Kagoshima, S.; Sugano, T.; Saito, G. *Synth. Met*. **1986**, *16*, 367.
(55) Rothaemel, B.; Ferro, L.; Cooper, J. R.; Schilling, J. S.; Weger, V.; Bele, P.; Brunner, H.; Schweitzer, D. *Phys. Rev. B* **1984**, *34*, 704.
(56) Heidmann, C.-P.; Barnsteiner, A.; Gross-Alltag, F.; Chandrasekhar, B. S.; Hess, E. *Solid State Commun*. **1992**, *84*, 711.
(57) Fortune, N. A.; Murata, K.; Ishibashi, M.; Tokumoto, M.; Kinoshita, N.; Anzai, H. *Solid State Commun.* **1991**, *77*, 265.
(58) Takano, Y.; Hiraki, K.; Yamamoto, H. M.; Nakamura, T.; Takahashi, T. *J. Phys. Chem. Solids* **2001**, *62*, 393.
(59) Kino, H.; Fukuyama, H. *J. Phys. Soc. Jpn.* **1996**, *65*, 2158.
(60) Seo, H. *J. Phys. Soc. Jpn.* **2000**, *69*, 805.
(61) Wojciechowski, R.; Yamamoto, K.; Yakushi, K.; Kawamoto, A. *Synth. Met.* **2003**, *135*−*136*, 587.
(62) Tajima, N.; Tamura, M.; Nishio, Y.; Kajita, K. *J. Phys. Soc. Jpn.* **2000**, *69*, 543.
(63) Kajita, K.; Tajima, N.; Ebina-Tajima, A.; Nishio, Y. *Synth. Met*. **2003**, *133*−*134*, 95.
(64) Kubo, Y.; Takano, Y.; Hiraki, K.; Takahashi, T.; Yamamoto, H. M.; Nakamura, T. *Synth. Met.* **2003**, *135*−*136*, 591.
(65) Tajima, N.; Ebina-Tajima, A.; Tamura, M.; Nishio, Y.; Kajita, K. *J. Phys. Soc. Jpn.* **2002**, *71*, 1832.
(66) Baram, G. O.; Buravov, L. I.; Degtyarev, L. S.; Kozlov, M. E.; Laukhin, V. N.; Laukhina, E. E.; Onishchenko, V. G.; Pokhodnya, K. I.; Sheinkman, M. K.; Shibaeva, R. P.; Yagubskii, E. B. *JETP Lett*. **1986**, *44*, 376.
(67) Crabtree, G. W.; Carlson, K. D.; Hall, L. N.; Copps, P. T.; Wang, H. H.; Emge, T. J.; Beno, M. A.; Williams J. M. *Phys. Rev. B* **1984**, *30*, 2958.
(68) Tokumoto, M.; Anzai, H.; Bando, H.; Saito, G.; Kinoshita, N.; Kajimura, K.; Ishiguro, T. *J. Phys. Soc. Jpn.* **1985**, *54*, 869.
(69) Laukhina, E. E.; Laukhin, V. N.; Khomenko, A. G.; Yagubskii, E. B. *Synth. Met*. **1989**, *32*, 381.
(70) Müller, H.; Svensson, S. O.; Fitch, A. N.; Lorenzen, M.; Xenikos, D. G. *Adv. Mater.* **1997**, *9*, 896.
(71) Müller, H.; Madsen, D.; Fitch, A. N.; Wanka, S.; Wosnitza, J. *J. Phys. IV* **2000**, *10*, Pr3-147.
(72) Wojciechowski, R.; Ulanski, J.; Lefrant, S.; Faulques, E.; Laukhina, E.; Tkacheva, V. *J. Chem Phys.* **2000**, *112*, 7634.
(73) Laukhina, E.; Tkacheva, V.; Chuev, I.; Yagubskii, E.; Vidal-Gancedo, J.; Mas-Torrent, M.; Rovira, C.; Veciana, J.; Khasanov, S.; Wojciechowski, R.; Ulanski, J. *J. Phys. Chem. B* **2001**, *105*, 11089.
(74) Tkacheva, V. A. Ph.D. Thesis, Institute of Problem of Chemical Physics of RAS, Chernogolovka, Russia, 2003.
(75) Leung, P. C. W.; Emge, T. J.; Beno, M. A.; Wang, H. H.; Williams, J. M.; Petricek, V.; Coppens, P. *J. Am. Chem. Soc.* **1985**, *107*, 6184.
(76) Molchanov, V. N.; Shibaeva, R. P.; Kaminskii, V. F.; Yagubskii, E. B.; Simonov, V. I.; Vainshtein, B. K. *Dokl. AN SSSR* **1986**, *286*, 637.
(77) Buravov, L. I.; Kartsovnik, M. A.; Kononovich, P. A.; Laukhin, V. N.; Pesotskii, S. I.; Schegolev, I. F. *Zh. Eksp. Teor. Fiz.* **1986**, *91*, 2198.
(78) Ginodman, V. B.; Gudenko, A. V.; Zherikhina, L. N. *Pis'ma v ZhETF* **1985**, *41*, 41.
(79) Tokumoto, M.; Bando, H.; Anzai, H.; Saito, G.; Murata, K.; Kajimura, K.; Ishiguro, T. *J. Phys. Soc. Jpn.* **1985**, *54*, 869.
(80) Laukhin, V. N.; Kostyuchenko, E. E.; Sushko, Yu. V.; Schegolev, I. F.; Yagubskii, E. B. *JETP Lett.* **1985**, *41*, 81.
(81) Murata, K.; Tokumoto, M.; Anzai, H.; Bando, H.; Saito, G.; Kajimura, K.; Ishiguro, T. *J. Phys. Soc. Jpn.* **1985**, *54*, 1236.
(82) Buravov, L. I.; Kartsovnik, M. V.; Kaminskii, V. F.; Kononovich, P. A.; Kostyuchenko, E. E.; Laukhin, V. N.; Makova, M. K.; Pesotskii, S. I.; Schegolev, I. F.; Topnikov, V. N.; Yagubskii, E. B. *Synth. Met.* **1985**, *11*, 207.
(83) Ginodman, V. B.; Gudenko, A. V.; Kononovich, P. A.; Laukhin, V. N.; Schegolev, I. F. *JETP Lett.* **1986**, *44*, 673.
(84) Ginodman, V. B.; Gudenko, A. V.; Kononovich, P. A.; Laukhin, V. N.; Schegolev, I. F. *Zh. Eksp. Teor. Fiz.* **1988**, *94* (5), 333.
(85) Kang, W.; Jérome, D.; Lenoir, C.; Batail, P. *Synth. Met.* **1988**, *27*, A353.
(86) Laukhin, V. N.; Ginodman, V. B.; Gudenko, A. V.; Kononovich, P. A.; Schegolev, I. F. in *The Physics and Chemistry of Organic*

Superconductors; Saito, G., Kagoshima, S., Eds.; Springer-Verlag, Berlin, Heidelberg: New York, 1990; p 122.
(87) Ginodman, V. B.; Gudenko, A. V.; Zasavitskii, I. I.; Yagubskii, E. B. *Pis'ma v ZhETF* **1985**, *42*, 384.
(88) Creuzet, F.; Creuzet, G.; Jérome, D.; Schweitzer, D.; Keller, H. J. *J. Phys., Lett.* **1985**, *46*, L-1079.
(89) Schirber, J. E.; Azevedo, L. J.; Kwak, J. F.; Venturini, E. L.; Leung, P. C. W.; Beno, M. A.; Wang, H. H.; Williams, J. M. *Phys. Rev. B* **1986**, *33*, 1987.
(90) Emge, T. J.; Leung, P. C. W.; Beno, M. A.; Schultz, A. J.; Wang, H. H.; Sowa, L. M.; Williams, J. M. *Phys. Rev. B.: Condens. Matter.* **1984**, *30*, 6780.
(91) Leung, P. C. W.; Emge, T. J.; Beno, M. A.; Wang, H. H.; Williams, J. M.; Petricek, V.; Coppens, P. *J. Am. Chem. Soc.* **1984**, *106*, 7644.
(92) Schultz, A. J.; Wang, H. H.; Williams, J. M. *J. Am. Chem. Soc.* **1986**, *108*, 7853.
(93) Merzhanov, V. A.; Kostyuchenko, E. E.; Laukhin, V. N.; Lobkovskaya, R. M.; Makova, M. K.; Shibaeva, R. P.; Schegolev, I. F.; Yagubskii, E. B. *Pis'ma v ZhETF* **1985**, *41*, 146.
(94) Hurdiquit, H.; Creuzet, F.; Jérome, D. *Synth. Met.* **1988**, *27*, A183.
(95) Hasegawa, Y.; Fukuyama, H. *J. Phys. Soc. Jpn.* **1986**, *55*, 3717.
(96) Gudenko, A. V.; Ginodman, V. B.; Kononovich, P. A.; Laukhin, V. N. *Zh. Eksp. Teor. Fiz.* **1990**, *98*, 627.
(97) Schweitzer, D.; Bele, P.; Brunner, H.; Gogu, E.; Haeberlen, U.; Henning, I.; Klutz, I.; Swietlik, R.; Keller, H. J. *Z. Phys. B* **1987**, *67*, 489.
(98) Schweitzer, D.; Gogu, E.; Hennig, I.; Klutz, T.; Keller, H. J. *Ber. Bunsen-Ges. Phys. Chem.* **1987**, *91*, 890.
(99) Zvarykina, A. V.; Kartsovnik, M. V.; Laukhin, V. N.; Laukhina, E. E.; Lyubovskii, R. B.; Pesotskii, S. I.; Shibaeva, R. P.; Schegolev, I. F. *Zh. Eksp. Teor. Fiz.* **1988**, *94* (9), 277.
(100) Laukhina, E. E.; Merzhanov, V. A.; Pesotskii, S. I.; Khomenko, A. G.; Yagubskii, E. B.; Ulanskii, J.; Kryszewski, M.; Jeszka, J. K. *Synth. Met.* **1995**, *70*, 797.
(101) Laukhina, E. E.; Ulanskii, J.; Khomenko, A. G.; Pesotskii, S. I.; Tkacheva, V. A.; Atovmyan, L.; Yagubskii, E. B.; Rovira, C.; Veciana, J.; Vidal-Gancedo, J.; Laukhin, V. N. *J. Phys I* **1997**, *7*, 1665.
(102) Murata, K.; Tokumoto, M.; Anzai, H.; Bando, H.; Saito, G.; Kajimura, K.; Ishiguro, T. *J. Am. Chem. Soc.* **1985**, *54*, 2084.
(103) Bobrov, V. S.; Zorin, S. N. *Pis'ma v ZhETF* **1984**, *40*, 345.
(104) Kagoshima, S.; Nogami, Y.; Hasumi, M.; Anzai, H.; Tokumoto, M.; Saito, G.; Mori, N. *Solid State Commun.* **1989**, *69*, 1177.
(105) Kagoshima, S.; Hasumi, M.; Nogami, Y.; Kinoshita, N.; Anzai, H.; Tokumoto, M.; Saito, G. in *The Physics and Chemistry of Organic Superconductors*; Saito, G., Kagoshima, S., Eds.; Springer-Verlag, Berlin, Heidelberg: New York, 1990; p 126.
(106) Kanoda, K.; Akiba, K.; Takahashi, T.; Saito, G. *Phys. Rev. B* **1990**, *42*, 6700.
(107) Nogami, Y.; Kagoshima, S.; Anzai, H.; Tokumoto, M.; Saito, G.; Mori, N. in *The Physics and Chemistry of Organic Superconductors*; Saito, G., Kagoshima, S., Eds.; Springer-Verlag, Berlin, Heidelberg: New York, 1990; p 130.
(108) Ravy, S.; Pouget, J.-P.; Moret, R.; Lenoir, C. *Phys. Rev. B* **1988**, *37*, 5113.
(109) Montgomery, L. K.; Geiser, U.; Wang, H. H.; Beno, M. A.; Schultz, A. J.; Kini, A. M.; Carlson, K. D.; Williams, J. M.; Whitworth, J. R.; Gates, B. D.; Cariss, C. S.; Pipan, C. M.; Donega, K. M.; Wenz, C.; Kwok, W. K.; Crabtree, G. W. *Synth. Met.* **1988**, *27*, A195.
(110) Beno, M. A.; Kini, A. M.; Montgomery, L. K.; Whitworth, J. R.; Carlson, K. D.; Williams, J. M. *Synth. Met.* **1988**, *27*, A219.
(111) Kushch, N. D.; Buravov, L. I.; Zvarykina, A. V.; Laukhin, V. N.; Khomenko, A. G.; Yagubskii, E. B. *Izv. AN SSSR, Ser. Khim.* **1990**, 1690.
(112) Madsen, D.; Burghammer, M.; Fielder, S.; Müller, H. *Acta Crystallogr., Sect. B* **1999**, *55*, 601.
(113) Shibaeva, R. P.; Kaminskii, V. F.; Bel'skii, V. K. *Sov. Phys. Crystallogr.* **1984**, *29*, 638.
(114) Buravov, L. I.; Zvarykina, A. V.; Laukhina, E. E.; Laukhin, V. N.; Lobkovskaya, R. M.; Merzhanov, V. A.; Aleinikov, N. N.; Korotkov, V. E.; Shibaeva, R. P.; Schegolev, I. F.; Yagubskii, E. B. *Mater. Sci.* **1988**, *14*, 17.
(115) Beno, M. A.; Geiser, U.; Kostka, K. L.; Wang, H. H.; Webb, K. S.; Firestone, M. A.; Carlson, K. D.; Nuñez, L.; Whangbo, M.-H.; Williams, J. M *Inorg. Chem.* **1987**, *26*, 1912.
(116) Shibaeva, R. P.; Lobkovskaya, R. M.; Yagubskii, E. B.; Kostyuchenko, E. E.; *Sov. Phys. Crystallog.* (English translation) **1986**, *31*, 267.
(117) Shibaeva, R. P.; Lobkovskaya, R. M.; Yagubskii, E. B.; Laukhina, E. E. *Sov. Phys. Crystallog.* (English translation) **1987**, *32*, 530.
(118) Shibaeva, R. P.; Lobkovskaya, R. M.; Yagubskii, E. B.; Kostyuchenko, E. E.; *Sov. Phys. Crystallog.* (English translation) **1986**, *31*, 657.
(119) Shibaeva, R. P.; Lobkovskaya, R. M.; Kaminskii, V. F.; Lindeman, S. V.; Yagubskii, E. B. *Sov. Phys. Crystallog.* (English translation) **1986**, *31*, 546.
(120) Konarev, D. V.; Kovalevsky, A. Yu.; Coppens, P.; Lyubovskaya, R. N. *Chem. Commun.* **2000**, 2357.
(121) Zvarykina, A. V.; Kononovich, P. A.; Laukhin, V. N.; Molchanov, V. N.; Pesotskii, S. I.; Simonov, V. I.; Shibaeva, R. P.; Schegolev, I. F.; Yagubskii, E. B. *JETP Lett.* **1986**, *43*, 329.
(122) Shibaeva, R. P.; Yagubskii, E. B.; Laukhina, E. E.; Laukhin, V. N. in *The Physics and Chemistry of Organic Superconductors*; Saito, G., Kagoshima, S., Eds.; Springer-Verlag, Berlin, Heidelberg: New York, 1990, p 342.
(123) Kartsovnik, M. V.; Laukhin, V. N.; Schegolev, I. F. *Zh. Eksp. Teor. Fiz.* **1986**, *90*, 2172.
(124) Laukhina, E.; Vidal-Gancedo, J.; Laukhin, V.; Veciana, J.; Chuev, I.; Tkacheva, V.; Wurst, K.; Rovira, C. *J. Am. Chem. Soc.* **2003**, *125*, 3948.
(125) Avramenko, N. V.; Zvarykina, A. V.; Laukhin, V. N.; Laukhina, E. E.; Lyubovskii, R. B.; Shibaeva, R. P. *Pis'ma v ZhETF* **1988**, *48*, 429.
(126) Wang, H. H.; Carlson, K. D.; Montgomery, L. K.; Schlueter, J. A.; Cariss, C. S.; Kwok, W. K.; Geiser, U.; Crabtree, G. W.; Williams, J. M. *Solid State Commun.* **1988**, *66*, 1113.
(127) Laukhina, E.; Tkacheva, V.; Chekhlov, A.; Yagubskii, E.; Wojciechowski, R.; Ulanski, J.; Vidal-Gancedo, J.; Veciana, J.; Laukhin, V.; Rovira, C. *Chem. Mater.* **2004**, in press.
(128) Yoneyama, N.; Miyazaki, A.; Enoki, T.; Saito, G. *Synth. Met.* **1997**, *86*, 2029.
(129) Kobayashi, H.; Kato, R.; Kobayashi, A.; Nishio, Y.; Kajita, K.; Sasaki, W. *Chem. Lett.* **1986**, 833.
(130) Kato, R.; Kobayashi, H.; Kobayashi, A.; Moriyama, S.; Nishio, Y.; Kajita, K.; Sasaki, W. *Chem. Lett.* **1987**, 507.
(131) Kajita, K.; Nishio, Y.; Moriyama, S.; Sasaki, W.; Kato, R.; Kobayashi, H.; Kobayashi, A. *Solid State Commun.* **1987**, *64*, 1279.
(132) Balthes, E.; Breining, A.; Kahlich, S.; Moldenhauer, J.; Schweitzer; D.; Bele, P.; Brunner, H.; Heinen, I.; Nuber, B.; Keller, H. J. *Synth. Met.* **1993**, *55*−*57*, 2859.
(133) Kobayashi, H.; Kawano, K.; Naito, T.; Kobayashi, A. *J. Mater. Chem.* **1995**, *5*, 1681.
(134) Balthes, E.; Schweitzer, D.; Heinen, I.; Keller, H. J.; Biberacher, W.; Jansen, A. G. M.; Steep, E. *Synth. Met.* **1995**, *70*, 841.
(135) Wosnitza, J.; Liu, X.; Schweitzer, D.; Keller, H. J. *Phys. Rev. B* **1994**, *50*, 12747.
(136) Tamura, M.; Yakushi, K.; Kuroda, H.; Kobayashi, A.; Kato, R.; Kobayashi, H. *J. Phys. Soc. Jpn.* **1988**, *57*, 3239.
(137) Kajita, K.; Nishio, Y.; Takahashi, T.; Sasaki, W.; Kato, R.; Kobayashi, H.; Kobayashi, A. *Solid State Commun.* **1989**, *70*, 1181.
(138) Kobayashi, H.; Kato, R.; Kobayashi, A.; Moriyama, S.; Nishio, Y.; Kajita, K.; Sasaki, W. *Synth. Met.* **1988**, *27*, A283.
(139) Kajita, K.; Nishio, Y.; Takahashi, T.; Sasaki, W.; Kato, R.; Kobayashi, H.; Kobayashi, A.; Iye, Y. *Solid State Commun.* **1989**, *70*, 1189.
(140) Terashima, T.; Uji, S.; Aoki, H.; Tamura, M.; Kinoshita, M.; Tokumoto, M. *Solid State Commun.* **1994**, *91*, 595.
(141) Tamura, M.; Kuroda, H.; Uji, S.; Aoki, H.; Tokumoto, M.; Swanson, A. G.; Brooks, J. S.; Agosta, C. C.; Hannahs, S. T. *J. Phys. Soc. Jpn.* **1994**, *63*, 615.
(142) Oshima, Y.; Ohta, H.; Okubo, S.; Koyama, K.; Motokawa, M.; Tamura, M.; Nishio, Y.; Kajita, K. *Synth. Met.* **2001**, *120*, 853.
(143) Lyubovskaya, R. N.; Lyubovskii, R. B.; Shibaeva, R. P.; Aldoshina, M. Z.; Gol'denberg, L. M.; Rozenberg, L. P.; Khidekel', M. L.; Shul'pyakov, Yu. F. *Pis'ma v JETF* **1985**, *42*, 380.
(144) Shibaeva, R. P.; Rozenberg, L. P. *Kristallografiya* **1988**, *33*, 1402.
(145) Wanka, S.; Beckmann, D.; Wosnitza, J.; Balthes, E.; Schweitzer, D.; Strunz, W.; Keller, H. J. *Phys. Rev. B* **1996**, *53*, 9301.
(146) Itskovsky, M. A.; Askenazy, S.; Maniv, T.; Vagner, I. D.; Balthes, E.; Schweitzer, D. *Phys. Rev. B.* **1998**, *58*, R13347.
(147) Balthes, E.; Schiller, M.; Schweitzer, D.; Heinen, I.; Strunz, W.; Steep, E.; Jansen, A. G. M.; Wyder, P. *Physica C* **1999**, *317*−*318*, 108.
(148) Nothardt, A.; Balthes, E.; Schmidt, W.; Schweitzer, D.; Kartsovnik, M.; Sheikin, I. *J. Phys. IV* **2004**, *114*, 351.
(149) Pasquier, C.; Joo, N.; Batail, P.; Schweitzer, D.; Jérome, D. *J. Phys. IV* **2004**, *114*, 239.
(150) Khasanov, S. S.; Zorina, L. V. Manuscript to be published.
(151) Sugano, T.; Sato, S.; Konno, M.; Kinoshita, M. *Acta Crystallogr., Sect. C* **1988**, *44*, 1764.
(152) Shibaeva, R. P.; Rozenberg, L. P.; Korotkov, V. E.; Karpov, O. G.; Kushch, N. D.; Yagubskii, E. B.; Neiland, O. Ya.; Medne, R. S.; Katsen, Ya. Ya. *Kristallografiya* **1989**, *34*, 1438.
(153) Kobayashi, H.; Takahashi, M.; Kato, R.; Kobayashi, A.; Sasaki, Y. *Chem. Lett.* **1984**, 1331.
(154) Korotkov, V. E.; Kushch, N. D.; Shibaeva, R. P.; Yagubskii, E. B. *Kristallografiya* **1992**, *37*, 908.
(155) Korotkov, V. E.; Shibaeva, R. P.; Kushch, N. D.; Yagubskii, E. B. in *The Physics and Chemistry of Organic Conductors*; Saito, G., Kagoshima, S., Eds.; Springer-Verlag, Berlin, Heidelberg: New York, 1990, p 306.
(156) Lyubovskii, R. B.; Laukhina, E. E.; Makova, M. K.; Yagubskii, E. B. *Synth. Met.* **1990**, *35*, 1.

(157) Shibaeva, R. P.; Rozenberg, L. P.; Simonov, M. A.; Kushch, N. D.; Yagubskii, E. B. *Kristallografiya* **1988**, *33*, 1156.
(158) Shultz, A. J.; Geiser, U.; Kini, A. M.; Wang, H. H.; Schlueter, J.; Cariss, C. S.; Williams, J. M. *Synth. Met.* **1988**, *27*, A229.
(159) Yagubskii, E. B. *J. Solid State Chem.* **2002**, *168*, 464.
(160) Doublet, M.-L.; Canadell, E.; Pouget, J.-P.; Yagubskii, E. B.; Ren, J.; Whangbo, M.-H. *Solid State Commun*. **1993**, *88*, 699.
(161) Yagubskii, E. B.; Kotov, A. I.; Laukhina, E. E.; Ignatiev, A. A.; Nagapetyan, S. S.; Shklover, V. E.; Struchkov, Yu. T.; Vetoshkina, L. V.; Ukhin, L. Yu. *Mater. Sci.* **1991**, *17*, 55.
(162) Yagubskii, E. B.; Kotov, A. I.; Laukhina, E. E.; Ignatiev, A. A.; Buravov, L. I.; Khomenko, A. G.; Shklover, V. E.; Nagapetyan, S. S.; Struchkov, Yu. T. *Synth. Met.* **1991**, *41*−*43*, 2515.
(163) Yagubskii, E. B.; Kushch, L. A.; Gritsenko, V. V.; Dyachenko, O. A.; Buravov, L. I.; Khomenko, A. G. *Synth. Met.* **1995**, *70*, 1039.
(164) Shibaeva, R. P.; Khasanov, S. S.; Narymbetov, B. Zh.; Rozenberg, L. P.; Kushch, L. A.; Yagubskii, E. B. *Russ. Crystallogr*. **1998**, *43*, 237.
(165) Wang, H. H.; Fox, Sh. B.; Yagubskii, E. B.; Kushch, L. A.; Kotov, A. I.; Whangbo, M.- H. *J. Am. Chem. Soc.* **1997**, *119*, 7601.
(166) Yagubskii, E. B.; Kotov, A. I.; Buravov, L. I.; Khomenko, A. G.; Shklover, V. E.; Nagapetyan, S. S.; Struchkov, Yu. T.; Vetoshkina, L. V.; Ukhin, L. Yu. *Synth. Met.* **1990**, *35*, 271.
(167) Dyachenko, O. A.; Gritsenko, V. V.; Shilov, G. V.; Laukhina, E. E.; Yagubskii, E. B. *Synth. Met.* **1993**, *58*, 137.
(168) Gritsenko, V. V.; Dyachenko, O. A.; Kushch, L. A.; Yagubskii, E. B. *Synth. Met.* **1998**, *94*, 61.
(169) Kushch, L. A.; Yagubskii, E. B.; Konovalikhin, S. V.; Shilov, G. V.; Atovmyan, L. O. *Russ. Chem. Bull.* **1999**, *48*, 1513.
(170) Kushch, L. A.; Gritsenko, V. V.; Buravov, L. I.; Shilov, G. V.; Dyachenko, O. A.; Merzhanov, V. A.; Yagubskii, E. B.; Rousseau, R.; Canadell, E. *J. Mater. Chem.* **1995**, *5*, 1633.
(171) Yagubskii, E. B. *Synth. Met.* **2003**, *134*−*135*, 385.
(172) Kontani, H. *Phys. Rev. B* **2003**, *67*, R180503.
(173) Miyazaki, T.; Kino, H. *Phys. Rev. B* **2003**, *68*, R220511.

CR0306642